SEDIMENTOLOGY the journal of the International Association of Sedimentologists

*Sedimentology* (2011) **58,** 170–219 doi: 10.1111/j.1365-3091.2010.01209.x

# Hot-spring Systems Geobiology: abiotic and biotic influences on travertine formation at Mammoth Hot Springs, Yellowstone National Park, USA

BRUCE W. FOUKE

*Departments of Geology, Microbiology, and Institute for Genomic Biology, University of Illinois Urbana-Champaign, 1301 West Green Street, Urbana, IL 61801, USA and Thermal Biology Institute, Montana State University, Leon Johnson Hall, Bozeman, MT 59717, USA (E-mail: fouke@illinois.edu)*

Associate Editor – Jim Best

**ABSTRACT**

Multiple abiotic and biotic factors combine in nature to influence the formation of calcium carbonate limestone deposits. Systems Geobiology studies of how micro-organisms respond to, or sometimes even control, the coupled effects of environmental change and mineralization will permit more accurate interpretation of the fossil record of ancient microbial life. Mammoth Hot Springs in Yellowstone National Park, USA, serves as a natural laboratory for tracking how the dynamic interplay of physical, chemical and biological factors come together to form hot-spring limestone (called 'travertine'). Systematic downstream correlations occur at Mammoth Hot Springs between travertine deposition (geomorphology, crystalline structure and geochemistry), microbial communities (mat morphology, pigmentation, and phylogenetic and metabolic diversity) and spring-water conditions (temperature, pH, geochemistry and flow). Field-based microscale and mesoscale experimentation indicates that microbes directly influence travertine growth rate and crystalline structure. At the macroscale, time-lapse field photography and numerical modelling suggest that travertine terrace geomorphology is influenced strongly by hydrology, heat dispersion and geochemistry. These results from Mammoth Hot Springs allow establishment of a conceptual framework across broad spatial and temporal scales in which to track how multiple geological and biological factors combine to control $CaCO_3$ crystal precipitation and the resulting formation of travertine deposits.

**Keywords** Mammoth Hot Springs, microbial ecology, *Sulfurihydrogenibium*, travertine, water chemistry.

## INTRODUCTION

Earth science exploration in the Twenty-First Century is moving from a focus on individual geological processes to questions of how multiple physical, chemical and biological phenomena simultaneously interact in nature. This shift in emphasis necessitates a broad cross-disciplinary integration of: (i) reductionist and holistic approaches; (ii) field and laboratory experimentation; and (iii) synthesis and prediction across broad spatial and temporal scales. A remarkable succession of recent technological advancements in the physical and life sciences now make this possible. For instance, knowledge of microbiological composition, distribution and function in natural environments (the 'OMICS' sciences; Blow, 2008) is being propelled by

rapidly expanding capacities in molecular sequencing and bioinformatics [National Research Council (NRC), 2007; Dinsdale *et al.*, 2008; Frias-Lopez *et al.*, 2008]. At the same time, new instrumentation is continually being developed for optical, mineralogical, structural, chemical, hydrological and sedimentological analyses at, or below, the 1 μm average diameter of single microbial cells (Stephens & Allan, 2003; Sweedlow *et al.*, 2003; Lipfert & Doniach, 2007; Garcia, 2008; Stock, 2008; U.S. DOE, 2008). As a result, a wide array of fundamental physical and chemical processes can now be simultaneously measured, correlated and mechanistically linked with biological processes that range from the single cell to entire ecosystems.

The emerging field of 'Systems Geobiology' links microscale and mesoscale geological, biological, physical and chemical processes with macroscale environmental processes (Fig. 1), the goal of which is to more accurately interpret the record of fossilized micro-organisms (biomarkers; Allen *et al.*, 2000*)* preserved in ancient rock [Banfield & Nealson, 1997; Agouron, 2001; American Society for Microbiology (ASM), 2001; Knoll, 2003; Konhauser, 2007; Dilek *et al.*, 2008; Ehrlich & Newman, 2009]. Understanding the relative influence of abiotic and biotic controls on calcium carbonate ($CaCO_3$) limestone deposition is an important focus area of this research (Schneidermann & Harris, 1985; Stanley, 2001; Ridgwell & Zeebe, 2005). Of the many terrestrial and marine environments in which limestone accumulates, limestone deposits in hydrothermal systems (called 'travertine'; Sanders & Friedman, 1967; Pentecost & Viles, 1994) provide an especially sensitive record of complex interactions between microbes and the environment (Chafetz & Folk, 1984; Folk, 1993, 1994; Pentecost, 1995, 2005; Ford & Pedley, 1996; Fouke *et al.*, 2000; Riding, 2000); this makes travertine an important target in the search for ancient microbial fossils that formed on the early Earth (Walter & Des Marais, 1993; Riding, 2000; Pentecost, 2005). The challenges now facing Systems Geobiology research in carbonate hot-spring ecosystems are to: (i) develop the conceptual, contextual, experimental and technical approaches required to simultaneously track biotic and abiotic interactions in modern environments; and (ii) directly apply these results to interpret ancient hot-springs travertine and other key terrestrial and marine environments of limestone deposition.

The largest assemblage of terrestrial hot springs in the world occurs in Yellowstone National Park (YNP) and is heated by the largest volcano on Earth (Smith & Siegel, 2000). Mammoth Hot Springs (MHS), at the northern boundary of YNP (Fig. 2A), is one of the only easily accessible hot-spring complexes in the world that remain in their natural state because of long-term protection by the United States National Park Service (NPS). Several decades of research at MHS has shown that modern travertine crystal fabric, chemistry and rapid precipitation rates ($\leq$5 mm day$^{-1}$) result from the complex interplay of both biotic and abiotic processes (Friedman, 1970; Fouke *et al.*, 2000, 2003; Zhang *et al.*, 2004; Kandianis *et al.*, 2008; Veysey & Goldenfeld, 2008). In addition, MHS and nearby Gardiner, Montana (Fig. 2A), contain a sequence of ancient Holocene and Pleistocene travertine deposits that permit interpretations from the modern hot springs to be directly applied to the geological record of fossil travertine deposits (Bargar, 1978; Sorey, 1991; Sturchio, 1992; Sturchio *et al.*, 1994; Sorey & Colvard, 1997). The intent of this review is to summarize the research at MHS, which quantifies the dynamic interplay of physical, chemical and biological processes that influence travertine deposition, to better understand broader questions for other environments of limestone deposition in the emerging field of Systems Geobiology.

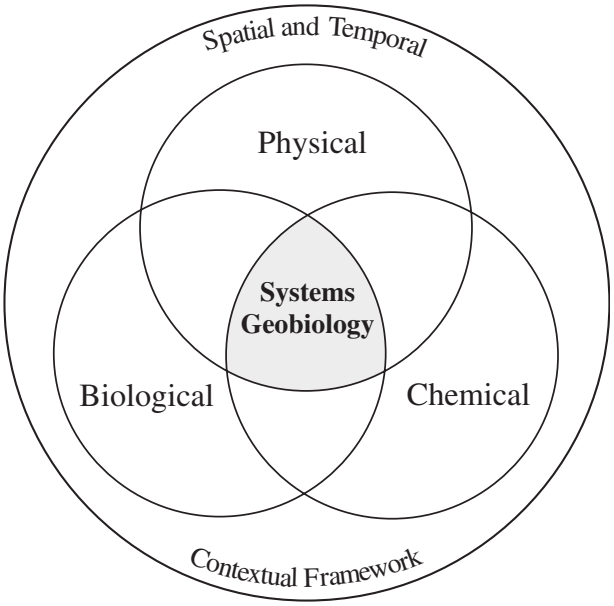


**Fig. 1.** Cross-disciplinary and contextual nature of Systems Geobiology research, in which simultaneous physical, chemical and biological analyses are linked directly to the spatial and temporal contextual framework.

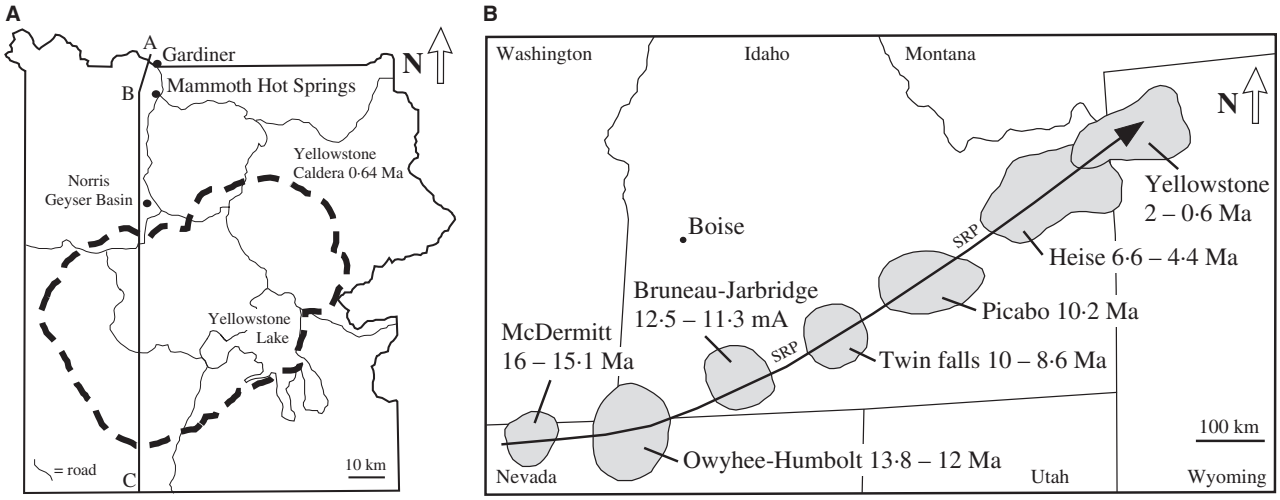


**Fig. 2.** Regional maps of Yellowstone National Park (YNP) caldera and the Snake River Plain (SRP) volcanic track. (A) Map of YNP illustrating the position of Mammoth Hot Springs (MHS) and Gardiner with respect to the Yellowstone caldera, the Norris Geyser Basin, Yellowstone Lake and the primary roads in Yellowstone (modified from Lowenstern & Hurwitz, 2008). (B) Trajectory of the Yellowstone hot spot track (dark line with arrowhead) that progresses from the original 16 to 15·1 Myr old McDermitt volcanic field, through the successive migration of SRP volcanic fields, to the current position of the 2 to 0·64 Ma Yellowstone volcanic plateau (modified from Pierce *et al.*, 2007).

## YELLOWSTONE GEOLOGICAL AND HYDROLOGICAL SETTING

Yellowstone National Park is a showcase of more than 12 000 hot springs, geysers, fumeroles and mud pots that are heated by the immense Yellowstone supervolcano (Fournier, 1989, 2005; Rye & Truesdell, 2007). The vent water at these sites exhibits a bimodal distribution in pH (Fig. 3) that reflects the complex interplay of regional hydrology, bedrock geology and potentially the metabolic activity of heat-loving micro-organisms (thermophiles). Yellowstone National Park straddles the Yellowstone Plateau, a crescent-shaped complex of high volcanic plateaus and mountainous terrain at the north-east end of the Snake River Plain in the western United States (Pierce *et al.*, 2007; Fig. 2B). All aspects of the geology, topography, climate and biota comprising the greater Yellowstone ecosystem reflect the direct thermal influence of the Yellowstone supervolcano, which initially formed over 16 Ma at a location near the Nevada-Oregon border (Fig. 2B). Since then, the south-west-moving North American plate has migrated over a relatively stationary mantle thermal plume ('hot spot'), which forms the Snake River Plain volcanic track and its present culmination at the 2 Myr old Yellowstone Plateau (Fig. 2B; Pierce *et al.*, 2007; Morgan *et al.*, 2009a). The supervolcano last erupted 640 ka to form the present elliptical $50 \times 80$ km Yellowstone volcanic caldera (Fig. 2A; Christiansen *et al.*, 2007). The crust underlying the caldera is composed of an upper silicic magma chamber at 5 to 10 km depth (Fig. 4) that has fuelled most of the volcanism over the past 2 Myr, as well as lower basaltic intrusions at 20 to 25 km depth that provide heat and $CO_2$-rich waters to the YNP hydrothermal system (Husen & Smith, 2004; Lowenstern & Hurwitz, 2008; Morgan *et al.*, 2009b). Hot springs immediately adjacent to the northern flank of the caldera occur atop a succession of Mesozoic sedimentary rocks overlain by welded ash flows (Fraser *et al.*, 1969), while thermal features within the caldera are underlain by a complex sequence of volcanic rhyolites and ash flows (Pierce *et al.*, 2007; Fig. 4).

Mammoth Hot Springs is the second largest site on Earth of active travertine deposition after Pamukkale, Turkey (Pentecost, 2005). Mammoth Hot Springs lies 40 km north of the caldera rim (Fig. 2A) in the subsiding Norris-Mammoth corridor that extends into the Corwin Springs Known Geothermal Resources Area (KGRA; Sorey, 1991; Fig. 4). Furthermore, MHS is the only major area of hydrothermal vent activity in YNP outside of the caldera (Sorey, 1991; Sorey & Colvard, 1997; Kharaka *et al.*, 1991, 2000; Rye & Truesdell, 2007). The complex subsidence structure of the Norris-Mammoth corridor has required intensive research efforts over several decades to determine the source and age of the spring-water that emerges at MHS (White *et al.*, 1975; Sorey, 1991; Sorey & Colvard, 1997). Mammoth Hot

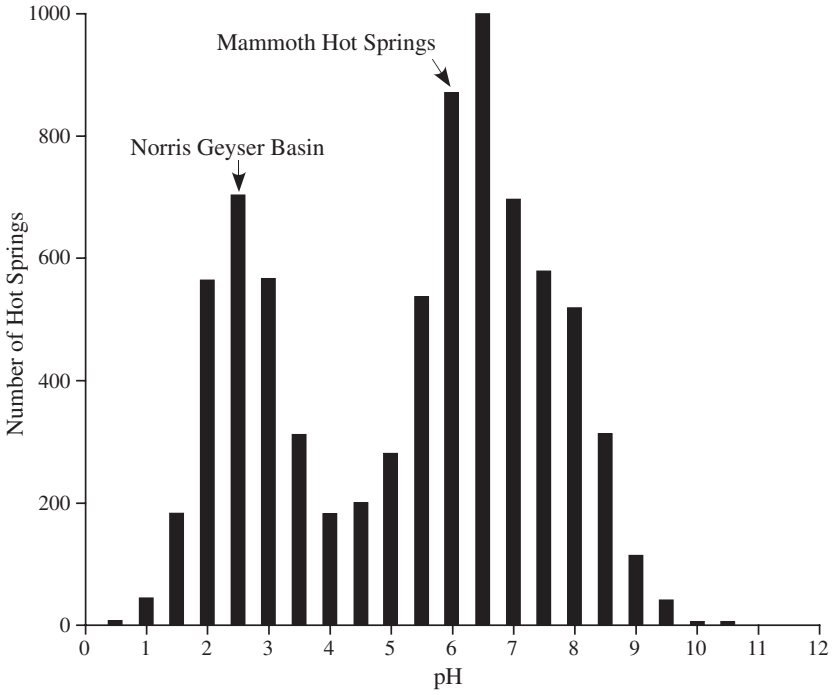


**Fig. 3.** Vent water pH values from hydrothermal features in Yellowstone National Park. The graph represents data collected from 7700 of the more than 12 000 geothermal vents in Yellowstone and is derived from analyses performed by the Yellowstone Center for Resources and made available through the Yellowstone NSF Research Coordination Network website (http://www.rcn.montana.edu/).

Springs spring-water $\delta$D and $\delta^{18}$O values suggest they have been derived from shallow subsurface recharge of Holocene and/or Pleistocene Gallatin Mountain snowmelt precipitated at 2·5 to 3 km elevation. These surface waters then flowed into the subsurface along the Swan Lake fault system (Kharaka *et al.*, 1991, 2000). Only in this northern part of Yellowstone are the meteoric water $\delta$D values sufficiently low and the subsurface geological plumbing adequate to deliver recharging meteoric waters deep into the caldera hydrological system (Rye & Truesdell, 2007). Theoretical estimates for recharge age and subsurface residence time are difficult to constrain and range from less than 2000 years to greater than 11 000 years (Rye & Truesdell, 2007). The $^{3}He/^{4}He$ values and concentrations of Cl, B and $CO_2$ at Mammoth imply that the meteoric recharge has been mixed in the subsurface with a magmatic water source derived from the Norris Geyser Basin (Kharaka *et al.*, 2000). An alternative model suggests that heat and volatiles are sourced from a separate, yet currently unknown, magmatic source emplaced under Bunsen Peak just south of Mammoth (Kharaka *et al.*, 1991, 2000).

The springs at MHS expel Ca–Na–$HCO_3$–$SO_4$ type $CO_2$-rich waters at a maximum temperature of 73°C and a pH of *ca* 6 (Fig. 3). Mammoth Hot Springs spring-water chemistry and travertine $\delta^{34}S$ and $^{87}Sr/^{86}Sr$ indicate that subsurface water–rock interactions have occurred at as much as 100°C with Mississippian-age Madison Group limestone and evaporite deposits (Kharaka *et al.*, 1991; Sorey, 1991; Sorey & Colvard, 1997; Fouke *et al.*, 2000; Rye & Truesdell, 2007). Spring-water emerging at MHS is therefore supercharged with dissolved $CO_2$ as a result of these subsurface water–rock interactions (Sorey, 1991). The small extent of spring-water deuterium fractionation detected in MHS spring-water (+0·2 to +0·4‰ $\Delta\delta$D SMOW; Friedman, 1970; Kharaka *et al.*, 1991) suggests that little to no boiling has taken place in the subsurface. Thermal water discharge at MHS reaches 600 $Ls^{-1}$, of which 10% erupts onto the MHS travertine terraces and 90% flows directly into the Gardiner River at the Fire Hole spring (Sorey, 1991; Sorey & Colvard, 1997). Temperature readings taken during drilling of the U.S. Geological Survey (USGS) Y-10 well that penetrated the entirety of the MHS travertine section (White *et al.*, 1975), combined with later borehole temperature logging (Sorey, 1991), indicate subsurface water temperatures of 72°C in the western portion of the MHS complex (Fig. 5C). The Y-10 borehole waters also exhibit a 4% higher ground water pressure head and a 10% elevation in dissolved Cl and $SO_4$ concentrations than the rest of the MHS complex (Sorey, 1991); this implies that deep ground water flows up into the MHS complex near the Y-10 well site in the south-west and then flows to the north-east (Sorey, 1991).

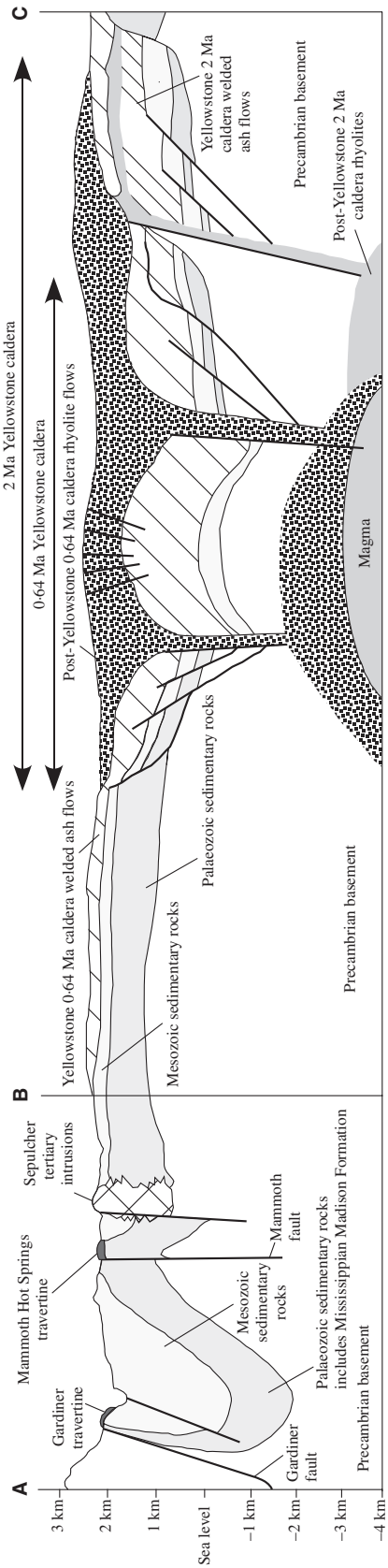


**Fig. 4.** Schematic north–south geological cross-section through Yellowstone National Park. The location of the A–B–C line-of-section is shown in Figure 2A. Section A–B illustrates the folded Palaeozoic and Mesozoic sedimentary rocks underlying MHS and Gardiner. Mammoth Hot Springs spring-water primarily derives its carbonate-rich chemistry as a result of subsurface water–rock interactions with limestone and evaporites comprising the Palaeozoic Mississippian Madison Formation. Section A–B is modified from Fraser *et al.* (1969) and Sorey (1991). Section B–C is a sketch of the Yellowstone caldera showing the volcanic rocks underlying all other hydrothermal features in YNP (modified from Rye & Truesdell, 2007).

## Overview of Mammoth Hot Springs travertine

The classification scheme for $CaCO_3$ deposits precipitated in 'terrestrial' settings includes the terms 'travertine' (precipitates from high-temperature springs, also called carbonate sinters), 'tufa' (precipitates from low-temperature springs, lakes, and waterfalls) and 'speleothem' (precipitates from waters in low-temperature to high-temperature subterranean caves or fracture systems; Sanders & Friedman, 1967). In the present review, the term 'travertine' will be used to refer to the modern and ancient limestone deposits that have precipitated in the 25°C to 73°C hot-spring outflow drainage systems at MHS (Pentecost & Viles, 1994). Furthermore, 'travertine' will be used in a purely descriptive sense, based solely on rock properties (i.e. grain-size, shape, composition and mineralogy) and without interpretation of the depositional environment. Travertine classification schemes that incorporate interpretations of water temperature, slope, geomorphology and biological processes (Pentecost *et al.*, 2003; Pentecost, 2005) have been established for other spring systems but do not apply consistently at MHS and, therefore, have not been used.

Long-term observation, sampling and monitoring at MHS has been conducted at Angel Terrace Spring AT-1, AT-2, AT-3 and Narrow Gauge (Fig. 5A and B). Travertine deposition shifts from site to site as the spring vents migrate, stop flowing and re-emerge in a new location (Weed, 1889; Allen & Day, 1935; Freidman, 1970; Bargar, 1978; Fouke *et al.*, 2000). The geomorphology of the travertine deposits at MHS was first described by Weed (1889), then Allen & Day (1935) and presented in more detail by Bargar (1978). Macro-scale (≥5 m thick) travertine deposits consistently form large stepped terraces with a flat top, distinct break in slope and an inclined front margin. Striking examples include Minerva Terrace, Main Terrace and Highland Terrace (Fig. 6A). Each terrace is composed of smaller interbedded mesoscale (0·5 to 1 m thick) travertine geomorphologies (Fig. 6B), which include terracettes, domes and fissure-ridges (Fig. 6B to E). In the case of terracettes and domes, spring-water is expelled from small (<10 cm diameter) cylindrical vents (Fig. 6D and E). Asymmetrical semi-circular terracette deposits form when the vents emerge on a hillside slope (Fouke *et al.*, 2000; Goldenfeld *et al.*, 2006; Fig. 6A and B). Symmetrically rounded travertine domes are deposited when the vent erupts on a flat surface (Chan & Goldenfeld, 2007; Fig. 6D), the best-known of which is

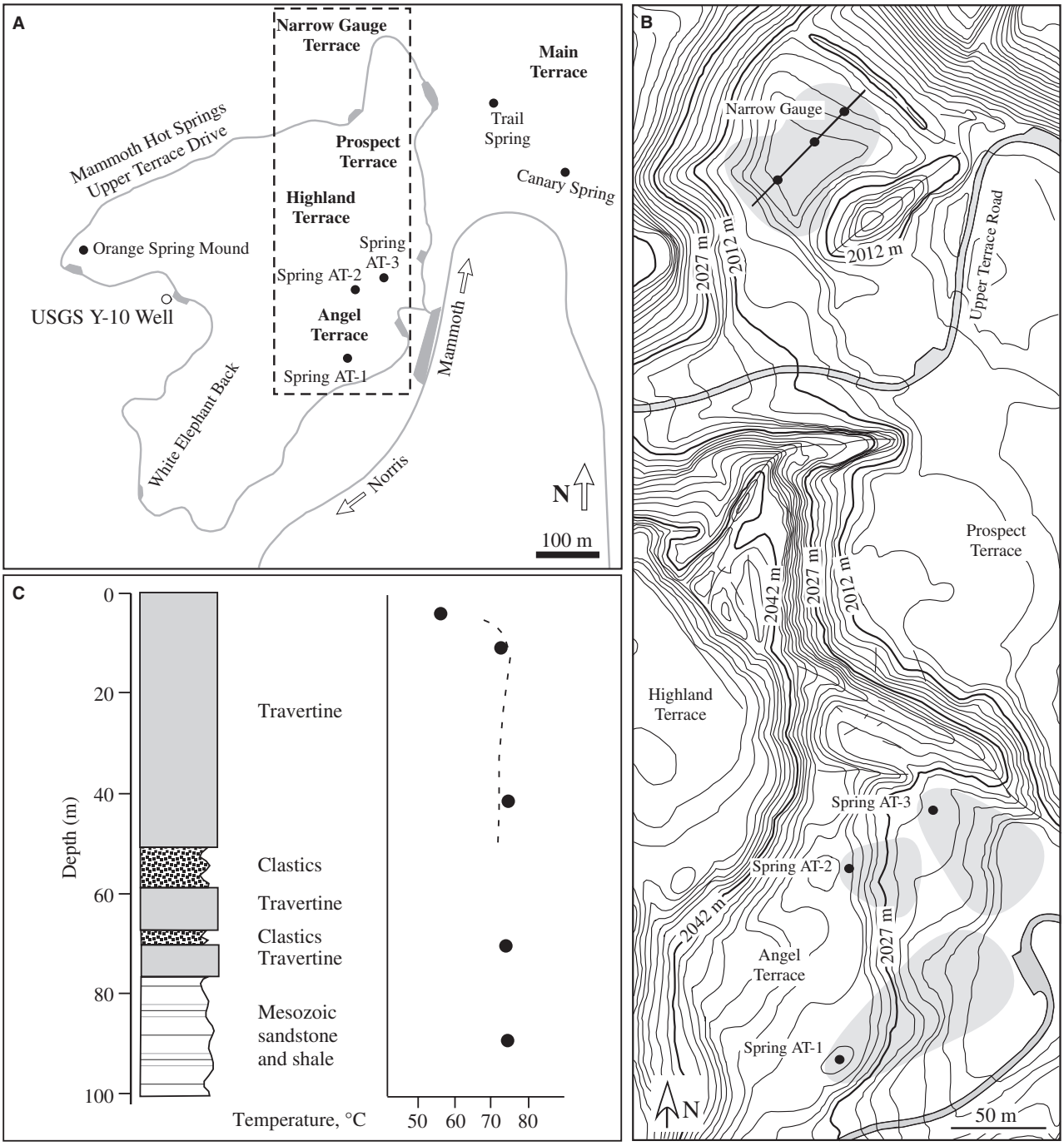


**Fig. 5.** Location of hot springs and the Y-10 well within the Mammoth Hot Springs complex. (A) Line tracing of an aerial photograph showing the location of hot springs and the USGS Y-10 well along the Upper Terrace Loop road at MHS. (B) Topographic map of MHS showing the location of the hot springs studied at Angel Terrace (AT-1, AT-2 and AT-3) and Narrow Gauge. Dark circles indicate the position of vents, dark lines are fractures and grey fields indicate outflow drainage patterns. Note that Narrow Gauge exhibits a series of vents that emerge along a fracture. (C) Stratigraphy and formation water temperatures from the USGS Y-10 well (modified from White *et al.*, 1978 and Sorey, 1991).

Liberty Cap (Fig. 6E). Travertine fissure-ridges form where hot-spring water emerges along a fracture and flows in opposite directions away from the fracture line source to form an elongate symmetrical travertine mound (Fig. 6C). Narrow Gauge is a complex hybrid deposit of all three of these geomorphologies, with individual vent point sources developing along a fracture to form terracettes, domes (Fig. 6D) and fissure ridges, all in one system. Smaller-scale (1 mm to 0·5 m)

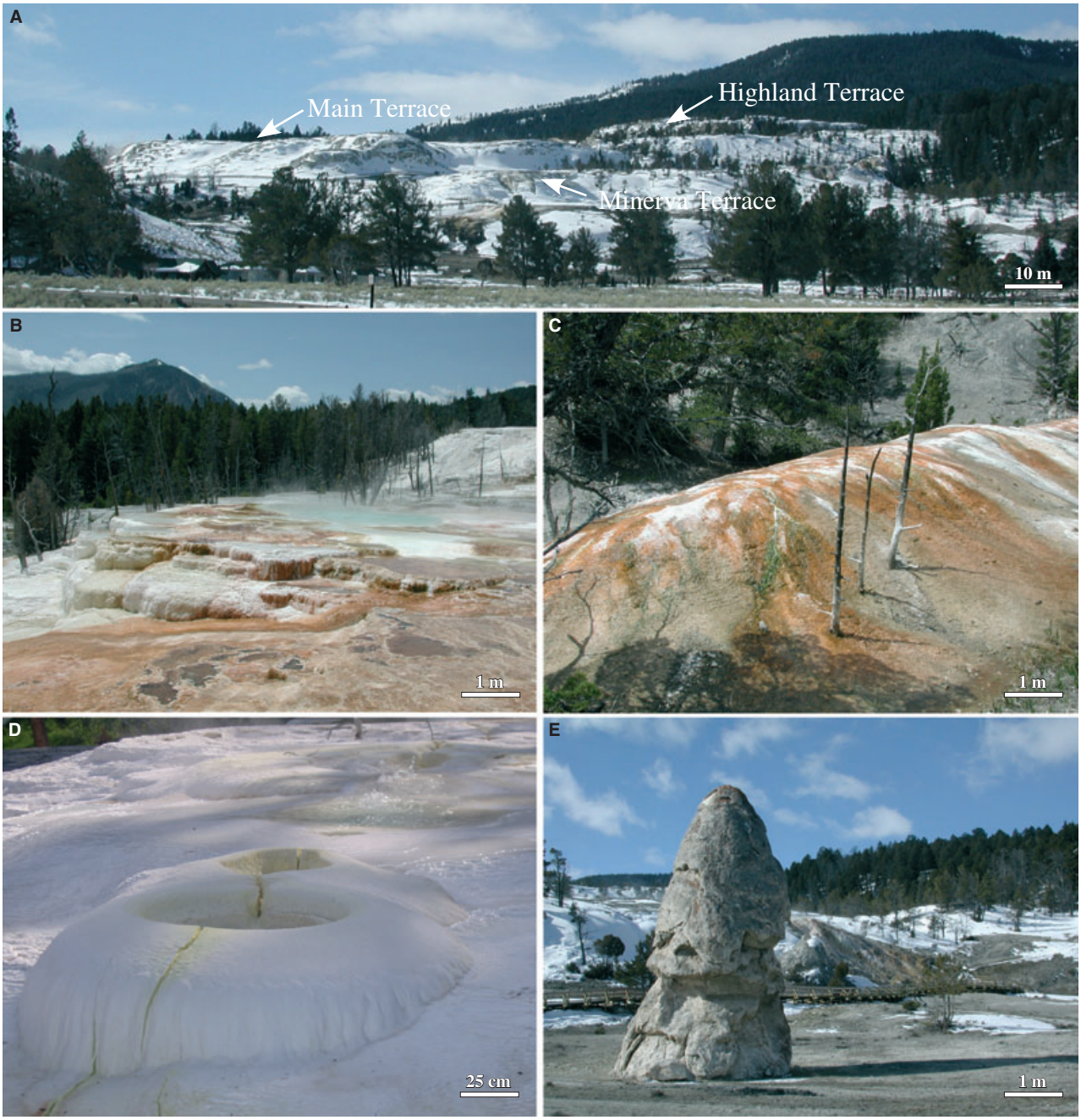


**Fig. 6.** Travertine geomorphology at Mammoth Hot Springs. (A) Westward view from the National Park Service Albright Visitors Center at MHS of the Minerva, Main and Highland Terrace complexes in January, 2008. (B) Westward view of travertine terracettes at Spring AT-3 (Fig. 7B) in July 2004. (C) Fissure-ridge travertine deposits on the eastern margin of Angel Terrace in July 2004. (D) A series of domed travertine deposits at Narrow Gauge (Chan & Goldenfeld, 2007) in January 2002, which are forming along a fracture containing yellow sulphur-rich travertine deposits. (E) The Liberty Cap travertine dome in January 2002.

step-shaped microterracettes form on the outer surface of terracette, dome and fissure-ridge deposits. In addition, the Mammoth–Gardiner corridor also contains a nearly continuous depositional time-series of modern-to-ancient hot-spring travertine accumulation that exhibits all three of the terracette, fissure ridge and dome geomorphologies. This accumulation includes a 73 m thick sequence of Recent and Holocene travertine deposits at MHS (Chafetz & Guidry, 2003; Fig. 5B) and Pleistocene travertine deposits in Gardiner, Montana (Sorey, 1991; Sturchio *et al.*, 1994).

Each position along the MHS outflow drainage system is composed of as many as four primary

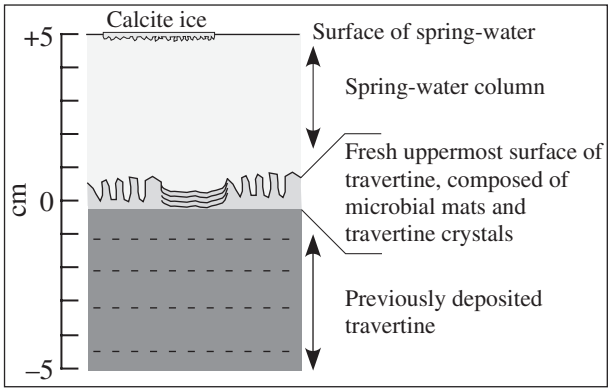


**Fig. 7.** Schematic cross-section of the travertine–microbe–water environments comprising the floor of hot-spring drainage systems at Mammoth Hot Springs.

components, which include (Fig. 7): (i) the overlying flowing spring-water; (ii) thin sheets of $CaCO_3$ crystals (calcite ice and calcified bubbles) that precipitate on spring-water surface tension in regions of slow flow rates; (iii) the fresh, actively precipitating, uppermost travertine surface that is interwoven with living microbial mats; and (iv) older underlying previously deposited travertine. In place (*in situ*) travertine crystallization experiments indicate that the average rate of $CaCO_3$ precipitation is lowest at the vent (0·2 mg $cm^{-3}$ $h^{-1}$) and highest in the immediately adjacent outflow regions of the drainage system (1·0 mg $cm^{-3}$ $h^{-1}$). As a result of these extremely high precipitation rates, the uppermost 0·5 cm thick surface of travertine substrate (Fig. 7) accumulates in as little as 15 to 75 days. This time scale is significantly shorter than the several months to years over which vents and outflow paths generally remain stationary (hot-spring outflow cycles are described in a later section). Therefore, if the hot spring has been consistently active and flowing for several weeks prior to sampling, then the uppermost layer of crystalline travertine can be assumed to have precipitated directly from the spring-water currently flowing over that specific sample site.

## MODERN MAMMOTH HOT SPRINGS TRAVERTINE–WATER–MICROBE SYSTEM

The intent of the present work at MHS has been to identify, understand and predict the interplay of physical, chemical and biological phenomena (Fig. 1) that control the formation of hot-spring travertine. To achieve this goal, the crystalline composition and geomorphology of the MHS travertine deposits were first described as a function of surface topography and downstream position within the drainage system. The geochemistry of the travertine and the overlying spring-water from which it precipitated was then superimposed on the travertine deposits. Finally, microbial community analyses were embedded strategically within the hot-spring geological and geochemical system. This process established the contextual framework for MHS summarized in Table 1, in which the geological and biological factors that influence modern travertine deposition at MHS were identified and tracked into the ancient travertine deposits at MHS and Gardiner.

The study of a natural system like MHS is confronted by the coupled challenges posed by scale and complexity (Anderson, 1972; Goldenfeld & Kadanoff, 1999; Schmidt & Lipson, 2009). To address and incorporate these factors, the primary physical, chemical and biological components of MHS were placed in a 'Powers of Ten' framework (Fig. 8; Morrison *et al.*, 1994; Dodick & Orion, 2006; Jones *et al.*, 2009). This type of evaluation illustrates that the MHS geobiological system spans a dynamic spatial range from $10^{-9}$ to $10^{5}$ m (Fig. 8). Furthermore, it shows that analyses at the scale of 1 mm to 1 cm are required to link macroscale fieldwork with microscale laboratory analyses (Fig. 8). This Powers of Ten framework guided experimental design, analytical measurement, modelling and eventual interpretation and synthesis of the multiple factors that control hot-spring travertine deposition.

Concentrated research on carbonate hot springs around the world has documented that multiple abiotic and biotic processes simultaneously engage in a constant, interactive balancing act to influence the crystalline fabric and geochemical composition of travertine precipitation (i.e. Friedman, 1970; Usdowski *et al.*, 1979; Amundson & Kelly, 1987; Chafetz *et al.*, 1991; Dreybrodt *et al.*, 1992; Fouke *et al.*, 2000; Pentecost, 2005). Specifically, the primary controls are a complex interplay of parameters that include: (i) spring-water chemistry (for example, pH, $HCO_3$, $pCO_2$, elemental abundance and resultant saturation state); (ii) physical processes (for example, temperature change, degassing, boiling, steaming, evaporation and dilution); (iii) hydrology (for example, flow rates, flux and surface area); and (iv) biotic activities (for example, microbial photosynthesis, respiration and biochemical effects; see literature summaries in Pentecost, 1995, 2005; Ford & Pedley, 1996; Fouke *et al.*, 2000). These physical, chemical and biological components,

 

**Table 1.** Summary of the travertine, spring-water and microbial community composition of each of the five MHS travertine depositional facies.

| System component | Vent facies | Apron and channel facies | Pond facies | Proximal-slope facies | Distal-slope facies |
|---|---|---|---|---|---|
| Travertine | Bowl-shaped depression surrounding the vent floored by well-indurated travertine mounds composed of botryoidal clusters of aragonite needles (≤80 μm) | Gently sloped fan-shaped channel floored with well-indurated streamer fabric pavements composed of botryoidal clusters of aragonite needles (≤20 μm) | Large semi-circular terracette ponds with a scalloped face formed by dendritic shrubs composed of aragonite needles (≤20 μm) | Small semicircular terracette to microterracette ponds with a scalloped face composed of aragonite needles (≤20 μm) forming dendritic shrubs | Small microterracette ponds with thick, rounded, lips and scalloped faces composed of blocky calcite (≤30 μm) forming dendritic shrubs and spherules |
| Spring-water | 73–66°C<br>6.0–6.7 pH<br>≤0.5 m water depth<br>Turbulent flow | 70–60°C<br>6.4–7.2 pH<br>≤3 cm water depth<br>Turbulent sheet flow | 62–39°C<br>6.7–8.0 pH<br>≤1 m water depth<br>Turbulent to laminar flow and roll waves | 63–35°C<br>6.9–8.0 pH<br>≤3 cm water depth<br>Turbulent flow and roll waves | 44–28°C<br>7.3–8.1 pH<br>≤3 cm water depth<br>Turbulent to laminar flow and roll waves |
| Microbial communities | Translucent to light beige to yellow mats with irregular bumpy surfaces, low diversity assemblage dominanted by *Sulfurihydrogenibium yellowstonensis* | Translucent to light beige microbial filaments and mats, low diversity assemblage dominanted by *Sulfurihydrogenibium yellowstonensis* | Variety of white, orange, brown and green microbial mats, high diversity assemblage of autotrophs and heterotrophs | Variety of white, orange, brown and green microbial mats, high diversity assemblage of autotrophs and heterotrophs | Variety of orange, brown and green microbial mats, high diversity assemblage of autotrophs and heterotrophs |

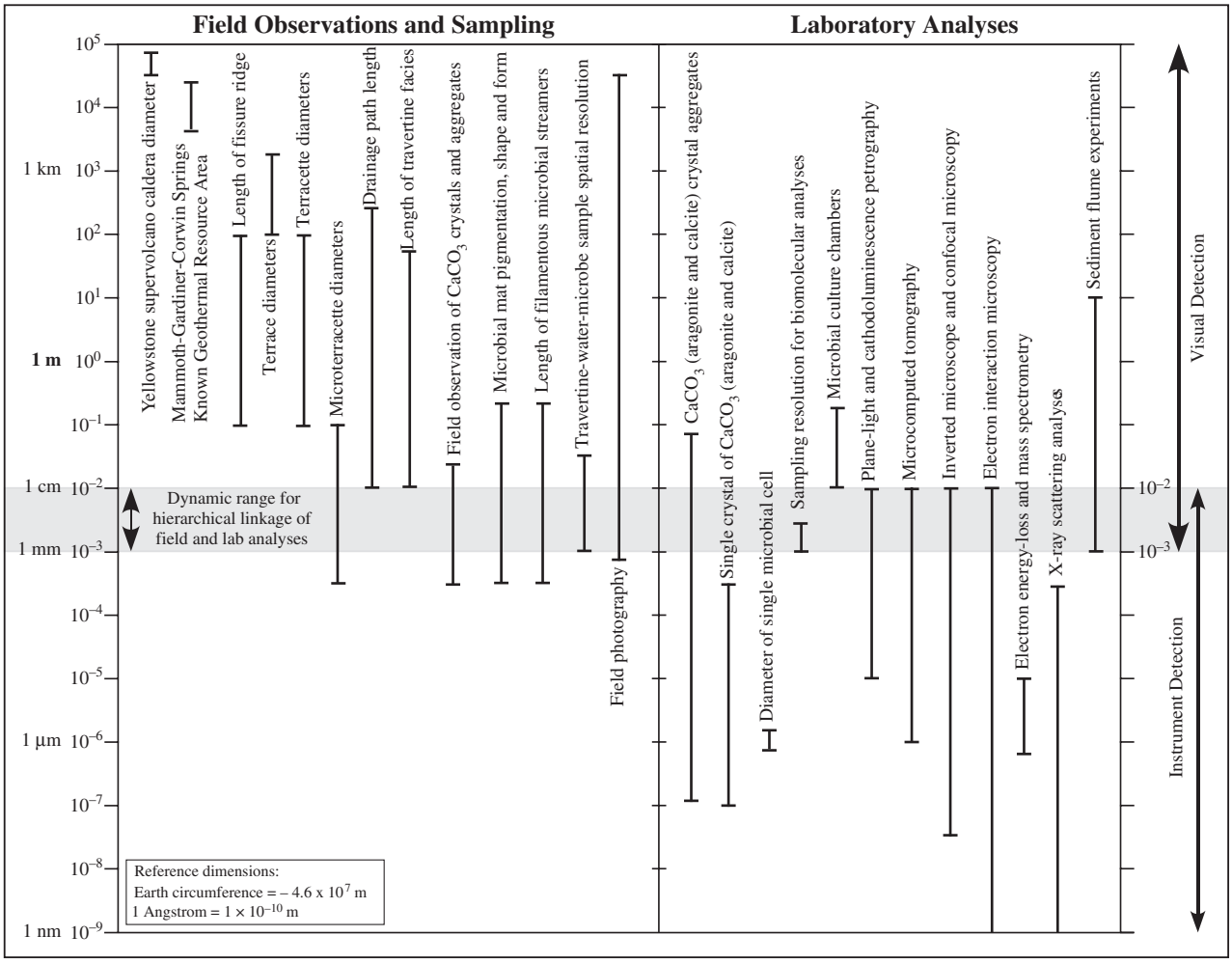


**Fig. 8.** The Powers of Ten hierarchical spatial structure of Mammoth Hot Springs.

which are different at each position along the primary flow path, act in concert to form a succession of different types of travertine along the hot-spring drainage system.

## Travertine depositional facies

The MHS drainage systems are floored by a downstream sequence of morphologically distinct travertine depositional facies (Fouke *et al.*, 2000, 2001; Fig. 9; Table 1). Each facies is a distinct type of sedimentary rock unit composed of a suite of specific characteristics (i.e. grain-size, shape, fabric, mineralogy and geomorphology) that reflect the combined physical, chemical and biological processes that were active in the environment of deposition (Gressly, 1838; Wilson, 1975; Walker & James, 1992; Cross & Homewood, 1997; Flügel, 2004). Mammoth Hot Springs travertine is unique from other limestone in that its formation is due almost exclusively to the *in situ* precipitation of $CaCO_3$ crystals directly from the flowing spring-water column, rather than from the transport and deposition of sedimentary particles (Fouke *et al.*, 2000; Kandianis *et al.*, 2008). Furthermore, the MHS travertine facies model has global application, having been observed consistently in other modern and ancient hot-spring systems around the world (Fouke *et al.*, 2000, 2001; Veysey *et al.*, 2008).

A downstream succession of vent, apron and channel, pond, proximal-slope and distal-slope facies occurs at MHS (Fouke *et al.*, 2000; Fig. 9; Table 1). The upstream and downstream boundary of each of these five travertine facies is determined by systematic changes in $CaCO_3$ crystal mineralogy, shape, size and geomorphology. Travertine fabrics previously described at MHS (Farmer & Des Marais, 1994a,b; Pentecost, 1995; Farmer, 2000) are included in the facies

 


B

| Facies | Vent | Apron and Channel | Pond | Proximal Slope | Distal Slope |
|---|---|---|---|---|---|
| T $^{o}$C | 73 – 66 | 70 – 60 | 62 – 39 | 65 – 35 | 44 – 28 |
| pH | 6·0 – 6·7 | 6·4 – 7·2 | 6·7 – 8·0 | 6·9 – 8·0 | 7·3 – 8·1 |
| Minerals | Aragonite | Aragonite | Aragonite and calcite | Aragonite and calcite | Calcite |

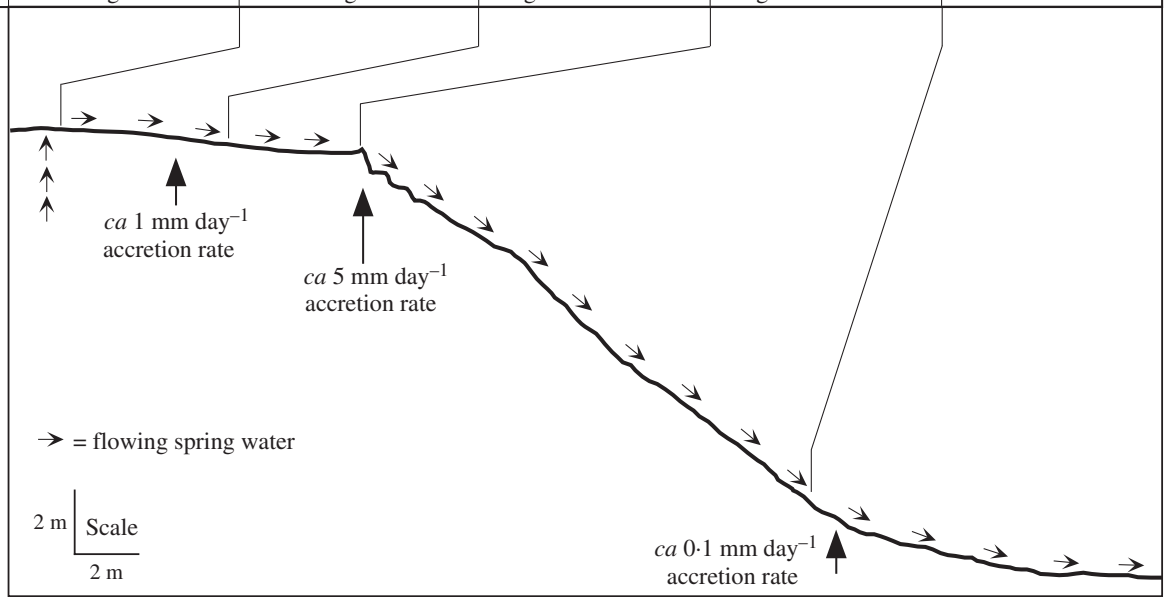


**Fig. 9.** Travertine depositional facies at Mammoth Hot Springs. (A) Field photograph of Angel Terrace Spring AT-1 (location shown in Fig. 5A). (B) Schematic cross-section of the travertine depositional facies (modified from Fouke *et al.*, 2003).

model (Fouke *et al.*, 2000). The composition and relative downstream sequence of the travertine facies is re-established as the hot springs shift their position as a result of changes in the flux of spring-water exiting the vent, as well as the closing of existing vents and the opening of new vents (Fouke *et al.*, 2000, 2001). The crystalline structure, chemistry and stratigraphy of the modern travertine facies therefore create a baseline with which to make accurate comparisons between modern springs, reconstruct ancient hot springs from fossil travertine deposits and identify diagenetic alterations (Fouke *et al.*, 2000; Chafetz & Guidry, 2003).

The vent facies is a shallow bowl-shaped depression (≤5 m in diameter) surrounding the vent orifice (≤3 cm in diameter) that is encrusted by hemispherical mounds of densely crystalline travertine (Fig. 10). These travertine mounds average 10 to 30 cm in diameter and periodically build to the water–air interface (Fig. 10). In thin-section, the vent facies travertine is composed of radiating bundles of long and relatively broad (≤80 μm × 5 μm) aragonite needles that nucleate from dark irregular micron-scale microcrystalline cores that are replaced microbial filaments (Fig. 11A).

The vent facies grades downstream into the apron and channel facies, which is floored by sinuous deposits of travertine called 'streamers' (Farmer, 2000) that reach tens of centimetres in length (Fig. 12A and B). Each streamer filament is composed of aragonite needle botryoids that are significantly smaller (≤20 μm × 0·5 μm) and less

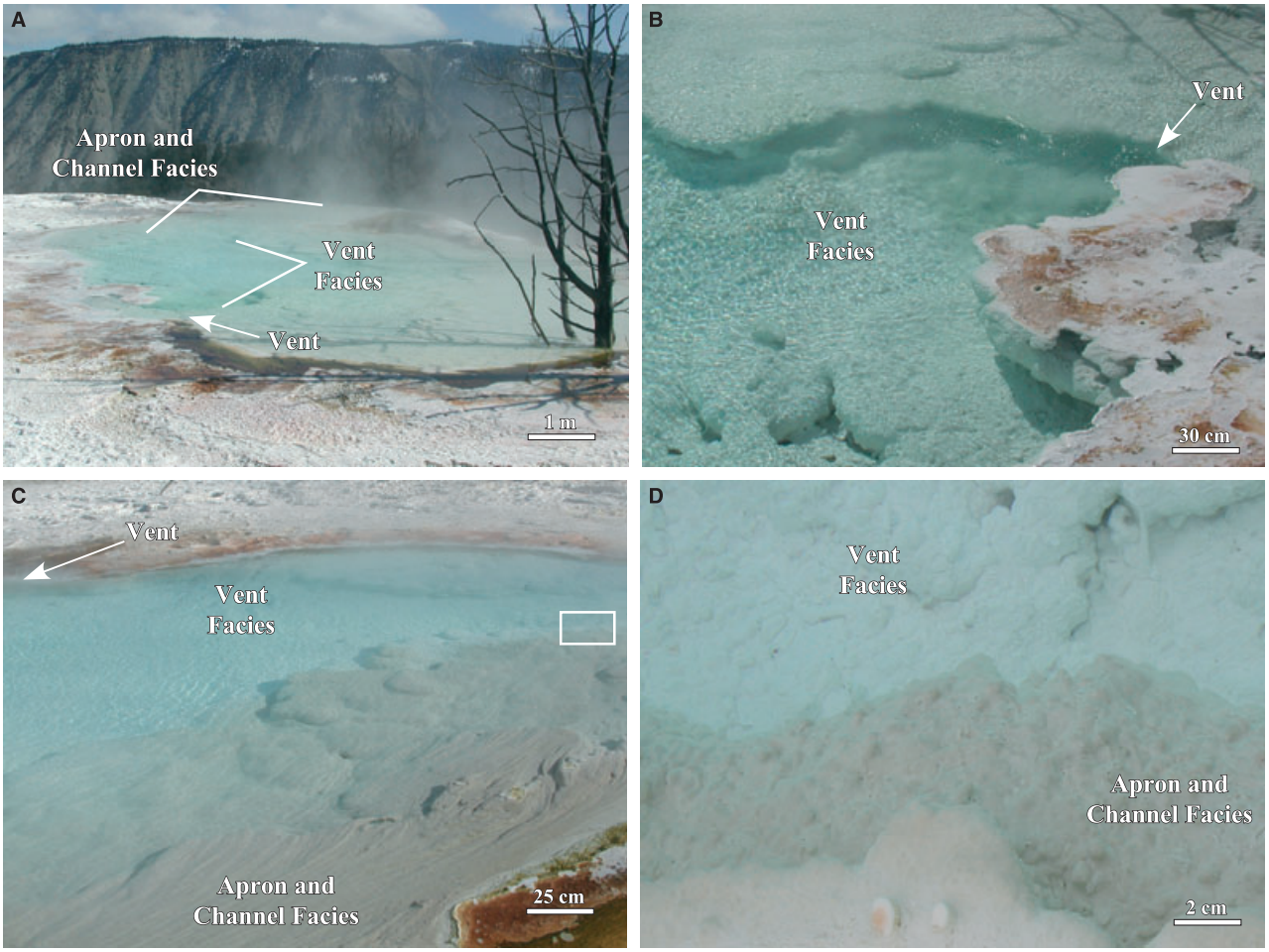


**Fig. 10.** Field photographs of the MHS travertine vent facies. (A) Overview of the vent facies and apron and channel facies at Spring AT-1 in July 2003. (B) Hot-spring water emerges from the vent at 73°C to form a turquoise pool floored with mounded white travertine deposits. (C) Gradational contact of the mounded white travertine of the vent facies with the characteristic beige sinuous streamer travertine of the apron and channel facies. (D) The irregular bumpy surface of the mounded travertine deposits in the transitional region from the vent to the apron and channel facies [enlargement of the area shown in panel (C)].

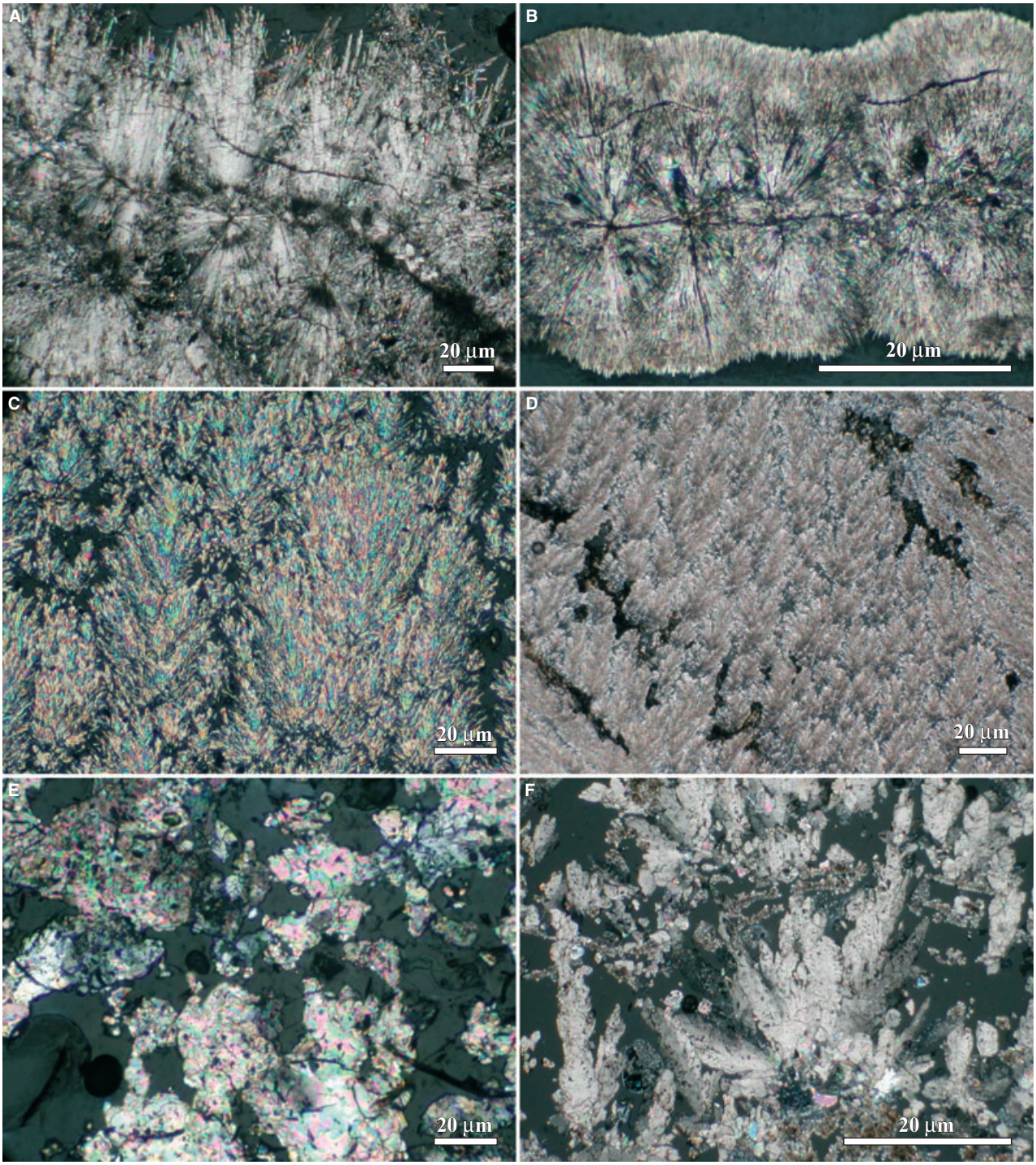


**Fig. 11.** Polarized-light photomicrographs of the characteristic crystal growth structure of Mammoth Hot Springs travertine. (A) Vent facies travertine composed of radiating bundles of long and broad aragonite needles (up to 80 μm × 5 μm). (B) Apron and channel facies travertine composed of radiating bundles of aragonite needles (up to 20 μm × 0·5 μm) that are shorter and thinner than those that precipitate in the vent facies. (C) Pond facies travertine composed of shrub-like clusters of fine aragonite needles (up to 10 μm × 0·25 μm). (D) Proximal-slope facies travertine composed of shrub-like clusters of fine aragonite needles (up to 10 μm × 0·25 μm) that are linear or concave-upward. (E) Distal-slope facies travertine composed of irregular blocky calcite (up to 20 μm × 20 μm). (F) Feather calcite crystals (up to 60 μm × 5 μm) that are common in the distal-slope facies and sometimes form on the floor of microterracettes in the proximal-slope facies.

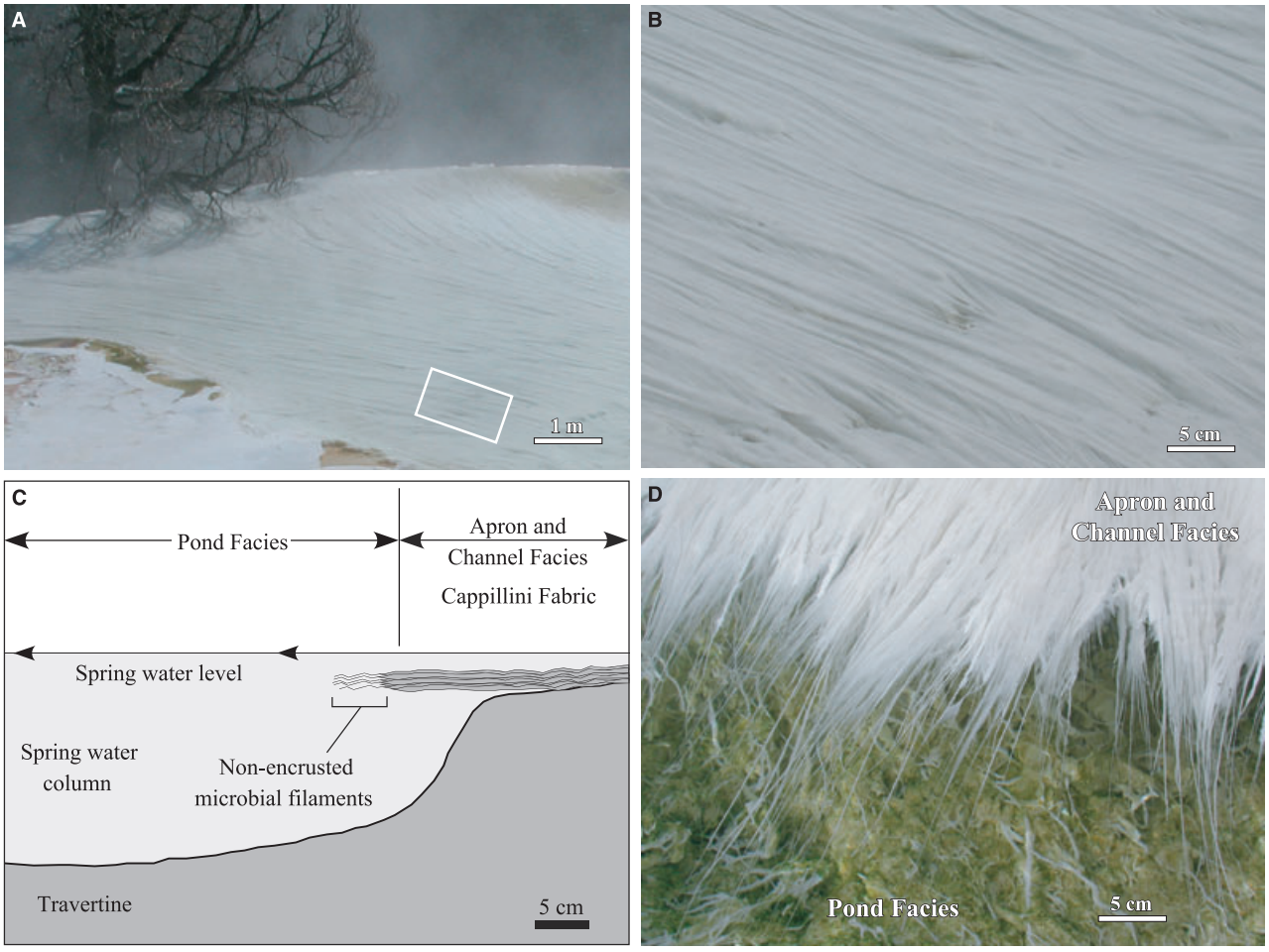


**Fig. 12.** Field photographs of the Mammoth Hot Springs travertine apron and channel facies at Angel Terrace Spring AT-1 in January 2004. (A) Overview of the apron and channel facies. (B) The characteristic sinuous streamer fabric of the apron and channel facies [enlargement of the area shown in panel (A)]. (C) Schematic cross-section of the abrupt transition from the apron and channel facies to the pond facies, with filamentous microbial mats that grow near the water surface and extend into the deeper water of the pond. During periods of increased spring-water outflow from the vent, the apron and channel facies travertine progrades into the pond at and near the water surface, forming a ledge that will eventually completely cover the pre-existing terracette if hot-spring water flow remains high. (D) Photograph of the transition from non-encrusted to travertine encrusted microbial filaments.

densely packed than the vent facies aragonite (Fig. 11A and B). The streamer filaments form as a result of the encrustation of filamentous thermophilic bacteria by radial bundles of aragonite needles (Fig. 11C and D). The encrusted microbial filaments become micritized as they decay, creating a solid microcrystalline core within each streamer filament. The transition from the apron and channel facies to the pond facies is a sharp contact located at the downstream position where the spring-water velocity slows dramatically as it enters the pond facies terracette pool (Fig. 12C and D). Streamer travertine deposits near the surface of the water extend laterally out into the downstream pond (Fig. 12C and D). If spring-water flux from the vent increases, a travertine streamer pavement will eventually entirely cover the immediately adjacent downstream pond facies terracette pool (Fig. 12C and D; hot-spring flow cycles described in later sections).

The pond facies is composed of metre-scale terracettes, which are tall (0·5 to 1·5 m high) hemispherical travertine ponds with buttresses that create a dam (or lip) that contains and slows the flowing spring water (Figs 9A, 13A and 13C). Each pond facies terracette forms on the flat-lying top margin of pre-existing terraces (Fig. 6B), unlike the smaller microterracettes of the proximal-slope facies that precipitate on the steeply inclined terrace foreslopes (Fig. 13C; described below). The pond facies exhibits a wide range in spring-water temperature and pH conditions and

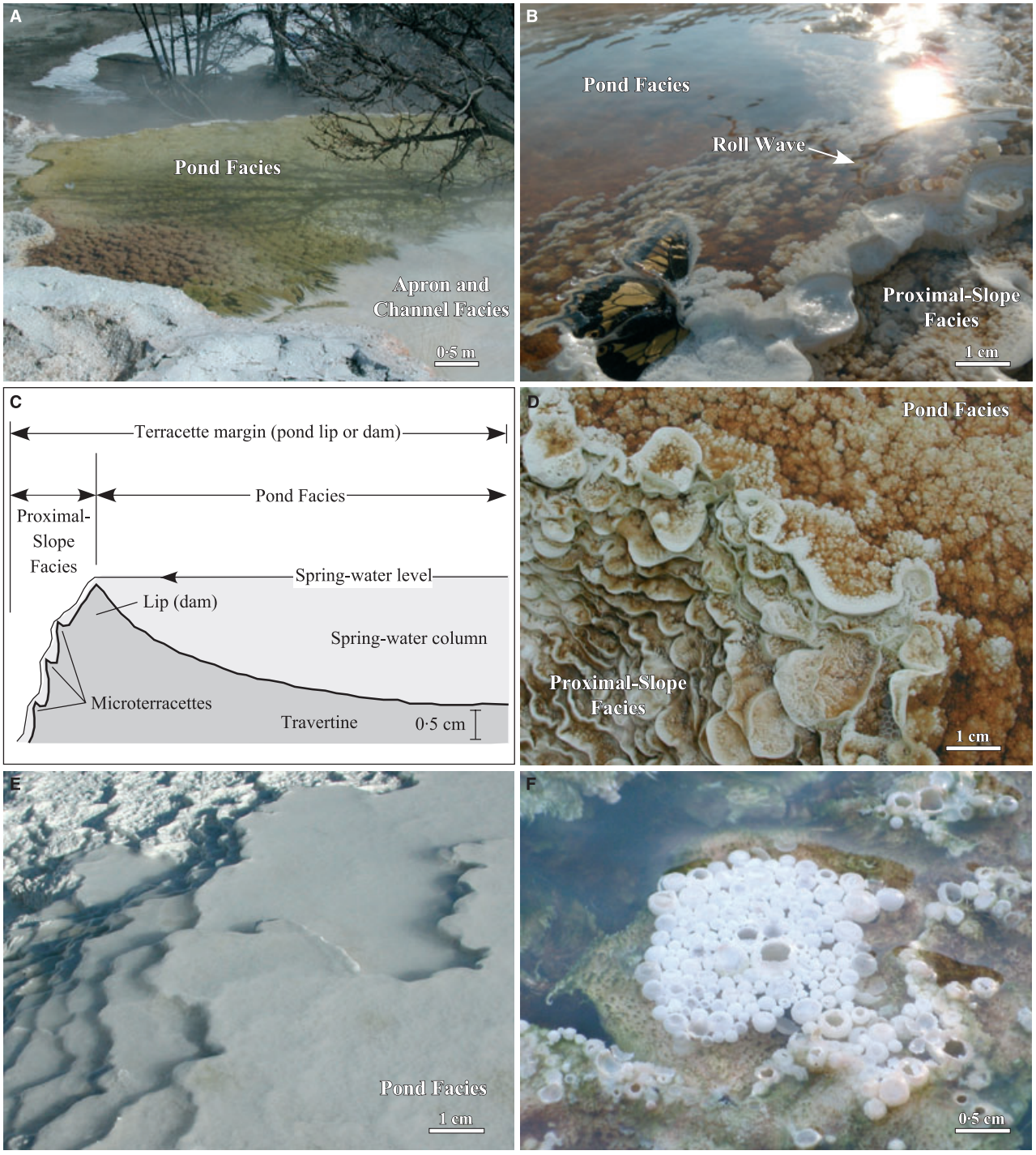


**Fig. 13.** Field photographs of the Mammoth Hot Springs travertine pond facies. (A) Overview of the abrupt downstream transition from the apron and channel facies to the pond facies at Spring AT-1 in January 2003. (B) Lip of the pond facies travertine dam at the margin of a terracette, showing formation of a roll wave, encrustation of a monarch butterfly and the abrupt transition to scalloped microterracettes of the proximal-slope facies (in July 2008). (C) Schematic cross-section of the pond facies lip. (D) Field photograph of the pond facies lip in July 2008. (E) Calcite ice rafts forming on the surface of microterracette ponds. (F) Travertine-encrusted water bubbles at the margin of a pond.

can be divided into: (i) high-temperature (≥58°C) ponds that contain rounded, shrub-like, clusters of aragonite up to 20 cm in diameter (Fig. 11A, C and D; Bargar, 1978; Pentecost, 1990) composed of small (20 μm × 0·5 μm) aragonite needles organized into small dendritic clusters (Fig. 11C); and

(ii) low-temperature (≤57°C) ponds that form ridged networks of microcrystalline aragonite 1 to 2 cm in height (Farmer, 2000). Thin carbonate 'ice-sheets' and calcified bubbles (Fig. 13E and F) composed of 50 to 100 μm diameter blocky to columnar calcite crystals and small (<10 μm) acicular aragonite (Fig. 14A to D) precipitate at the pond air–water interface (Allen & Day, 1935;

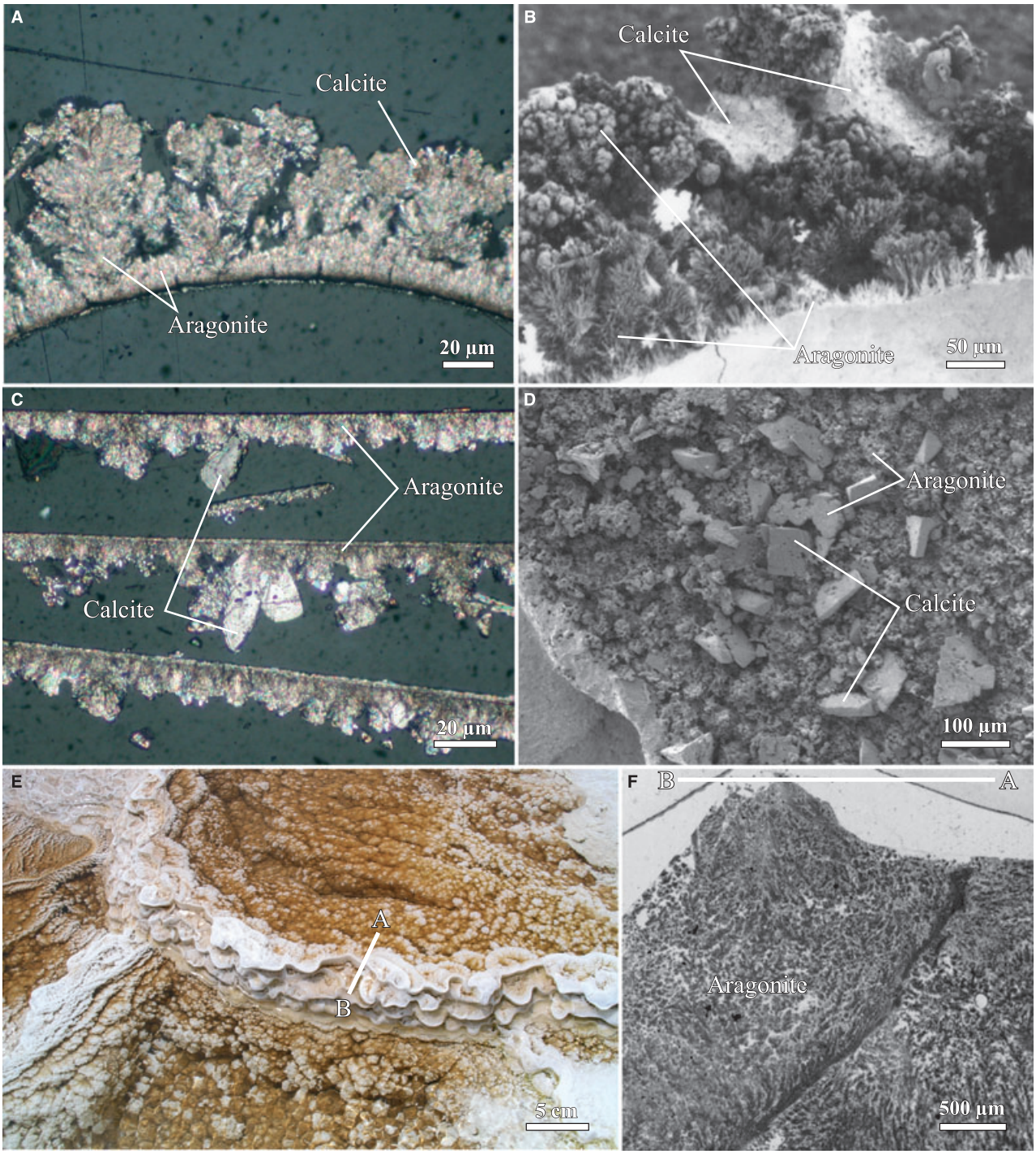


**Fig. 14.** Petrography of travertine comprising encrusted bubbles, calcite ice and microterracette pond lips. (A) and (B) Paired polarized-light photomicrograph and SEM image of aragonite and calcite crystals encrusting a hot-spring water bubble in pond facies travertine [the field photograph is shown in panel (F)]. (C) and (D) Paired polarized-light photomicrograph and SEM image of aragonite and calcite crystals comprising calcite ice sheets. (E) and (F) Field photograph and plane-light photomicrograph of the lip of a microterracette in the proximal-slope facies.

 

Bargar, 1978; Chafetz *et al.*, 1991; Fouke *et al.*, 2000). Thicker ice sheets form when pond flow decreases (Allen & Day, 1935; Bargar, 1978). In addition, aragonite needles form dumb-bell-shaped aragonite needle aggregates ('fuzzy dumb-bell' of Folk *et al.*, 1985; Buczynski & Chafetz, 1991; Chafetz & Buczynski, 1992; Folk, 1993, 1994). Fuzzy dumb-bells on the underside of calcite ice sheets are flattened on one side, reflecting their growth at the water–air interface (Fig. 14C and D).

The proximal-slope facies begins immediately downstream of the pond facies on the steepened foreslope of travertine terraces, creating cascading arrays of microterracettes that vary considerably in length (Fig. 15). Three categories of proximal-slope microterracettes have been observed. The first are *ca* 5 cm to 1·5 m diameter microterracettes that exhibit a well-defined pond and lip similar in shape and form to the larger pond facies terracettes (Fig. 15C and D). The second are mounded microterracettes on approximately the same 5 cm to 1·5 m diameter scale, but which do not have a well-established pond and form on lower angle slopes (Fig. 15F and E). The third category is composed of small 1 mm to 1 cm diameter fluted and scalloped microterracettes that grow on the front face of both pond facies terracettes (Fig. 13C and D) and proximal-slope facies microterracettes (Fig. 16D, E and F; Chafetz & Folk, 1984; Guo & Riding, 1992). All three classes of proximal-slope microterracettes are composed of similar aragonite needle clusters organized into shrub-like growth structures that grow in either linear or concave upward trajectories (Figs 11D, 14E and F).

A gradual transition takes place into the distal-slope facies as the mineralogy transitions from aragonite to calcite and the travertine forms broad low-relief microterracettes on very low-angle slopes (Fig. 16A and B). Each microterracette is connected laterally to others, which is distinct from the individually enclosed small scalloped microterracettes that occur in the proximal-slope facies (Fig. 15B and C). The floor of each microterracette pond in the distal-slope facies is filled with encrusted pine needles and 1 to 3 mm diameter calcite spherules (Fig. 16C and D). However, the low spring-water flow velocities present in the distal-slope facies require that a mechanism other than current driven spring-water motion is responsible for the spherule morphology. The distal-slope facies microterracette and spherule travertine is composed of two distinct types of calcite crystal growth. The first are 5 to 30 μm diameter blocky to prismatic calcite crystals (Fig. 11E) that are sometimes aggregated into branching irregular stalks. The second are dendritic calcite 'feather crystals' growing on the floor of microterracette ponds (Fig. 11F; Chafetz & Folk, 1984; Folk *et al.*, 1985; Guo & Riding, 1992).

## Spring-water flow dynamics

The hot springs at MHS exhibit significant spatial and temporal fluctuations in temperature and chemistry as a result of changing water depth, flux and extents of mixing along the course of their outflow drainage channels. This effect creates a succession of gradually varied (in the interior of each facies) to rapidly varied (at the downstream margin of each facies) open-channel flow conditions. Velocities range from less than 10 cm $s^{-1}$ in the pond facies to over 35 cm $s^{-1}$ in the proximal-slope facies (Fouke *et al.*, 2000; Veysey *et al.*, 2008). Associated variations in vent flux vary from 10 to 60 l $s^{-1}$ over time periods of a few weeks to months (Veysey *et al.*, 2008). A hydraulic jump occurs as the spring-water shallows from the vent facies to the apron and channel facies (Figs 9 and 10). Conversely, hydraulic drops occur at the apron and channel facies contact with the pond facies (Figs 9 and 12). Because of this hydraulic variability, it has been necessary to identify the primary flow path (Veysey *et al.*, 2008; Fig. 17) as a means to accurately sample, analyse and link travertine–water–microbe feedback interactions from upstream to downstream positions within the travertine facies model. Consistent utilization of the primary flow path has also provided the contextual framework for reconstruction of the spring-water pH, temperature and flux from ancient hot-spring travertine facies (Veysey *et al.*, 2008).

Because advection dominates these drainage systems, the primary flow path has been defined by spring-water flux, temperature and pH in the context of the travertine facies accumulation patterns (Veysey *et al.*, 2008). A single flow path (Fig. 17) can be defined in a Lagrangian frame of reference as the points traversed by a parcel of water as it migrates from the hot-spring vent facies to the distal-slope facies. Given a contiguous area covered by spring-water within a drainage system, the primary flow path is the set of points at a given distance from the vent that are traversed by the largest volume of water. The primary flow path can rarely be identified

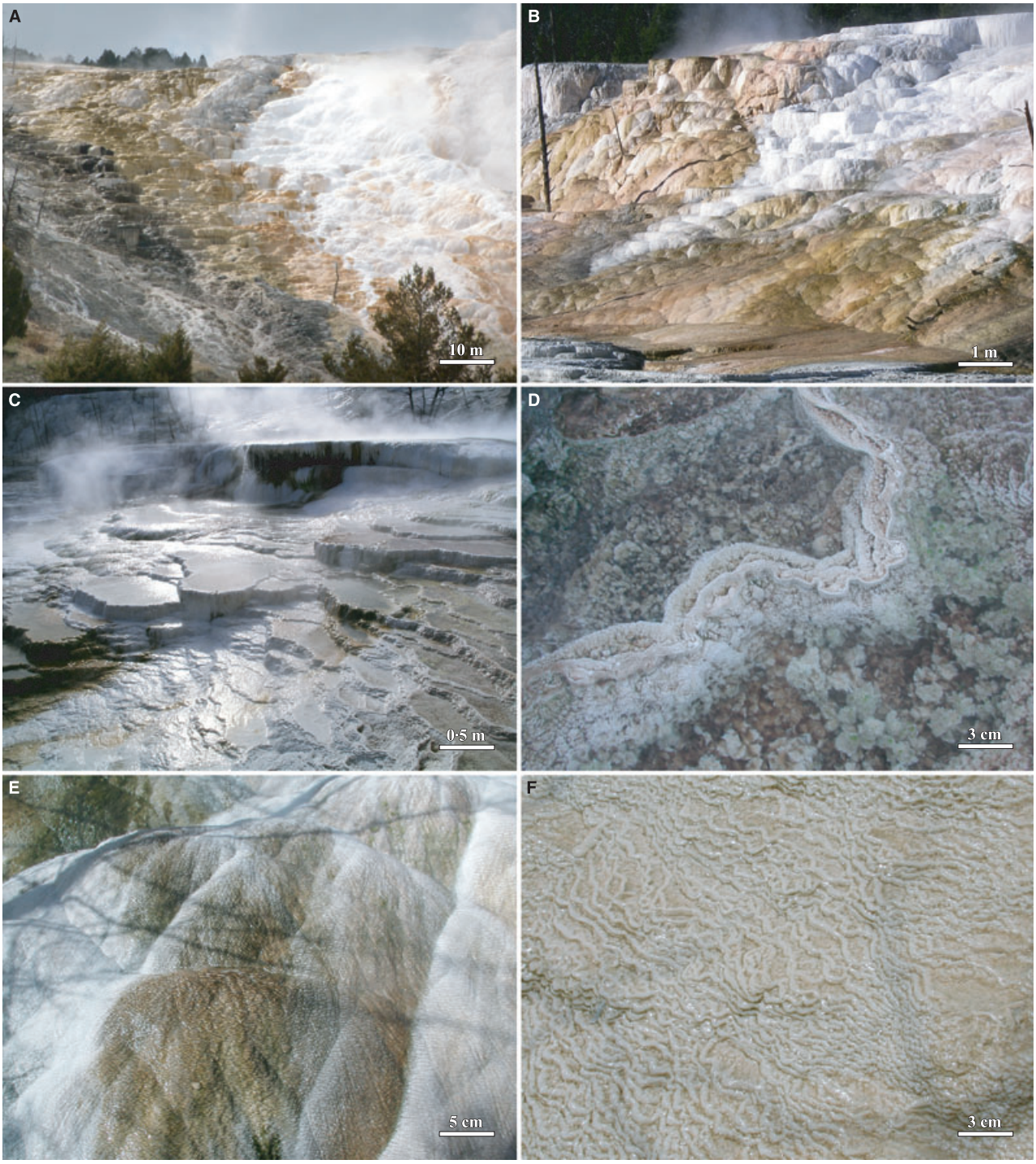


**Fig. 15.** Field photographs of the Mammoth Hot Springs travertine proximal-slope facies. (A) Overview of the 50 m high proximal-slope facies at Canary Springs in July 2009. (B) Overview of the 10 m high proximal-slope facies at Spring AT-2 in November 2008. (C) Microterracettes comprising the proximal-slope facies at Spring AT-3 in October 2005. (D) Enlargement of a microterracette pond lip at Spring AT-1 in November 2002. (E) Rounded microterracettes comprising the proximal-slope facies at Spring AT-1 in November 2002. (F) Microterracettes forming on the proximal-slope facies at Spring AT-3 in January 2007.

by visual inspection, particularly in the type of shallow turbulent flow present in the apron and channel, proximal-slope and distal-slope facies. Therefore, the primary flow path is best identified as the trajectory along which temperature decreases most slowly as a function of distance

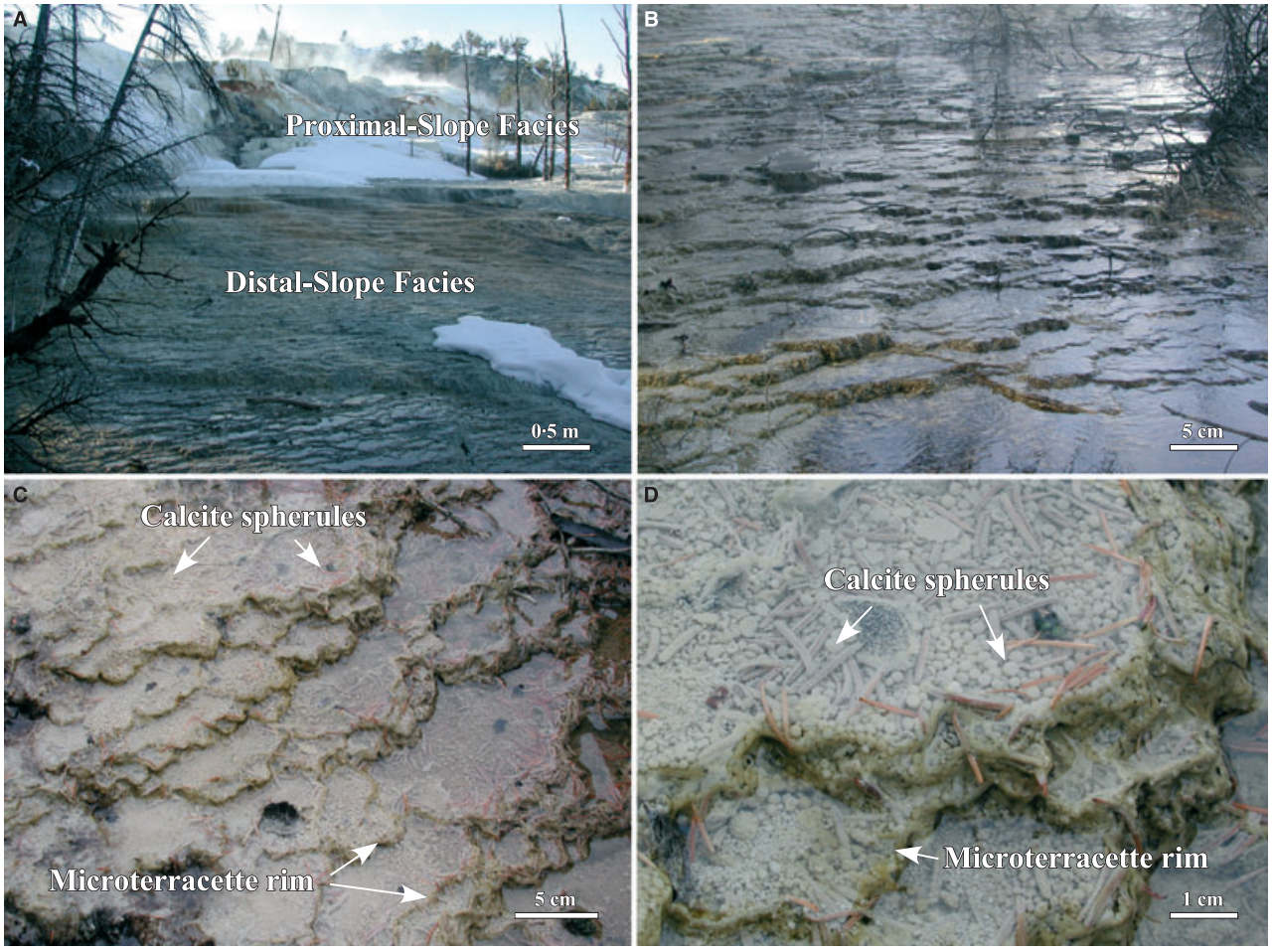


**Fig. 16.** Field photographs of the Mammoth Hot Springs travertine distal-slope facies. (A) Overview of the gradual transition and associated decrease in slope from the proximal-slope facies to the distal-slope facies at Spring AT-1 in January 2000. (B) Broad and shallow microterracettes that are characteristic of the distal-slope facies. (C) and (D) Each microterracette has a distinct margin and is floored with small calcite spherules, as well as decaying pink-tinted and travertine-encrusted pine needles.

and is the local minimization of $dT/dr$ (T = temperature, r = distance along the flow path (Veysey *et al.*, 2008). In a practical field-based sense, the primary flow path is determined from co-ordinated field measurements of temperature and pH at successively larger arcs of distance with movement away from the vent. When combined with qualitative observations within the facies model, this approach allows sampling strategies to be established that account for mixed flow paths, regardless of variations in water depth, velocity or changes in underlying topography (Fig. 17).

Large-amplitude interfacial waves (called 'roll waves') are a common hydraulic feature at MHS. These waves have a consistent shape and speed that is created by instabilities in the gravity-driven turbulent sheet flow of spring-water as it progresses down slope (Ponce & Maisner, 1993; Balmforth & Mandre, 2004; D'Alessio *et al.*, 2009). Although roll waves do not occur in the vent, apron and channel, pond and distal-slope facies, they are often observed rhythmically pulsing down the proximal-slope facies. Spring-water near the lip of pond terracettes and microterracettes forms millimetre-scale buildups as a result of surface tension (Fig. 13B). Once the surface tension is overwhelmed by the mass of the accumulating spring-water, it is released to spill over the pond lip where it generates regular and widely-spaced roll waves that propagate down the steeply inclined proximal slope. Qualitative field observations suggest that the frequency and distribution of the roll waves exhibit no spatial or temporal correlation with travertine microterracettes, thus implying they are not directly involved in their formation.

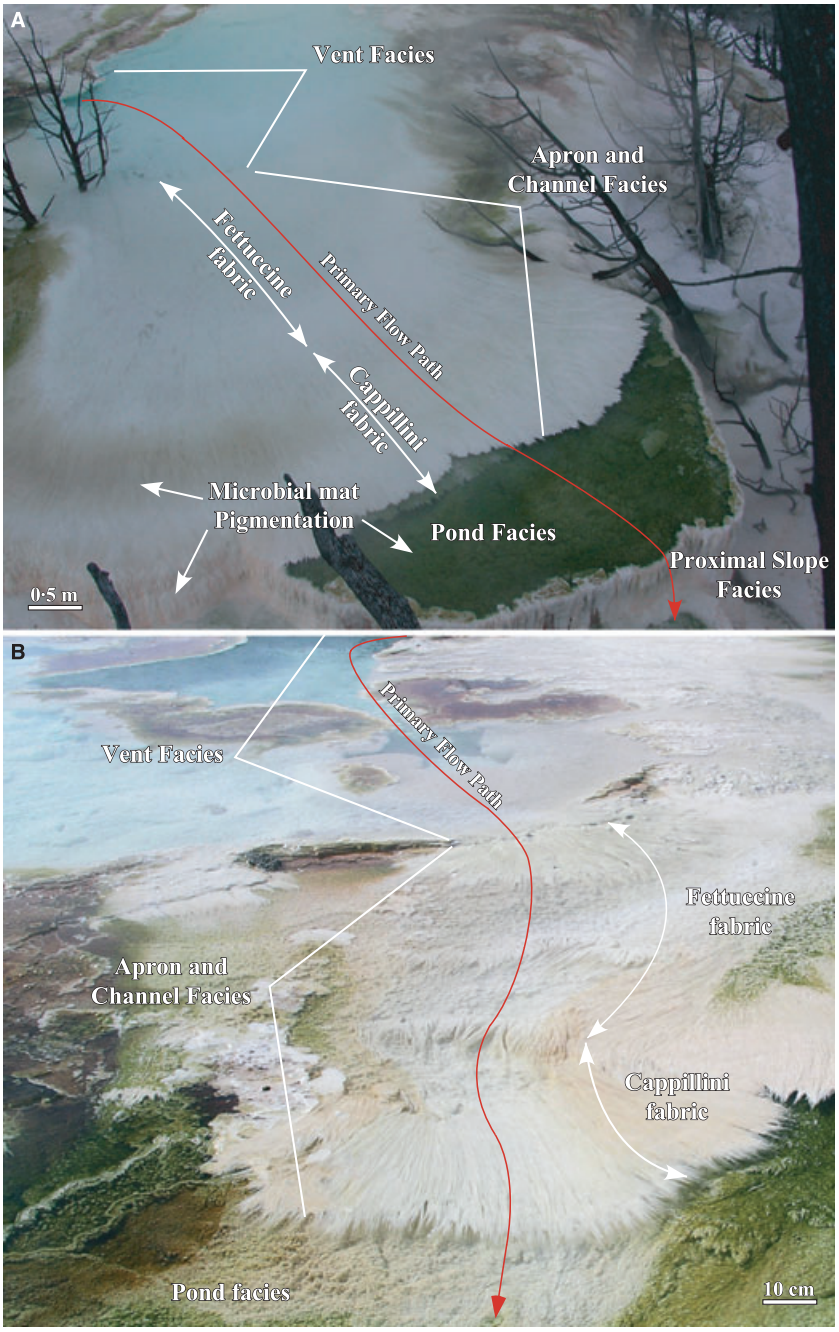


**Fig. 17.** Field photographs indicating the position of the primary flow path within the vent, apron and channel, pond and proximal-slope facies at Mammoth Hot Springs. (A) Spring AT-1 in November 2002. (B) Spring AT-3 in November 2005.

## Spring-water and travertine geochemistry

After the spring-water emerges from the ground in the vent facies and flows downstream to the distal-slope facies, the temperature has cooled to 25°C and the pH has increased two units, primarily as a result of the loss of dissolved carbon dioxide gas [$CO_2$ (g)]. These changes along the primary flow path serve to increase the capacity of the spring-water to precipitate $CaCO_3$ in accordance with the following chemical reaction:

$$Ca^{++}(aq) + 2HCO_3^-(aq) \rightarrow CaCO_3(s) + CO_2(g) + H_2O$$

The equilibrium saturation state with respect to aragonite ($\Omega_a$) of the emerging spring-water at the vent is 1·49 + 0·11, which is considered an overestimation because of strong kinetic effects that are observed throughout the system (Kandianis *et al.*, 2008). Therefore, $\Omega_a$ is effectively near, or just slightly above, a value of one and the vent spring-water is thus unlikely to be capable of

self-sealing the vent with travertine precipitation. It is not until after the spring-water leaves the vent, comes into contact with the atmosphere and rapidly degasses $CO_2$, that the remarkably high rates of $CaCO_3$ precipitation are attained (Fouke *et al.*, 2000; Kandianis *et al.*, 2008). As a result, the frequent closure and migration of vents at Mammoth is probably the result of gravity-driven compression and closure of subsurface vent conduits as the travertine settles under its own weight during rapid accumulation.

Mammoth Hot Springs spring-water temperature and pH indicate that the broadest variability occurs in the pond facies, whereas the narrowest range occurs in the vent and distal-slope facies (Fig. 18A). The vent is held fixed by the steady influx of homogeneous source water. Conversely, spring-water temperature and $CO_2$ fugacity in the distal-slope facies asymptotically approaches equilibrium with respect to both the atmosphere and travertine; this accounts for the overall lower rate of travertine precipitation measured downstream (Fouke *et al.*, 2000) and explains the decreased variation in pH (Fig. 18A). The temporal fluctuations in temperature exhibit the same trend (Fig. 18A) and are consistent with data from temperature loggers placed in the pond and proximal-slope facies (±9°C with differences in day-time and night-time air temperatures as large as 20°C, Veysey *et al.*, 2008). Facies-specific changes in downstream $\delta^{13}C$ and $\delta^{18}O$ values of both the spring-water and travertine have also been observed (Fig. 18C and D). With respect to the oxygen isotope values, equilibration between atmospheric $CO_2$, DIC and $H_2O$ is nearly instantaneous and thus no fractionation is expected during abiotic degassing (Truesdell & Hulston, 1980). However, the small positive shift in spring-water $\delta^{18}O$ values suggests that some downstream evaporation is occurring (Fig. 18C; Gonfiantini, 1986).

To evaluate the relative influence of $CO_2$ degassing (Friedman, 1970; Pentecost, 1995; Guo *et al.*, 1996) versus biological photosynthesis (Amundson & Kelly, 1987; Guo *et al.*, 1996; Pedley *et al.*, 2009), the measured travertine isotopic values have been compared with calculated isotopic values for travertine in thermodynamic equilibrium with the spring-water in each facies (Fig. 19A and B). The small fractionation of oxygen and carbon isotopes between aragonite and calcite does not change with temperature or precipitation rate and, thus, will not change across the mineralogical transition from the vent to the distal-slope facies. Downstream co-variations in travertine and spring-water aqueous geochemistry were used to identify specific sites along the primary flow path where biological activity may be most likely to influence travertine deposition (Fig. 20). For example, the entire MHS drainage system is influenced strongly by $CO_2$ degassing as indicated by Rayleigh-type fractionation calculations of spring-water $\delta^{13}C$ values versus dissolved inorganic carbon (DIC) concentrations (Fig. 18B; Fouke *et al.*, 2000). However, the relative ordering of spring-water $\delta^{13}C$ versus DIC co-variations (Fig. 18A) is not consistent with the actual downstream sequence of depositional facies. This observation suggests that biological processes that impact dissolved $CO_2$ concentrations may be influential in the apron and channel facies, as well as the pond facies (Fig. 18A). The pond facies (Fig. 20) is a site where spring-water flux is low enough and microbial biomass large enough that it might control spring-water chemistry and thus overprint the geochemical fractionation effects of $CO_2$ degassing recorded in the travertine (Figs 18B, 18C, 18D, 19A and 19B).

Another target for studying biological influence on travertine deposition is the steep redox gradient of the apron and channel facies, informally referred to as the MHS 'Perfect Geochemical Storm'. Biogeochemical cycling of sulphur at this position may strongly influence the environmental chemistry, microbial metabolic pathways and resulting travertine geochemistry (Inskeep *et al.*, 2005; Fig. 20C). The $\delta^{34}S$ compositions of dissolved sulphate in the spring-water and the sulphate in the travertine do not change significantly along the primary flow path (Fig. 19C). These data have identified an unexpected fractionation effect that may be biological in origin, where the travertine is consistently as much as 3‰ heavier than the dissolved sulphate in the spring-water (Fig. 19C).

## Microbial communities

Microbial mat morphology and pigmentation provide a valuable field-based indication of microbial diversity and distribution in hot-spring drainage systems throughout YNP (Brock, 1978; Hugenholtz *et al.*, 1998; Ward & Castenholz, 2000; Dyer, 2003; Sheehan *et al.*, 2005). An especially striking example of this is the correlation between microbial pigments and spring-water geochemistry in chemotrophic mat communities inhabiting siliceous acid–sulphate–chloride hot-spring drainage channels in the Norris Geyser Basin (Inskeep & McDermott, 2005). Analogous relationships occur

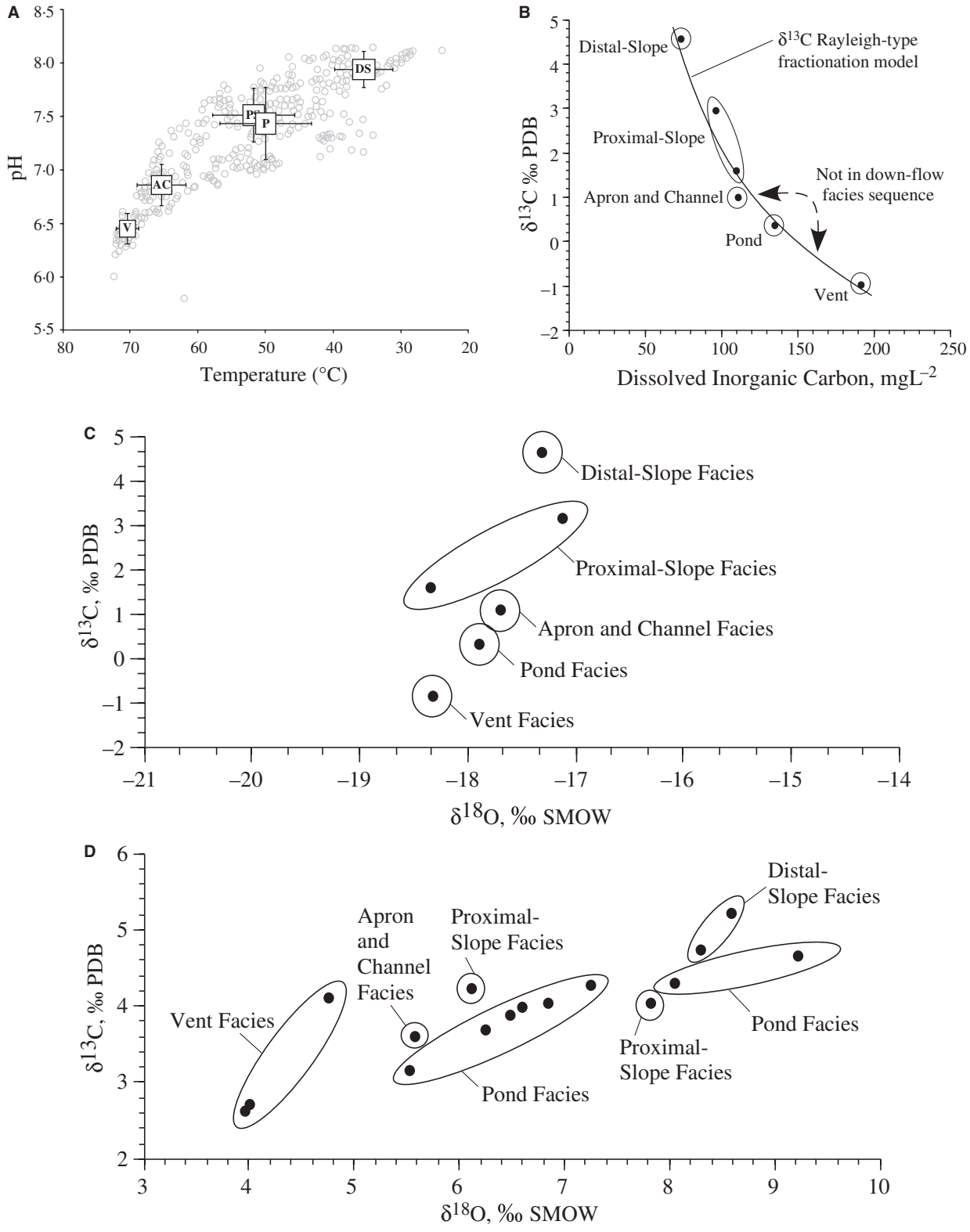


**Fig. 18.** Travertine and spring-water geochemistry at Mammoth Hot Springs Spring AT-1 and Spring AT-3. (A) The distribution of 343 triplicate paired measurements of spring-water temperature and pH. Error bars indicate one standard deviation (modified from Veysey *et al.*, 2008). (B) Co-variations in spring-water total dissolved inorganic carbon (DIC) versus its $\delta^{13}C$ value. (C) Co-variations in spring-water oxygen versus carbon-isotopic composition. (D) Co-variations in travertine oxygen versus carbon-isotopic composition [(B), (C) and (D) modified from Fouke *et al.*, 2000].

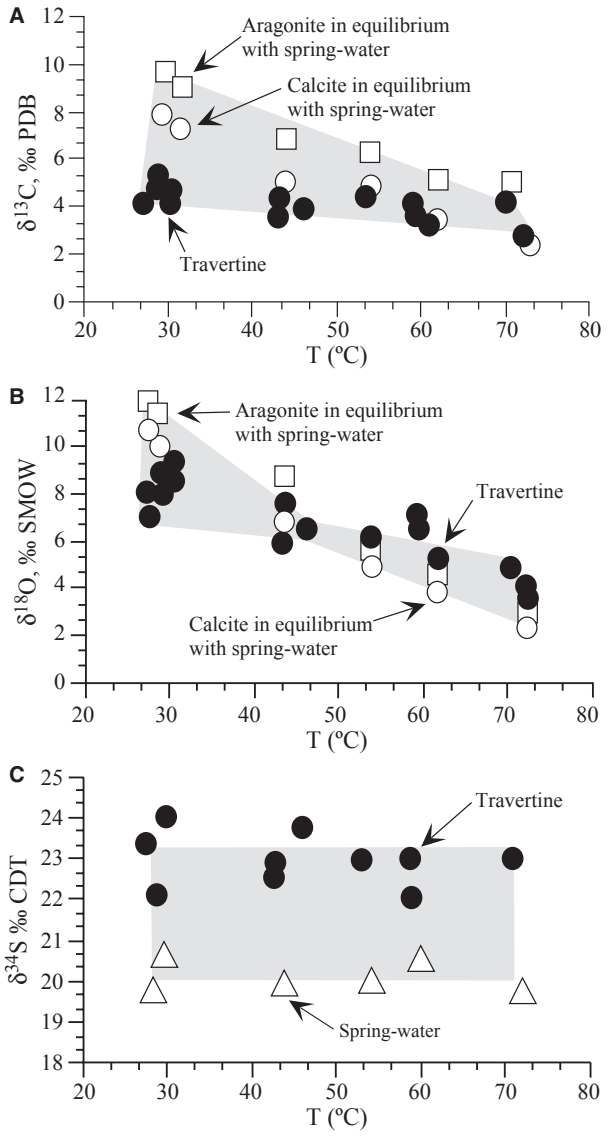


**Fig. 19.** Comparison of Mammoth Hot Springs spring-water and travertine oxygen isotope geochemistry and calculated equilibrium values for calcite and aragonite from Spring AT-1 (modified from Fouke *et al.*, 2000). Shaded regions denote non-equilibrium fractionation effects. (A) Temperature versus $\delta^{13}C$. (B) Temperature versus $\delta^{18}O$. (C) Temperature versus $\delta^{34}S$.

at MHS along transects from: (i) upstream to downstream along the primary flow path; (ii) shallow-to-deep water within vent pools; and (iii) laterally across spring-water drainage channels (Fig. 17). The microbial mats at Angel Terrace and Narrow Gauge (Fig. 21) range from less than 0·5 to 3 mm in thickness, with the thickest mats developed in the deep and slower moving water of the pond facies. The overall thin nature of the MHS mats relative to other sites in YNP (Stal, 2000; Inskeep & McDermott, 2005) presumably results from the extremely high rate of travertine precipitation (Kandianis *et al.*, 2008). This rapid mineralization serves to dilute the mats with crystal growth during rapid entombment of the growing mat surface.

Each of the travertine depositional facies is distinctly different in microbial mat morphology and pigmentation (Fig. 21). The vent facies contains thin (<1 mm) translucent to light beige microbial mats that form an irregular bumpy surface on the mounded substrate deposits of travertine (Fig. 10). High concentrations of sulphur crystals in the vent facies sometimes further tints the vent mats a dark greenish-yellow (Fig. 6D). Filamentous microbial clusters up to 5 cm in length and 1 mm in diameter sometimes grow in clusters at the shallow-water margins of the travertine bowl surrounding the vent. The apron and channel facies is floored by translucent to light beige Aquificales-dominated microbial filaments and mats (Fouke *et al.*, 2003) that form the sinuous travertine streamer fabric (Fig. 12). These mats abruptly end downstream where naked non-$CaCO_3$ encrusted microbial filaments, up to 10 cm in length extend near the water surface as a thin sinuous sheet into the deeper pooled water of the pond facies (Fig. 12C and D). Remarkably, the rate of travertine mineral precipitation is so high in the apron and channel facies (≤3 mm day$^{-1}$) that the filamentous mats are fully cemented to form a solid substrate just a few centimetres upstream from the non-encrusted filaments (Fig. 12). During dusk each day, these filamentous microbial mat communities exhibit a bright pink salmon-coloured pigment. At the time the field photograph in Figure 21A was taken at Narrow Gauge, spring-water flux from the vent had recently increased and the deep salmon coloured mats of the apron and channel facies streamers were prograding over the pond facies and had begun to encrust the proximal-slope facies. These pigments track high-temperature diurnal biogeochemical cycling and anoxygenic photosynthesis in the apron and channel facies (Madigan, 2005).

The pond and proximal-slope facies contain a wide variety of microbial mat morphologies and pigmentations. The most common of these microbial mats are briefly described here. The highest temperature (63 to 65°C) pond facies contain translucent mats that have a bleached appearance caused by the white colour of the travertine shrub deposits with which they grow (Fig. 21A). Conversely, microbial mats in the intermediate temperature (55 to 63°C) ponds exhibit bright orange and dark brown pigments that are mixed

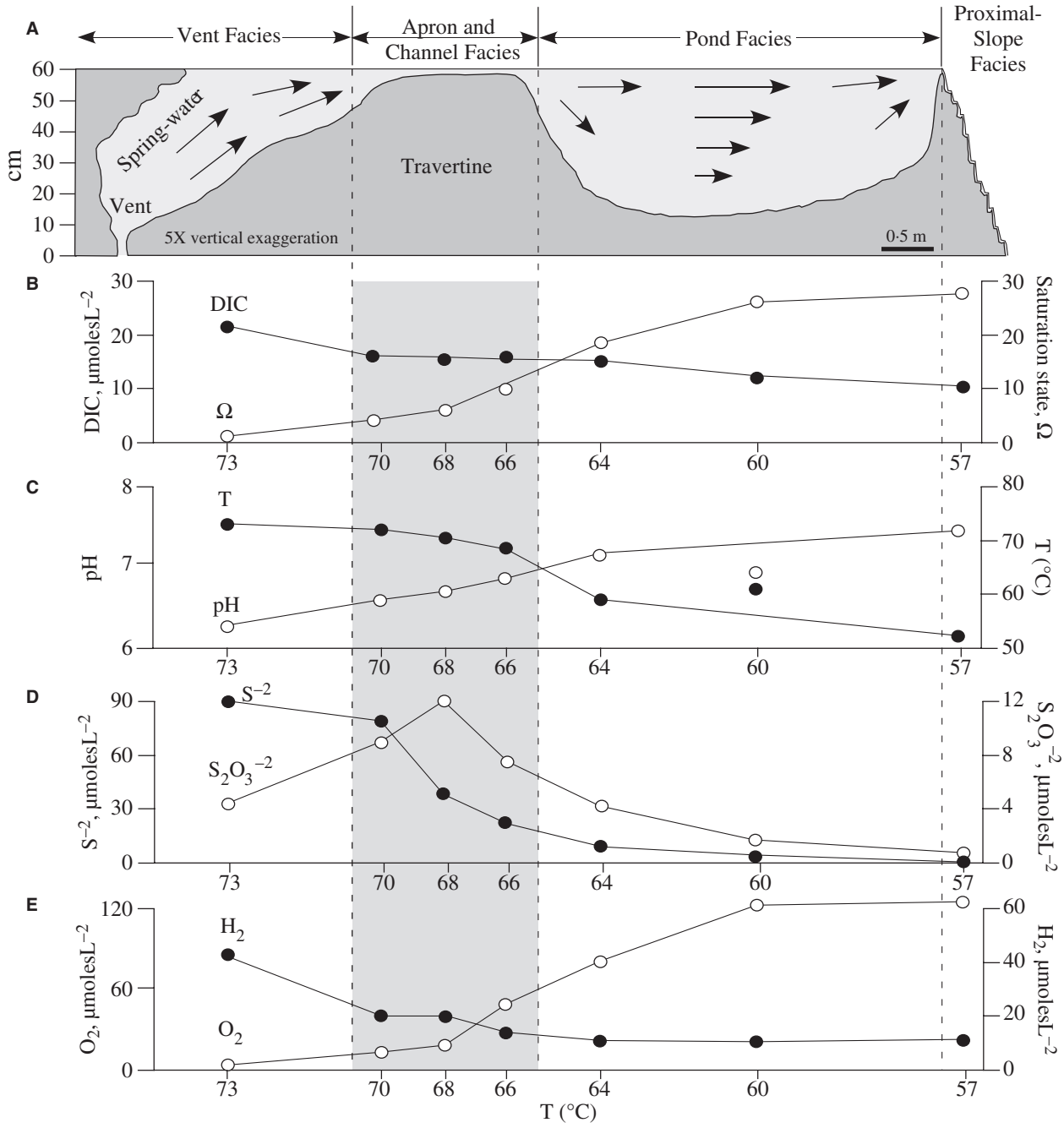


**Fig. 20.** Geomorphology and geochemistry of the vent, apron and channel, pond and proximal-slope facies at Mammoth Hot Springs. (A) Schematic cross-section (5× vertical exaggeration). Spring-water velocities at the surface of the pond are faster than those at the base. (B) to (E) Spring-water geochemistry from vent to proximal-slope facies along the drainage system.

in with areas of translucent mats. These mats assume the morphology of the pond facies travertine with which they are growing, and range from ridged-network (Fig. 21B) to shrub textures (Fig. 13B and D). The lowest temperature (35 to 55°C) ponds exhibit an extremely wide variety of dark green to brown and even black microbial mats (Fig. 21C to F). One of the most common varieties of microbial mats are thick, light to dark green in colour, and form fields of small vertical cylinders that eventually rise to the upper surface of the pond spring-water (Fig. 21C and D). Although not yet studied in detail, each mat cylinder (also called a 'gas lift-off structure') is

 

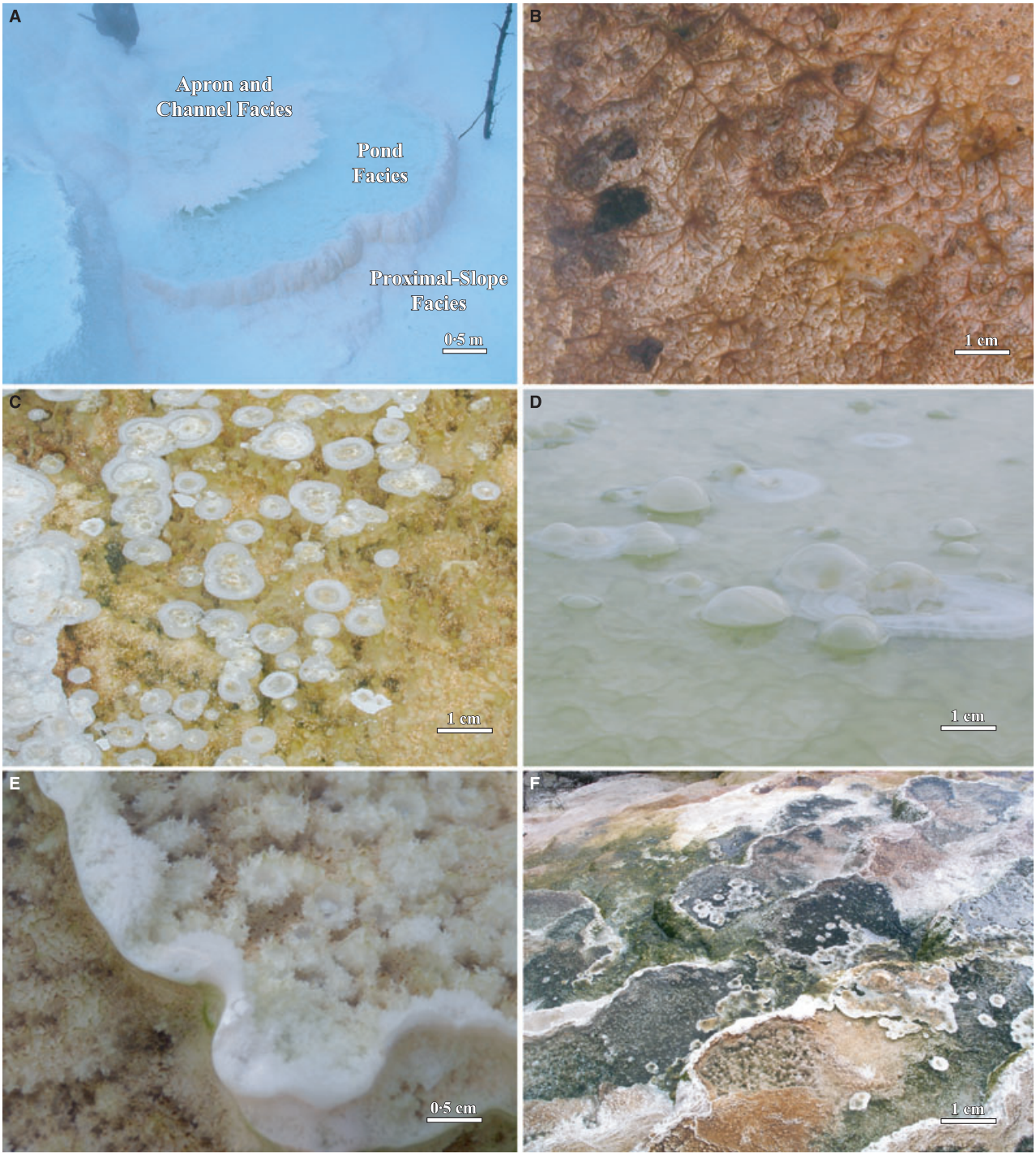


**Fig. 21.** Field photographs of microbial mat communities inhabiting the travertine facies. (A) Bright salmon-coloured microbial mats at dusk in the apron and channel and proximal-slope facies at Narrow Gauge in November 2008. (B) Brown ridged network microbial mats in the mid-temperature pond facies at Spring AT-3 in June 2004. (C) and (D) Green gas lift-off microbial mats and associated gas bubbles encrusted in calcite ice in the lower temperature pond facies at Spring AT-1 in November 2002. (E) Heavily travertine-encrusted gas lift-off microbial mats around a microterracette lip in the proximal-slope facies at Spring AT-3 in October 2005. (F) Multi-coloured microbial mats in the microterracettes of the proximal-slope facies at Spring AT-1 in January 2001.

apparently derived from the accumulation of gas bubbles within the mats that gradually float to the pond surface and stretch the mat upward with it. A similar mechanism, but with presumably lower volumes of trapped gas, may also influence the formation of the ridged network fabrics

(Fig. 21B). Once the mat cylinders reach the pond surface, concentric rings of calcite ice sheets form at the water–air interface (Fig. 21C). Furthermore, gas sometimes does escape from the mats and accumulates under the calcite ice sheets, creating gas-filled and travertine encrusted bubbles (Fig. 21D). Finally, the distal-slope facies contains thin, light brown microbial mats that exhibit the microterracette and spherule morphologies of the travertine with which they grow (Fig. 16C and D).

Culture-independent molecular surveys further substantiate that the microbial communities at MHS are highly correlated with the downstream succession of travertine depositional facies (Fouke *et al.*, 2003). Polymerase chain reaction (PCR) amplification and sequencing of microbial 16S rRNA genes with universally-conserved bacterial primers identified over 553 unique partial and 104 complete sequences (derived from more than 14 000 clones) affiliated with 221 unique species that represent 21 bacterial divisions (Fig. 22A; Fouke *et al.*, 2003). These sequences exhibited less than 12% similarity in bacterial community composition between each of the travertine depositional facies. As expected with decreasing temperature, microbial community diversity increased downstream from seven and 21 ribotypes, respectively, in the vent and apron and channel facies, and to 84 and 70, respectively, in the proximal-slope (Fouke *et al.*, 2003). 16S rRNA ribotypes affiliated with uncultured Crenarchaeota, Euryarchaeota and Korarchaeota have also been detected using universal Archaeal primers in samples from the vent facies at Angel Terrace. Although several potential biases exist that prevent direct reconstruction of microbial community structure from 16S gene sequence clone libraries (Hurst *et al.*, 2002), the libraries presented in Fouke *et al.* (2003) are sufficient to make reliable first-order estimates of bacterial community composition. Some of the most prominant bacteria affiliated with clones detected in the vent facies and apron and channel facies is Aquificales (pBB, OPB 30, OPS1). Conversely, the microbial communities in the pond, proximal-slope and distal-slope facies are significantly more diverse, including Green Non-Sulphurs (OPB65, *Chloroflexus*), Green Sulphurs (*Chlorobium*), Aquificales, cyanobacteria (*Synechococcus* and *Spirulina*) and other members of the Bacteroides, Cytophagales, Flexibacter and Firmicutes. 16S rRNA gene sequence analysis of the bacteria inhabiting steam that rises from each travertine facies identified only three sequences that were identical or similar to those detected in the hot-spring system (Bonheyo *et al.*, 2005). The remaining 90% of the steam clone library contained sequences that have not previously been identified at MHS, implying that they may have been transported into the park as bioaerosols (Bonheyo *et al.*, 2005).

The downstream facies partitioning of the bacterial communities has been shown graphically by establishing Operational Taxonomic Units (OTUs) from the clone libraries (Martin *et al.*, 2010). Operational Taxonomic Units are utilized because they provide a means to identify different organisms while avoiding the difficulty of defining, and consistently applying, the concept of a 'species' to microbes that reproduce asexually (Stackebrandt & Goebel, 1994). By convention, each OTU is defined as a distinct 16S rRNA gene sequence determined at 0·5%, 1% and 3% cutoffs in similarity to gene sequences previously identified in other environments and submitted to GenBank (Stackebrandt & Goebel, 1994). The lower OTU bound at 0·5% is based on the PCR sequence error rate (Tindall & Kunkel, 1988; Barnes, 1992), whereas the upper bound at a difference of 3% is the standard used in most studies (Stackebrandt & Goebel, 1994). Of the 237 OTUs identified using the 1% cutoff, 91% were found to occur in only one of the travertine facies (Fig. 23B; Martin *et al.*, 2010). Similar microbial community partitioning was observed for the 0·5% and 3% cutoffs (90% and 93% partitioning, respectively). Furthermore, consistency between accumulation curves (after Hughes *et al.*, 2001) based on the three OTU cutoff definitions with theoretical exponential curves, suggests that the sampling procedure, assumptions of random sampling and environmental sequence saturation were adequate enough in the data set of Fouke *et al.* (2003) to map microbial distributions (Martin *et al.*, 2010). This observation further confirms that the hot-spring microbial communities are correlated strongly with the travertine depositional facies. Accumulation curves based on 3%, 1% and 0·5% OTU definitions consistently support the sampling procedure and the assumption of random sampling (Martin *et al.*, 2010). Furthermore, computational analysis of the relative abundance or cover of the Fouke *et al.* (2003) clone libraries, segregated into substrate versus spring-water column clones, can now be used in future studies to identify microbial candidates for linking metabolic activity with travertine precipitation (Martin & Goldenfeld, 2006a,b; Martin *et al.*, 2010).

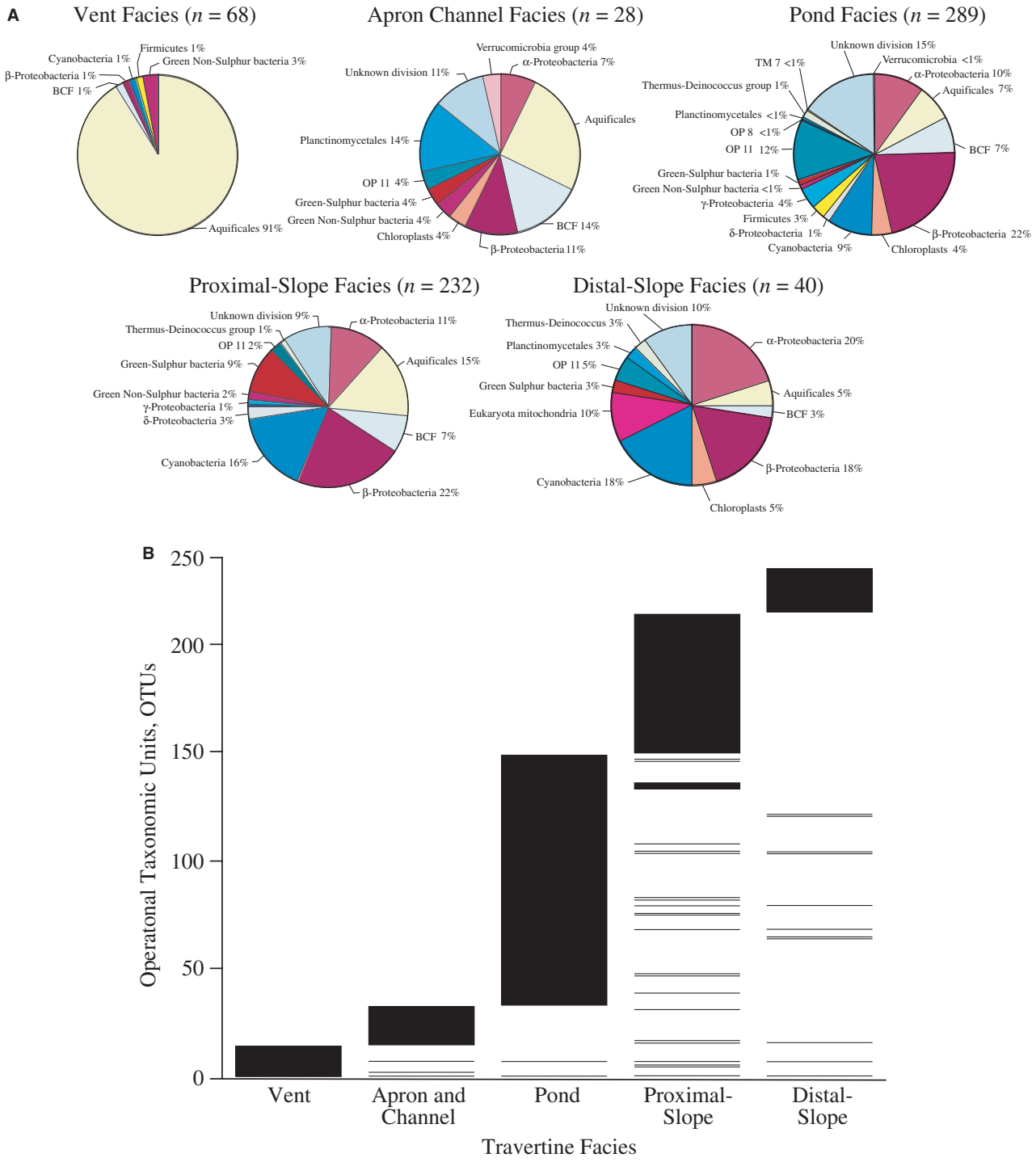


**Fig. 22.** Molecular analyses of the diversity and distribution of Mammoth Hot Springs bacterial communities within travertine depositional facies. (A) Pie diagrams illustrating the division-level proportion of the total number of 16S rRNA gene sequences comprising the clone libraries derived from each travertine facies. (B) The facies-specific downstream distribution of bacterial species at the 1% Operational Taxonomic Unit (OTU) definition.

## Downstream transect of microbial community diversity

Thermophilic and mesophilic microbes and their community associations have specific preferences for temperature, pH, nutrients, flow fields and other key environmental parameters (Brock, 1978; Hugenholtz *et al.*, 1998; Madigan, 2001; Nordstrom *et al.*, 2005; Madigan *et al.*, 2006; Takacs-Vesbach *et al.*, 2008). Thus, the extreme range of

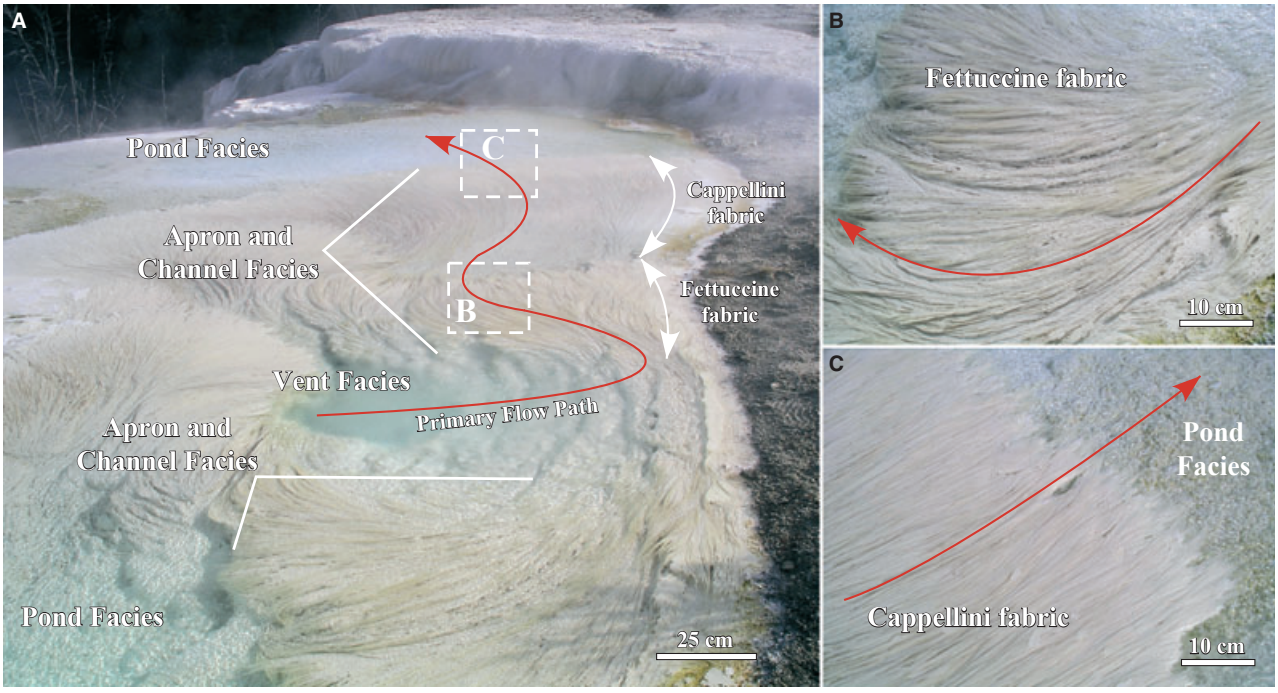


**Fig. 23.** Field photographs of the modern microbial mats and travertine comprising the apron and channel facies at Spring AT-2 in October 2005. (A) Trajectory of the primary flow path through the upstream Fettuccine fabric and downstream Cappillini fabric. (B) Enlargement of the Fettuccine fabric. (C) Enlargement of the Cappillini fabric.

environmental conditions present along the primary flow paths at MHS would be expected to contain a high diversity of micro-organisms. However, the sharp partitioning of the MHS microbial diversity with respect to the downstream succession of travertine facies is unexpected. The reproducibility of the multiple-field sampling intervals from each facies suggests that this is an accurate screen of the normal *in situ* inhabitants of each facies (Fouke *et al.*, 2003; Martin *et al.*, 2010). Only two 16S rRNA gene sequences, which are affiliated with Aquificales pBB and $\beta$-ProteobacteriaI (OPB 30) bacteria, were detected in all five travertine facies. These autotrophic thermophiles may be able to tolerate extreme changes in temperature, pH, $pCO_2$, nutrient availability and flow rate conditions that are outside of their prime niche (Madigan *et al.*, 2006). It is also possible that these gene sequences were washed down from upstream facies. Downstream cell transport may take place via cell movement and gliding within substrate biofilms and microbial mats, cell suspension in the water column, cells clinging to the fur of bison and elk that occasionally enter the streams and cell attachment to $H_2O$ molecules that rise as steam from the water–air interface (bioaerosols; Bonheyo *et al.*, 2005). Therefore, it is possible that a higher proportion of downstream bacterial transport is occurring, but at levels below detection. However, the bacterioplankton OTUs detected in the water column, which are presumably most susceptible to being flushed downstream, were not typically detected downstream (Fouke *et al.*, 2003; Martin *et al.*, 2010). Furthermore, the facies boundaries proved to be nearly absolute with respect to detected bacterial 16S rRNA gene sequences (Fouke *et al.*, 2003). Although specific 16S rRNA gene sequences were observed over a range of conditions within each travertine facies, OTUs were not found to cross the facies boundaries.

The bacterial communities inhabiting environments equivalent to the pond facies have been studied previously at Bath Lake, Narrow Gauge, Roland's Well and other unnamed springs within the New Highland and Angel Terrace complexes (Fig. 7A). Inhabitants include the purple sulphur anoxygenic phototrophic bacterium *Thermochromatium tepidum* (Madigan, 2003, 2005) that co-exists with the obligate phototroph *Chloroflexus aurantiacus* (Giovannoni *et al.*, 1987) at temperatures of 50 to 65°C and a pH of 6·5 (Ward *et al.*, 1989, 2001). *Thermochromatium tepidum* is proposed to be the primary producer in these high-temperature environments, given the absence of cyanobacteria, continuous anoxia and the lack of bacteriochlorophyll *a* (Giovannoni *et al.*, 1987; Ward *et al.*, 1989). This primary

production is supported by carbon isotope fractionations between DIC and lipid biomarkers, which suggest that the sulphate-reducing *Chloroflexus* and other chemo-organotrophs are growing photoheterotrophically on carbon derived from *T. tepidum* (van der Meer *et al.*, 2003; Madigan, 2005). *Chloroflexus* forms orange mats and contains bacteriochlorophyll (Bchl) *c* or *d* and chlorosomes (Pierson & Castenholz, 1995), and shares physiological and biochemical properties with both the purple and green anoxygenic phototrophs (Madigan, 1984, 1988; Giovannoni *et al.*, 1987). Other members of the communities include the cyanobacteria *Synechococcus* and *Spirulina* (Ward & Olson, 1980; Papke *et al.*, 2003). Marked increases in methanogenesis upon sulphate depletion indicated that methane production in Bath Lake microbial mats is limited by sulphate-reducing bacteria, and thus mirrors that of anaerobic degradation in marine sediments (Ward & Olson, 1980).

## HALLMARKS OF MAMMOTH HOT SPRINGS TRAVERTINE FORMATION

Mammoth Hot Springs exhibits systematic downstream correlations amongst travertine facies (geomorphology, crystalline structure and geochemistry), microbial communities (phylogenetic diversity, mat morphology and pigmentation) and spring-water parameters (temperature, pH, geochemistry and flow; Figs 9, 18, 19, 20 and 22); this begs the question of how these synchronously changing components of the natural hot-spring system might reflect interacting geological and biological phenomena that control travertine deposition. Possibilities include: (i) the travertine and microbes are not directly mechanistically linked with each other but are instead simultaneously controlled by the same suite of changing environmental conditions; (ii) the microbes respond to environmental conditions and, in turn, control travertine formation; (iii) the travertine precipitates in direct response to environmental conditions and, in turn, influences the microbial communities; or (iv) a combination of all three processes. To evaluate systematically these options, three of the hallmark attributes of the MHS travertine deposits have been chosen for study. These attributes include: (i) travertine terracettes and microterracettes at the macroscopic scale (tens of centimetres to tens of metres; Goldenfeld *et al.*, 2006; Veysey & Goldenfeld, 2008); (ii) travertine streamer fabrics at the mesoscopic (millimetre to centimetre) and microscopic (micrometre to millimetre) scales (Fouke *et al.*, 2000; Veysey *et al.*, 2008); and (iii) travertine growth rate (Kandianis *et al.*, 2008) which affects all travertine geomorphologies and depositional size classes.

### Travertine terracettes and microterracettes

An important emphasis of the work at MHS has been to determine whether the physical presence and metabolic activity of microbial communities are required to form the terraced travertine deposits universally observed in high-temperature and low-temperature springs (Pentecost, 2005). To test this at the macroscopic scale, a pattern analysis study of the travertine terracettes and microterracettes in the pond and proximal-slope facies (Figs 14 and 16) was completed by integrating time-lapse photography with time-dependent computer simulation modelling (Veysey & Goldenfeld, 2008). Three years of time-lapse photography, taken from a fixed position on the MHS Canary Springs boardwalk, indicates that: (i) once a spring starts flowing, the sloping ground surface is covered initially by many small microterracettes; (ii) the margin or 'lip' of a downstream microterracette grows faster than that of its directly upstream neighbours; and (iii) eventually this microterracette deepens and broadens to the point where upstream microterracettes are drowned and incorporated to form a significantly larger terracette (Veysey & Goldenfeld, 2008). This upslope drowning sequence was predicted independently with cell dynamical system (CDS) and differential equation modelling (Goldenfeld *et al.*, 2006). The latter approach integrates turbulent spring-water flow with the aqueous conditions that govern travertine precipitation, and indicates that the shape of the microterracettes and terracettes is scale-invariant (Veysey & Goldenfeld, 2008). The CDS models are based on theoretical principles of fluid and crystal growth dynamics, and have produced sub-metre to metre-scale synthetic travertine geomorphologies that are strikingly similar in shape and form to those observed in the pond and proximal-slope facies. This macroscale consistency between natural and modelled patterns implies that the terracette and microterracette geomorphologies may be controlled primarily by abiotic physical and chemical processes (i.e. heat diffusion, $CO_2$ degassing and hydrology; Goldenfeld *et al.*, 2006; Veysey & Goldenfeld, 2008).

### Travertine streamers

Accurate reconstruction of microbial community structure and activity from solid-phase travertine crystalline fabric and chemistry is essential to: (i) improve the identification of microbial life preserved in modern and ancient carbonate rocks (biomarkers); and (ii) better understand the origin and ecology of early microbial life on the ancient Earth (Riding, 2000; Knorre & Krumbein, 2000). Research on microbial $CaCO_3$ biomineralization has provided valuable guides that can now be used to identify mechanistic linkages between micro-organisms and the structural and chemical properties of carbonate rock deposits (Thompson & Ferris, 1990; Buczynski & Chafetz, 1991; Teng *et al.*, 1998; van Lith *et al.*, 2003; Chekroun *et al.*, 2004; Ferris *et al.*, 2004; Bosak & Newman, 2005). Three modes of mineralization have been observed: (i) abiotic or inorganic precipitation that is independent of biological influences; (ii) biologically-induced precipitation that is initiated by the physical presence and/or biogeochemical activity of an organism (for example, cellular matrix-mediated); and (iii) biologically controlled precipitation that is determined directly by a living organism (for example, skeletal carbonates; Lowenstam, 1981; Lowenstam & Weiner, 1982; Mann, 2001; Weiner & Dove, 2003). However, quantitatively diagnosing which of these modes were dominant for a specific facies-constrained travertine at MHS has required a combination of morphological characterizations (Chafetz & Folk, 1984; Jones & Renaut, 2003a,b) and geochemical reconstructions (Arp *et al.*, 2001), as well as microscopy and mineralogy (Neuweiler *et al.*, 1999).

The distinct sinuous fabric of the streamer deposits comprising the apron and channel facies (Fig. 12) is formed as a direct result of travertine entombment of filamentous microbial mats. The streamer fabric can only form when a thriving filamentous microbial community is present at the time of travertine deposition. Therefore, ancient travertine streamer deposits are an unequivocal microbial fossil, as well as a sensitive indicator of the spring-water temperature, pH and flux of the ancient environment in which the microbes lived (Veysey *et al.*, 2008). However, it cannot be deduced from the apron and channel facies streamer fabric alone whether the filamentous microbes directly control travertine precipitation, or simply serve as a passive substrate for rapid mineralization.

To investigate the extent to which microbes may influence travertine streamer formation, detailed mesoscale field inspection, sampling and microscale laboratory analyses were completed of the apron and channel facies at multiple springs in the MHS complex over a period of several years (Veysey *et al.*, 2008). This analysis identified distinct upstream to downstream differences in the structure of the streamer travertine within the apron and channel facies, as well as in the composition of the filamentous microbial communities (Fig. 22; Fouke *et al.*, 2003; Martin & Goldenfeld, 2006a,b; Martin *et al.*, 2010). The upstream 69°C to 71°C portion of the facies, called the 'Fettuccine' travertine streamer fabric, contains large individual microbial filaments that reach 2 mm in diameter and 10 cm in length (Fig. 23A and B). These widely spaced (≤0·5 cm) filaments have thick sheets of draped extracellular polymeric substances (EPS) between filaments that contain abundant elliptical holes presumably created by water turbulence, gravity stretching and gas bubble release (Fig. 23B). The downstream 65°C to 69°C portion, named the 'Cappellini' travertine streamer fabric is composed of filaments that are smaller in diameter (≤0·5 mm), shorter (≤2 cm) and tightly packed with significantly less EPS and no space between filaments (Fig. 23C). As a result, the Fettuccine and Cappellini fabrics directly mimic the morphology of the filamentous microbial mats that they preserve and are well-preserved in Holocene and Pleistocene age travertine deposits of Mammoth, the Gardner quarries and other locations around the world (Veysey *et al.*, 2008). Similar upstream–downstream changes in microbial filament diameters have been observed in other $CaCO_3$ and $SiO_2$ hot spring mineral deposits around the world (Lynne & Campbell, 2003; Pentecost, 2005).

Integrated high-resolution structural analyses of the microbial filaments and associated travertine streamer deposits at MHS are currently in progress. Initial results indicate that each individual decimetre-long microbial filament is composed of small (5 to 20 mm) intertwined microbial filaments and coccoidal cells (Fig. 24C). The surface of each microbial filament is encrusted by small, densely packed aragonite needles, whereas larger aragonite needles grow in the EPS-rich interstitial void spaces in which significantly larger aragonite needles are precipitated (Fig. 24D and E). Micro-computed tomography (Micro-CT) indicates that once each microbial filament is encrusted, the microbial biomass is rapidly decayed and recrystallized,

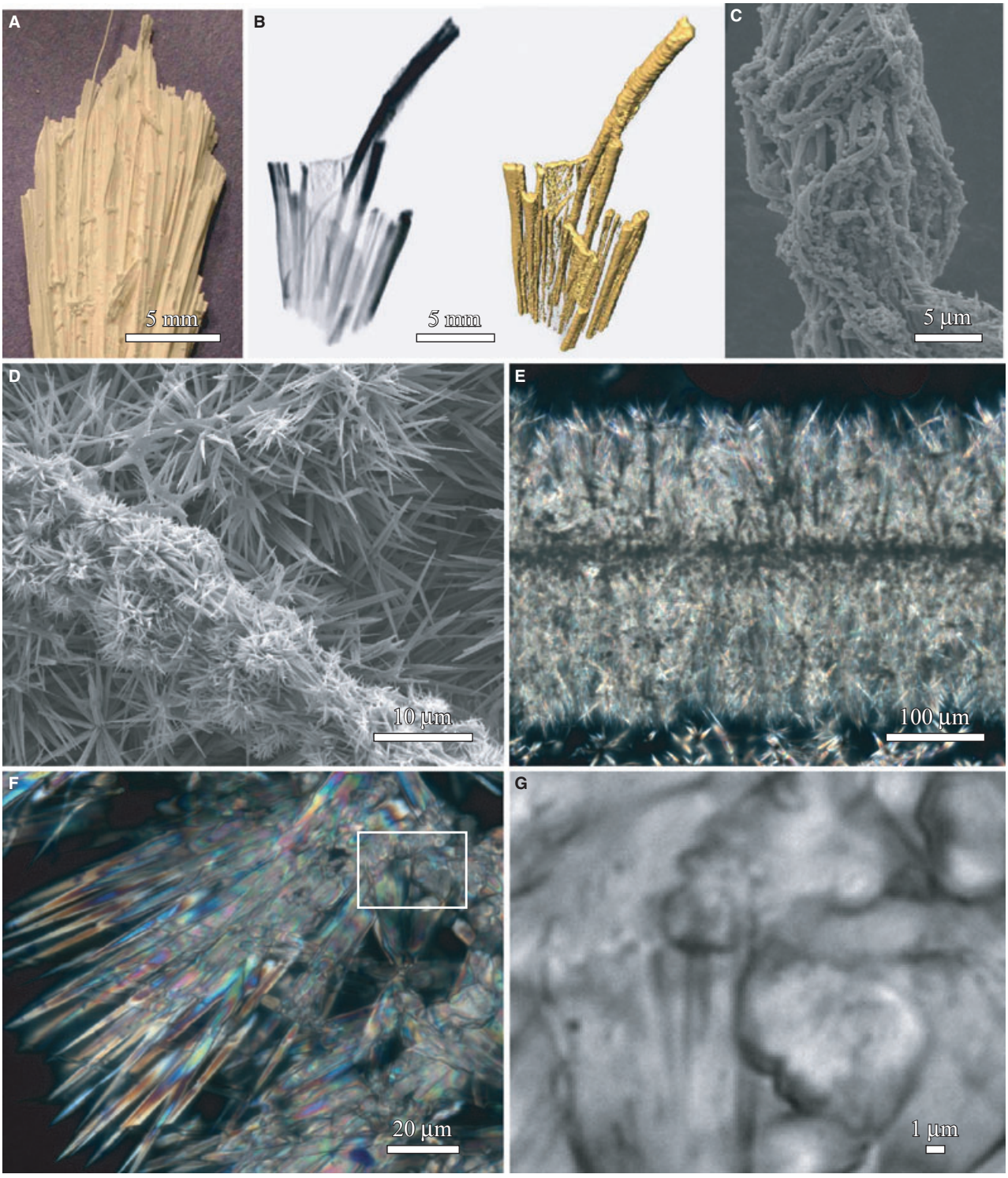


**Fig. 24.** Integrated high-resolution analyses of the travertine apron and channel facies Cappillini fabric. The sample was collected from the field site shown in Figure 23C. (A) Hand sample photograph of dried specimen. (B) MicroCT images depicting raw X-ray data (left) and rendered surfaces (right). (C) SEM image of the microbial filaments on which the travertine is precipitated, illustrating that each larger filament observed in the field is composed of small interwoven microbial filaments and coccoidal cells. (D) SEM image of a microbial filament encrusted by small aragonite needles and surrounding EPS-rich pore space in which significantly larger aragonite needles have precipitated (modified from Kandianis *et al.*, 2008). (E) to (G) Transmitted plane-light photomicrographs of a single travertine-encrusted microbial filament at increasingly higher magnification, reaching 1 µm resolution.

forming a solid organic matter rich core within each travertine streamer filament (Fig. 24A and B). Inverted plane-light microscopy at a 1 μm resolution suggests that there are multiple previously undocumented microcrystalline morphologies within each streamer deposit (Fig. 24F and G).

### Travertine growth rate

The rate of $CaCO_3$ precipitation (Lasaga, 1998), in the stages of both nucleation and crystal growth (Berner, 1980), is a primary factor in evaluating carbonate crystallization dynamics. Accordingly, any geological or biological component that significantly lowers or raises the energy required for these closely linked processes to occur will respectively increase or decrease the overall precipitation rate. Numerous investigators have conducted *in vitro* kinetic experiments, and proposed phenomenological $CaCO_3$ rate laws that accurately predict these reactions as a function of measurable physical and chemical environmental conditions (Morse, 1983; Inskeep & Bloom, 1985; Burton & Walter, 1987; Zhong & Mucci, 1989; Ferris *et al.*, 2004). The most universal form of these equations is: $R = k_R = k_{\mathrm{emp}} A(\Omega - 1)^n$ (Morse, 1983), where $R$ is the precipitation rate, $k_{\mathrm{emp}}$ is the empirical rate constant, $A$ is the reactive mineral surface area, $\Omega$ is the bulk solution $CaCO_3$ saturation state [$\{Ca^{++}\}$ $\{CO_3^{2-}\}$ $K_{sp\ CaCO3}^{-1}$] and $n$ is the reaction order with respect to the saturation state. However, rate laws alone cannot directly discriminate between the geological and microbiological mechanisms that may control $CaCO_3$ precipitation.

Therefore, Kandianis *et al.* (2008) conducted a controlled field experiment at Spring AT-3 using an *in situ* kinetic apparatus (ISKA; Fig 25A to D) in which aragonite saturation state ($\Omega_a$), microbial biomass concentration and microbial viability were measured quantitatively to determine their relative influences on the rates of travertine mineralization in an advection-dominated transport regime. The spring-water $\Omega_a$ value of 3·63 ± 0·09 in the MHS apron and channel facies, which is near that of normal sea water, suggests that: (i) the natural steady-state aragonite precipitation rate is 2·5 times greater than that observed when microbial biomass on the aragonite mineral surface is *ca* 80% depleted by 0·2 μm filtration (Fig. 25E); and (ii) inhibiting microbial viability with ultraviolet (UV) irradiation has no significant effect on the mean precipitation rate. The indigenous microbial communities were exposed to UV light at an intensity of 254 nm at 30 mJ $cm^{-2}$. For the Aquificales filamentous microbes being tested (Fouke *et al.*, 2003), this level of UV radiation destroyed their ability to reproduce by forming thymine dimmers and ensuing codon misreading during DNA replication (Scrima *et al.*, 2008). The microbial cells remained intact throughout the field experiment and the UV irradiation exposure did not extensively affect the microbial biomolecules (i.e. proteins and lipids) and EPS. Therefore, cell membrane-bound biomolecules and EPS concentrations in the microbial mat biomass may explain the observed 2·5 times increase in $CaCO_3$ precipitation rate with increasing biomass (Kandianis *et al.*, 2008). This observation is consistent with observations of increased rates of calcite tufa precipitation in controlled laboratory experiments (Rogerson *et al.*, 2008; Pedley *et al.*, 2009). Previous studies on metazoan aragonite biomineralization, primarily in bivalves, have demonstrated that proteins, polysaccharides and lipids alter $CaCO_3$ nucleation rates by changing the activation energy for precipitation (Mann, 2001; Weiner & Dove, 2003). Therefore, by analogy, this implies that microbial biomolecules and EPS may have a similar effect on hot-spring travertine precipitation at MHS. Furthermore, high-resolution inverted fluorescence microscopy analyses indicate that each experimental condition (natural, filtered and UV irradiated) produced different micro-scale sequences of aragonite and calcite precipitation. In summary, this expansion of the concept of a 'biomarker' to include $CaCO_3$ precipitation rate, mineralogy, chemistry, crystalline structure and porosity is significant, in that this basic suite of parameters is used universally to describe limestone mineralization and diagenesis.

## MICROBIAL METABOLIC INFLUENCE ON TRAVERTINE FORMATION

The microbial communities inhabiting each of the MHS travertine facies must control chemical reactions and synthesize molecules (metabolize) to grow and replicate in the natural hot-spring environment (Madigan *et al.*, 2006). Each microbial cell is composed of chemical constituents extracted directly from the local spring-water and substrate environments via anabolic processes. These constituents are broken down to release energy via catabolic processes needed for biochemical synthesis (biosynthesis) of new

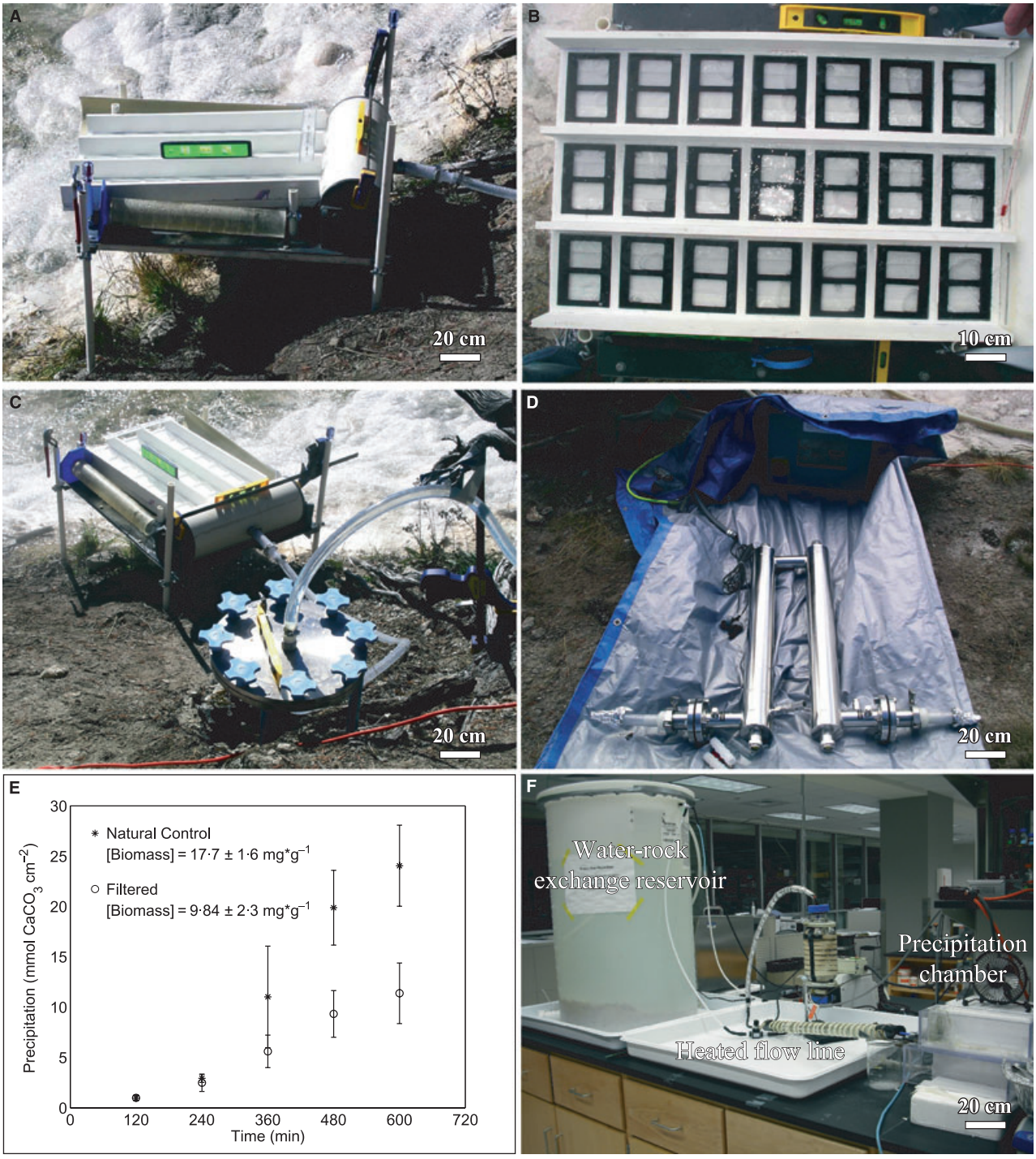


**Fig. 25.** Controlled travertine-microbe–water interaction experiments in the field and in the laboratory. (A) *In situ* kinetic apparatus (ISKA) deployed at MHS Spring AT-3 in October 2005 (modified from Kandianis *et al.*, 2008). (B) Three parallel runways with precipitation slides in the ISKA. (C) In-line 0·22 μm filtration device. (D) In-line UV radiation device. (E) Mean $CaCO_3$ precipitation as a function of experimental duration for the natural control and filtration treatments (modified from Kandianis *et al.*, 2008). (F) Laboratory photograph of the kinetic apparatus.

cell material and other functions such as transport and motility (Madigan *et al.*, 2006). The microbial metabolic activities most relevant to controlling travertine precipitation are those that influence the saturation state of spring-water $CaCO_3$ by impacting the following pH sensitive

$CO_2$ dissociation reactions (Stumm & Morgan, 1996):

$$CO_2 + H_2O \Leftrightarrow H_2CO_3$$

$$H_2CO_3 \Leftrightarrow HCO_3^- + H^+$$

$$HCO_3^- \Leftrightarrow CO_3^{2-} + H^+$$

$$CO_3^- + Ca^+ \Leftrightarrow CaCO_3$$

The suite of microbial metabolic processes potentially capable of affecting these carbonate reactions include: (i) the consumption or production of $CO_2$ during oxidation–reduction coupled metabolic reactions and photosynthesis (Konhauser, 2007; Ehrlich & Newman, 2009); (ii) the consumption or production of organic and inorganic acids (Konhauser, 2007; Ehrlich & Newman, 2009); and (iii) the biosynthesis of membrane bound biomolecules and enzymes on outer cell walls that affect $CaCO_3$ nucleation kinetics (Kandianis *et al.*, 2008). Futhermore, the presence and activity of microbes at the time of ancient travertine deposition can be inferred from biomarkers incorporated into the $CaCO_3$ crystals such as microbial biomolecules (i.e. lipids) and catabolic waste products (i.e. isotopes and reduced electron acceptors).

## Screening of microbial community composition and metabolism

Mammoth Hot Springs microbial mat communities in the vent facies and apron and channel facies are dominated by chemoautotrophic metabolisms, including S oxidation and anoxygenic photosynthesis (Fouke *et al.*, 2003; Martin & Goldenfeld, 2006a,b). Conversely, microbial communities in the pond, proximal-slope and distal-slope facies contain a diverse mixture of photoautotrophic and heterotrophic metabolic activities (Fouke *et al.*, 2003; Martin & Goldenfeld, 2006a,b; Martin *et al.*, 2010). A survey is currently underway of cell densities and the metabolic genes associated with sulphate reduction, nitrogen fixation, reverse tricarboxylic acid cycling, and the Calvin–Benson–Bassham pathway. Direct cell counts of filamentous and auto-fluorescent micro-organisms in the vent facies and apron and channel facies were low ($\leq 2 \times 10^5$ cells ml$^{-1}$). Conversely, the pond and proximal-slope facies had high auto-fluorescent cell counts ($\leq 1{\cdot}8 \times 10^6$ cells ml$^{-1}$) as well as high bacteriochlorophyll *a* concentrations, both of which are consistent with photoautotrophic primary production. The specific amplicons that were mapped within each travertine facies included: (i) dissimilatory sulphite reductase (*dsr*A); (ii) nitrogenase reductase (*nif*H); (iii) ribulose-1,5-bisphosphate-carboxylase/oxygenase (RuBisCO) Form IA/IB (*cbb*L), Form II (*cbb*M) and Form ID (*cbb*L_ID); and (iv) $\beta$-ATP-citrate lyase (*acl*B). The presence of *dsr*A in all five facies suggests the presence of sulphate-reducing bacteria throughout the drainage system, which is consistent with metabolic inferences derived from the 16S RNA clone libraries (i.e. *Desulfovibrio* sp.; Fouke *et al.*, 2003) and previous *dsr*A analyses at MHS (Fishbain *et al.*, 2003). Active phototrophy in the pond facies is indicated by changes in RuBisCO gene expression over the diurnal cycle, as well as the presence of three novel Form II gene sequences. Furthermore, phylogenetic analyses of cDNA generated from mRNA transcripts identified three distinct Form IA/IB gene sequences in the pond and proximal-slope facies, and in the pond facies. A 20% decrease in night-time sulphate concentrations in pond facies spring-water suggests that enhanced rates of sulphate reduction take place when oxygenic photosynthesis is reduced (Giovannoni *et al.*, 1987).

Lipid biomarkers and organic matter $\delta^{13}C$ fractionation were analysed to track the dynamics of carbon cycling within each travertine depositional facies. Phospholipid fatty acids (PLFA) and glycolipid fatty acids (GLFA) are partitioned distinctly between each travertine facies (Zhang *et al.*, 2004) and directly track the microbial community partitioning indicated from the clone libraries (Fouke *et al.*, 2003; Martin *et al.*, 2010). Because lipids can be trapped and preserved within the modern solid-phase travertine, their extraction from ancient travertine may permit the reconstruction of microbial community palaeoecology (Ward *et al.*, 2001). The microbial mat biomass $\delta^{13}C$ values decrease from $-16{\cdot}1‰$ in the vent facies to $-23{\cdot}5‰$ in the distal-slope facies, whereas the isotopic compositions of PLFA and GLFA have variations similar to those of total biomass (Zhang *et al.*, 2004). Fatty acid $^{13}C$ enrichment in the vent facies relative to the total biomass implies that these Aquificales-dominated communities are using the reversed tricarboxylic acid cycle (rTCA). Conversely, fractionations between fatty acids and total biomass suggest that $CO_2$ fixation in the pond, proximal-slope and distal-slope is dominated by the photosynthetic Calvin cycle (Zhang *et al.*, 2004).

### *Sulfurihydrogenibium*-dominated communities in the apron and channel facies

Microbial molecular analyses [16S rRNA gene sequence clone libraries, terminal-restriction fragment length polymorphism (T-RFLP) fingerprinting] of the filamentous microbial mats in the apron and channel facies indicate they are dominated by the Aquificales bacterium *Sulfurihydrogenibium* (Fouke *et al.*, 2003). This community structure is substantiated by metagenomic analyses (described below), which suggest that *Sulfurihydrogenibium* makes up 90% of the filamentous mats (Inskeep *et al.*, 2010). *Sulfurihydrogenibium* accounts for 86% of the 16S rRNA gene sequences detected in the Fettucine fabric, and 72% in the Cappellini fabric. One unique *Sulfurihydrogenibium* population (clone F1-C1-2) was predominant in the Fettucine fabric and nearly absent from the Cappellini fabric, whereas the opposite was true for clone C1-A1-B. The 16S rRNA clone libraries and metagenomic analyses also provide information on the less-dominant bacterial members of this community, including novel lineages of the Clostridiales and Planctomycetes (Fouke *et al.*, 2003; Inskeep *et al.*, 2010).

Metagenome bioinformatic analysis of these *Sulfurihydrogenibium* communities has identified strategic gene targets with which to link filamentous microbial metabolism with travertine precipitation (Inskeep *et al.*, 2010). Results suggest that *Sulfurihydrogenibium* is a chemolithoautotroph that fixes $CO_2$ using the reductive rTCA cycle (ATP citrate lysase *acl*B gene; Reysenbach *et al.*, 2009; Inskeep *et al.*, 2010). These metabolisms are substantiated independently by the lipid composition and $^{13}C$ enrichment detected in the *Sulfurihydrogenibium* filamentous mats (Zhang *et al.*, 2004). The rapid 3 mm $day^{-1}$ extension rate of *Sulfurihydrogenibium* observed in the apron and channel facies (Fouke *et al.*, 2003) suggests that the rate of this rTCA metabolism may be high enough to locally draw down $CO_2$ and enhance the rate of travertine precipitation. *Sulfurihydrogenibium* also has the ability to oxidize reduced forms of S using $O_2$ as the electron acceptor. This suggestion is based on the presence of a suite of sulphide oxidation (sox) genes in the genome and a sulphide-quinone glutathione reductase family of flavoproteins (sqr) that catalyse the oxidation of sulphide to elemental sulphur (Nakagawa *et al.*, 2005; Reysenbach *et al.*, 2009; Inskeep *et al.*, 2010). This observation is consistent with changes in spring-water aqueous $H_2S$ (high to low) and $O_2$ (low to high) concentrations observed downstream through the apron and channel facies (Fig. 20).

The biochemical pathway of $CO_2$ fixation via sulphur oxidation (sox system) that is utilized by *Sulfurihydrogenibium* is remarkably similar between hot-spring chemolithoautotrophs and anoxygenic photolithotrophs (Ghosh & Dam, 2009). Volatiles such as $CH_4$, $H_2S$ and $H_2$ degas as the spring water flows through the apron and channel facies, and $CO_2$ and $H_2S$ undergo chemical reactions that, in turn, place restrictions on microbial community activity (Fouke *et al.*, 2003). The filamentous *Sulfurihydrogenibium* are therefore primary producers that catalyse a variety of energetically favourable redox reactions that synchronously influence $CaCO_3$ precipitation (Kandianis *et al.*, 2008). Gene coding for the oxidation of hydrogen and thiosulphate was not observed in the *Sulfurihydrogenibium* genome and metagenome (Reysenbach *et al.*, 2009; Inskeep *et al.*, 2010). This observation suggests that *Sulfurihydrogenibium* is unable to oxidize hydrogen and, therefore, does not support previous hypotheses that high-temperature MHS microbial communities are primarily driven by microaerophyllic H-based oxidation rather than S oxidation (Spear *et al.*, 2005). Furthermore, preliminary application of fluorescence induction and relaxation (FIRE) analyses in the apron and channel facies suggest that the *Sulfurihydrogenibium*-dominated microbial community is also capable of anoxygenic photosynthesis.

The apron and channel facies is a non-equilibrium system, in that the spring-water: (i) has extremely low dissolved oxygen ($\sim\rho O_2 \leq 0{\cdot}2$ atm.); (ii) is oversaturated with respect to $CO_2$, $H_2$, $CH_4$ and $H_2S$ (*ca* 75 to 150 μmol); and (iii) is in significant redox non-equilibrium with varying amounts of reduced dissolved chemical species (Fouke *et al.*, 2000; Kandianis *et al.*, 2008). Energetic modelling of other analogous hot-spring drainage systems in Yellowstone has shown that downstream changes in chemical composition, rather than temperature, determine the energy supply to the microbial communities (Amend & Shock, 2001; Amend *et al.*, 2004; Meyer-Dombard *et al.*, 2005; Shock *et al.*, 2010). As a result, there are a limited number of possible exergonic reactions that will link sulphur cycling driven by *Sulfurihydrogenibium* metabolic activity with carbonate precipitation. These primary reactions include (Inskeep *et al.*, 2005):

$$H_2S(aq) + 0 \cdot 5O_2(aq) \Leftrightarrow S^0 + H_2O$$

$$H_2S(aq) + 2O_2(aq) \Leftrightarrow SO_4^{2-} + 2H^+$$

$$H_2S(aq) + H_3AsO_4 \Leftrightarrow S^0 + H_3AsO_3 + H_2O$$

$$H_2S(aq) + H_2AsO_4^- + H^+ \Leftrightarrow S^0 + H_3AsO_3 + H_2O$$

$$H_2S(aq) + 2Fe^{3+} \Leftrightarrow S^0 + 2Fe^{2+} + 2H^+$$

$$H_2S(aq) + 0{\cdot}25NO_{3-} + 0{\cdot}5H^+ \Leftrightarrow S^0 + 0{\cdot}25NH_{+4} + 0{\cdot}75H_2O$$

## HOT SPRING HYDROLOGICAL CYCLES AND MICROBIAL FEEDBACK

The integrated biotic and abiotic processes that influence MHS travertine formation operate within repeating systems-level cycles that are controlled by changes in the flux of spring-water emerging from the vent. Over a period of 12 consecutive years (1997 to 2009), a continuous long-term suite of field observation, measurement, photography and sampling has been compiled at Springs AT-1, AT-2 and AT-3, Narrow Gauge and Canary Springs (Fig. 5). This observation has revealed significant diurnal variations in water chemistry and microbial communities, but almost no seasonal variability (Fouke *et al.*, 2000; Veysey *et al.*, 2008). New vents open, vents shift their position during changes in spring-water outflow and old vents eventually stop flowing (Fouke *et al.*, 2000, 2001, 2003). Therefore, the composition, geometry and three-dimensional patterns of travertine facies deposition create a sensitive record of these long-term spring dynamics in both modern and ancient hot-spring systems. Long-term observations indicate that all hot springs in the MHS complex exhibit a remarkably similar hydrological life history, which includes a cycle composed of five distinct phases of spring-water discharge and associated travertine deposition.

In Phase 1, the vent forms and spring-water slowly erupts from the ground for only a day or two at relatively low temperature (40°C to 50°C) and high pH (7·0 to 7·5). Phase 2 is then initiated when spring-water reaches a temperature of 73°C, a pH of 6·0 and a flux discharge rate of as much as 20 to 60 l $s^{-1}$, which is the observed range of vent conditions at MHS (Veysey *et al.*, 2008). The five-fold sequence of travertine depositional facies (Fig. 9) is established rapidly over the next few weeks and then continues to accumulate over the next several months to years. The vertical and lateral position of each travertine facies during Phase 2 is influenced strongly by variations in the flux of spring-water emerging from the vent, as well as the pre-existing slope and topography of the ground surface on which the spring erupted (Veysey *et al.*, 2008). In the case of Springs AT-1, AT-2 and AT-3, the vents emerge within a few metres of the margin of Angel Terrace and the resultant Phase 2 drainage pathways generally reach 30 to 50 m in length. Phase 2 spring-water drainage patterns at Narrow Gauge are similar in scale to those at Angel Terrace, but accumulate within a bowl-shaped topographic low that serves to truncate the downstream extent of the distal slope facies. In contrast, Phase 2 at Canary Spring on Main Terrace is significantly larger in scale, with drainage pathways and associated travertine deposits that reach more than 300 m in length (Fig. 15B).

After anywhere from one to three years, Phase 3 is triggered by a significant increase in the flux of spring-water emerging from the vent, which can also be accompanied by a lateral shift in the position of the vent of as much as 1 m. The higher flux rate at the vent creates an accelerated primary flow path that delivers hotter and less chemically evolved spring-water, and microbial communities, to further downflow positions within the drainage system. As a result, the site of precipitation for each travertine depositional facies also shifts downstream. The most striking example of this is the rapid (mm $day^{-1}$) lateral migration of the apron and channel facies. Sustained increase in outflow flux eventually permits the apron and channel facies to completely cover or encrust the pond facies terracette that was immediately downstream during the previous Phase 2 period of travertine deposition (Fig. 26A). The filamentous Aquificales-dominated microbial communities on which the apron and channel facies travertine precipitate, grow just below the surface of the flowing spring-water. Therefore, the apron and channel facies travertine forms a 'pavement' that grows out and over the downstream terracette pond (Figs 12C, 12D and 26A). As the apron and channel facies travertine reaches the pond lip, it first forms stalagmite-type deposits (Fig. 26B) that eventually coalesce and blanket the front buttress of the terracette (Fig. 26C). The resulting effect on the hot-spring drainage outflow is to create a waterfall within the apron and channel facies; this increases the spring-water $\delta^{13}C$ while decreasing the DIC as a result of enhanced turbulence-driven $CO_2$ degassing (Fig. 18B to D). If the vent flux then remains high, a thick apron and channel facies travertine will form over the


**Fig. 26.** Field photographs of the life history of a Mammoth Hot Springs travertine hot spring. (A) Progradation of the modern apron and channel facies at Spring AT-1 (November 2002) over the pond facies as vent flow increases. (B) Progradation of the modern apron and channel facies at Spring AT-3 (October 2005) over the lip of the pond facies as vent flow increases. (C) Progradation of the modern apron and channel facies at Spring AT-1 (November 2002) over the proximal-slope facies as vent flow increases. (D) Progradation of recent (*ca* 100 years old) apron and channel facies over the pond facies at Highland Terrace. (E) Retrogradation and stranding of the modern vent facies and apron and channel facies at Spring AT-1 (November 2002) as vent flow decreased. (F) Upstream retrogradation of the modern apron and channel facies at Spring AT-1 (January 2001) as vent flow decreased.

pond lip (Fig. 26C). These lateral and downward shifts in travertine depositional facies are commonly observed in the Holocene and Pleistocene travertine stratigraphy of MHS and Gardiner (Fig. 26D). The amount of vertical travertine accumulation in these ancient travertine deposits

is significantly larger than that observed in Holocene travertine deposited atop the MHS complex; this requires that Phase 3 was sustained for longer periods of time in the past than in the modern.

Phase 4 begins with a rapid decrease in the flux of spring-water from the vent, during which time the entire drainage system instantaneously progresses into a low flow retrograde mode. Under these conditions, each temperature and pH defined section of the primary flow path shortens significantly and migrates to upstream positions. As a result, the site of precipitation for each travertine depositional facies also shifts upstream and 'back-steps' to locations significantly closer to the vent (Fig. 26E and F). Finally, Phase 5 occurs when all spring-water outflow from the vent has ceased and the drainage system becomes dry. At this stage, all of the travertine deposits are exposed to the atmosphere and subjected to physical erosion and diagenetic alteration. A new spring-water system later emerges that will start the cycle again and rapidly precipitate travertine, and bury the older deposits.

At least two different microbial $CaCO_3$ biomineralization responses appear to be associated with these Phase 1 to Phase 5 hot-spring hydrological cycles. Under high-flow conditions, it is advantageous for microbes to increase crystal growth rates to support filament growth at locations further downstream (Fig. 26F). The filamentous mats grow just below the uppermost surface of the spring-water sheet flow and, thus, instantaneously shift the lateral position of travertine encrustation to track the shift in niche environment as the flow increases (Fig. 26F). Presumably, this is the same microbial catalytic effect identified with the ISKA experimentation (Kandianis *et al.*, 2008). In contrast, under low-flow conditions, it is advantageous for the micro-organisms to retard $CaCO_3$ crystal growth to prevent becoming stranded downstream in lower-temperature aqueous environments (Fouke *et al.*, 2003; Veysey *et al.*, 2008). Therefore, $CaCO_3$ precipitation is influenced by the different responses of an organism to survive environmental change.

## HOLOCENE AND PLEISTOCENE TRAVERTINE

The Mammoth–Gardiner corridor contains a depositional sequence of ancient Pleistocene and Holocene hot-spring travertine deposits that are directly analogous to the active modern deposits at MHS. As a result, the modern MHS travertine facies model can be used as a comparative standard with which to reconstruct and gauge the spring-water chemistry, hydrodynamics and microbial ecology that was present during deposition of the ancient travertine (Veysey *et al.*, 2008). The Mammoth–Gardiner corridor deposits include: (i) Holocene travertine deposits (≤100s to 10 000 YBP) at MHS that were penetrated by the USGS Y-10 well (Fig. 5A and C), which were shown to be 73 m thick and range from 0 to 7700 ± 440 YBP (White *et al.*, 1975; Sorey, 1991; Sturchio, 1992); and (ii) Pleistocene travertine deposits (as old as 31 000 YBP) in Gardiner, Montana (Fig. 27), which were precipitated during small-scale retreats of the Pinedale Glacier (Sorey, 1991; Sturchio *et al.*, 1994).

Recent travertine deposits (≤100s YBP) form a veneer tens of metres in thickness at various sites across the top and sides of the MHS complex. These travertine deposits are exposed in cross-sectional outcrops along the Upper Terrace Drive, as well as along the many boardwalks that transect the centre of the MHS complex (Fig. 26D). The Y-10 well travertine is interbedded near the base with siliciclastic sandstones, whereas the whole section directly overlies Cretaceous siliciclastic sandstones and mudstones (Figs 4 and 5C; White *et al.*, 1975; Chafetz & Guidry, 2003). A *ca* 100 m thick sequence of Pleistocene travertine terraces was deposited on the mountain slopes immediately south of Gardiner, Montana (Fig. 27; Fraser *et al.*, 1969; Sorey, 1991). The complex stratigraphic relationships between glacial diamictites and travertine (Fig. 28F) have been coupled with uranium-series age dating of the travertine. Results indicate that the Gardiner Pleistocene hot springs were active from as early as 38 700 YBP to as recently as 19 500 YBP, during which the Pinedale Glacier filled the valley floor (Sturchio *et al.*, 1994).

Highly variable degrees of meteoric diagenesis have affected the Holocene and Pleistocene travertine outcrops and core (Guidry & Chafetz, 2003a,b). However, the primary depositional fabrics commonly are preserved and consistent with those observed in the modern MHS hot-spring travertine facies (Fig. 28). Quarrying in the Gardiner Pleistocene terraces has also exposed continuous 5 m thick outcrops that cut parallel to flow through thick, well-exposed, sequences of ancient proximal-slope travertine (Fig. 29). Future studies will be able to utilize these distinct stratigraphic packages of proximal-slope progradation and aggradation to correlate and reconstruct ancient depositional, hydrological and

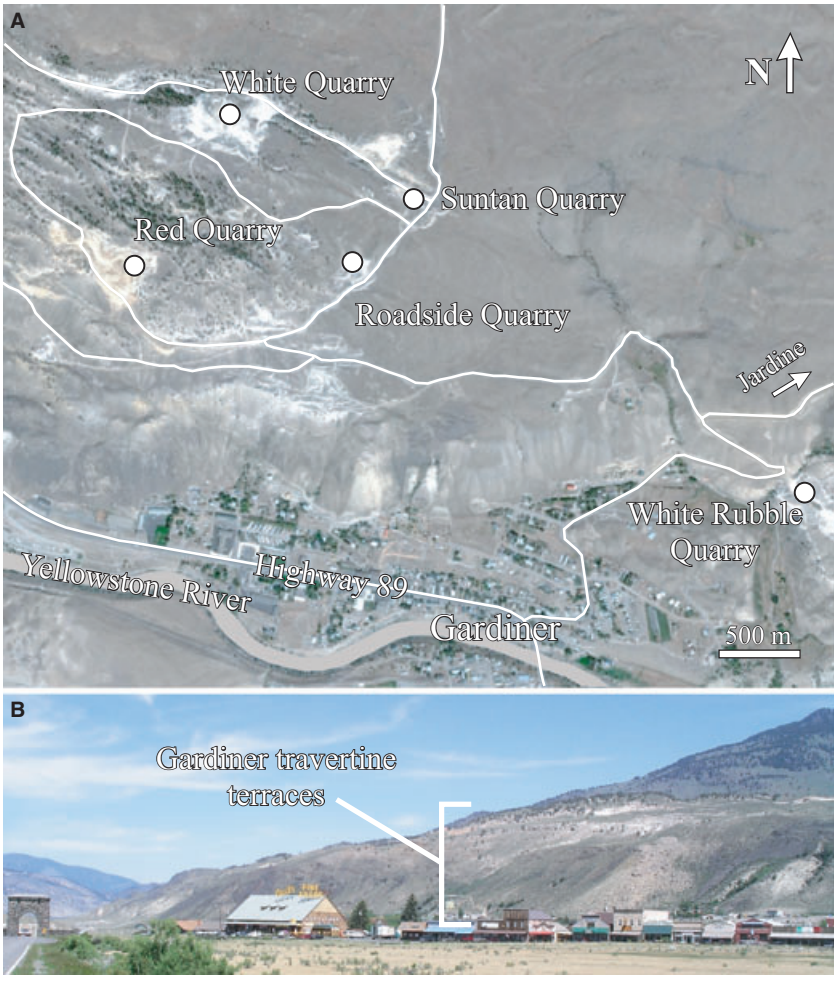


**Fig. 27.** The travertine terraces of Gardiner, Montana. (A) Aerial photograph with line tracings showing the location of quarries and roads. (B) Field photograph from the northern entrance of Yellowstone National Park.

diagenetic events. Diagenetic alteration of the ancient travertine crystalline microfabrics and geochemical compositions is highly variable and patchy, ranging from the extremes of excellent preservation to complete diagenetic alteration. Plane-light and cathodoluminescence-light (CL) petrography of travertine from Highland Terrace, the Y-10 core and the Gardiner Quarry have documented a complex multi-stage paragenetic sequence of post-depositional (diagenetic) events; this includes partial to complete replacement of original non-CL proximal-slope facies travertine with bright orange CL feather calcite crystals during meteoric diagenesis (Fig. 30). Travertine meteoric alteration has also been documented by the enrichment of Mg, depletion of Sr and Ba (Sturchio *et al.*, 1994) and co-varying decreases in $\delta^{18}O$ and $\delta^{13}C$ (Guidry & Chafetz, 2003a,b). Conversely, excellent preservation of at least some original travertine geochemistry is implied by primary fluid inclusion homogenization temperatures of 48°C to 62°C in Holocene pond-facies travertine from Highland Terrace (Fig. 31). The modern MHS facies model will be utilized similarly in future studies as a base line comparative standard with which to reconstruct spring-water environmental conditions from ancient travertine (Fig. 9).

## BROADER SYSTEMS GEOBIOLOGY IMPACTS OF MAMMOTH HOT SPRINGS RESEARCH

The research at Mammoth Hot Springs (MHS) summarized in this review can now be expanded to inform broader Systems Geobiology investigations of the interactions between life and Earth through geological time. The discrepancy in the interpretation of controlling processes at different length-scales highlights the challenges implicit to correlating measurements and interpretations across a broad 'Powers of 10' spectrum (Fig. 8). This concluding section will address how MHS


**Fig. 28.** Field photographs of modern and ancient travertine facies. (A) Modern microterracettes in the proximal-slope facies at Spring AT-1 in November 2002. (B) Microterracettes dated at *ca* 100 years before present (YBP) in the proximal-slope facies at Highland Terrace at Mammoth. (C) Microterracettes in the proximal-slope facies at the Gardiner travertine quarry dated at *ca* 30 000 YBP. (D) Cross-section of streamer fabrics in the apron and channel facies at Highland Terrace dated at *ca* 100 YBP. (E) Cross-section of layered travertine shrubs comprising pond facies at the Gardiner travertine quarry dated at *ca* 30 000 YBP. (F) Gardiner travertine stratigraphy at Sun Tan Quarry exhibiting basalt and glacial diamictite dated at *ca* 30 000 YBP.


**Fig. 29.** Field photograph of a wall left after excavation of travertine from the Gardiner White Quarry. The outcrop is a cross-section parallel to the flow direction within the proximal-slope facies and has been dated at *ca* 30 000 YBP. Primary bedding planes within the outcrop are highlighted with black lines, illustrating changes in geomorphology during simultaneous aggradation and progradation of the Proximal-Slope Facies travertine deposits.

travertine–water–microbe research has begun to link abiotic and biotic controls across large spatial hierarchies, and provided results for direct application to other important modern and ancient environments of $CaCO_3$ deposition.

## Strategic physical, chemical and biological characterization

Multi-disciplinary research at MHS has required that multiple physical, chemical and biological components be measured. However, initially it was unknown specifically which of the many parameters making up these components would be logistically feasible to measure and scientifically necessary to determine controls on travertine formation. Thus, a minimal set of parameters was chosen to simultaneously track abiotic and biotic processes (Fig. 8). Travertine analyses included measurements of geomorphology, crystal growth (size, shape, porosity and structural organization at multiple scales), mineralogy, surface area and elemental and isotopic geochemistry (Ca, Mg, Sr, Mn, Fe, $SO_4$, $\delta^{13}C$, $\delta^{18}O$, $\delta^{34}S$ and $^{87}Sr/^{86}Sr$). Spring-water measurements included temperature, pH, flow dynamics (primary flow path, depth, velocity and flux) and elemental and isotopic geochemistry (DO, DIC, alkalinity, S, $SO_4$, $NO_4$, Ca, Mg, Sr, Mn, Fe, Si, $\delta^{13}C$, $\delta^{18}O$, $\delta^{34}S$ and $^{87}Sr/^{86}Sr$). Finally, microbial community analyses included community structure and phylogenetic diversity (field and microscope observations, 16S rRNA gene sequence clone libraries and T-RFLP), metabolic activity as inferred from gene composition (16S rRNA, T-RFLP and metagenomics) and biochemistry (lipids and their $\delta^{13}C$ signatures). This short list of travertine–water–microbe parameters can serve as a reasonable starting point for Systems Geobiology characterization of other environments of limestone deposition.

## Linking geological and biological controls across broad spatial scales

As previously described, modelling suggests that the formation of macroscopic travertine accumulation patterns may be controlled primarily by

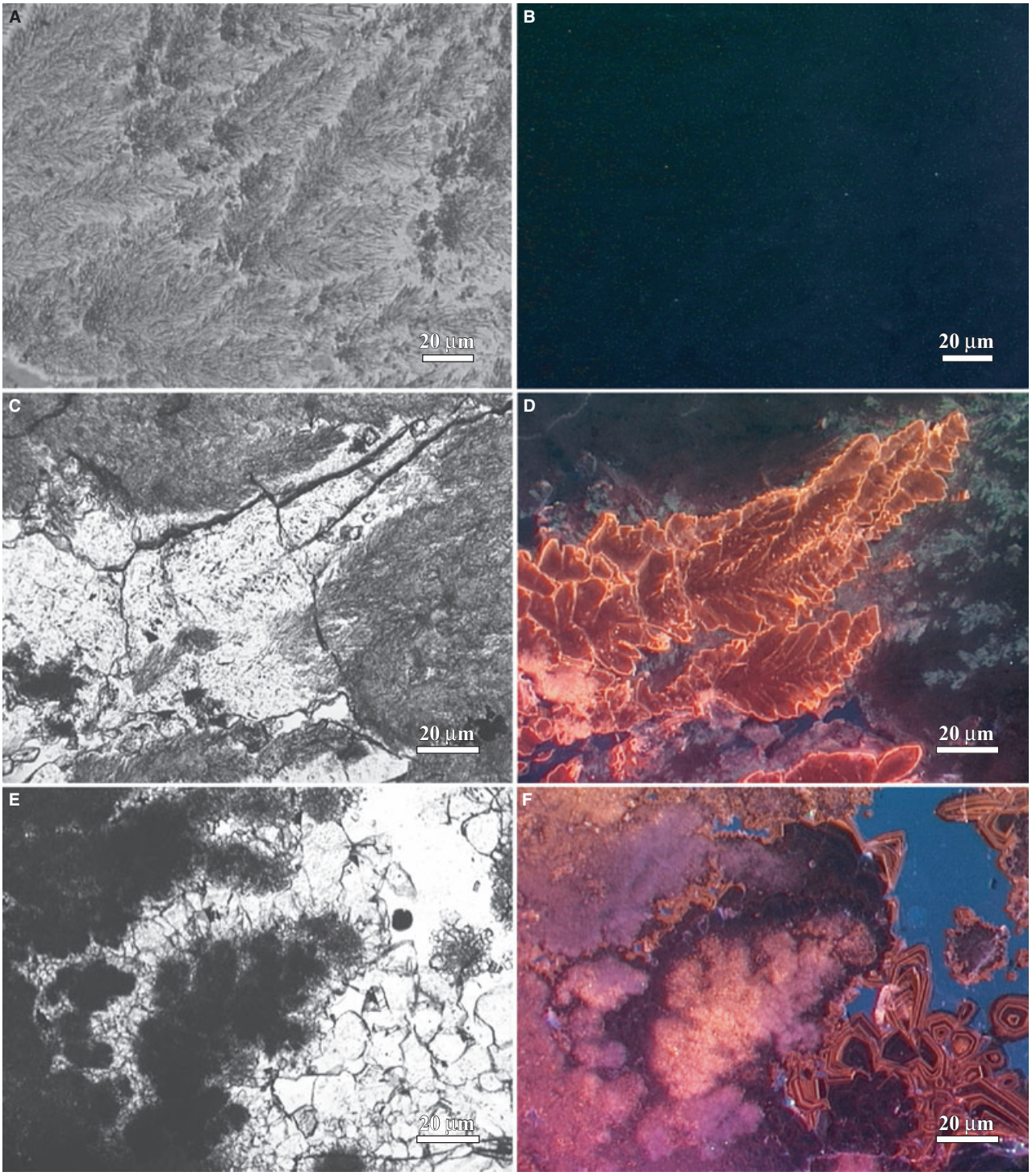


**Fig. 30.** Paired plane-light (left images) and cathodoluminescence (CL)-light (right images) petrography of modern and ancient travertine at Mammoth Hot Springs and Gardiner. (A) and (B) Modern non-CL proximal-slope facies travertine from Spring AT-1. (C) and (D) Recent (*ca* 100 YBP) proximal-slope facies travertine from Highland Terrace at MHS. Bright orange CL feather calcite crystals are diagenetically replacing non-CL aragonite shrubs. (E) and (F) Ancient (*ca* 30 000 YBP) pond facies travertine from Sun Tan Quarry at Gardiner. Non-CL travertine shrubs have been replaced by mauve CL calcites, and multiple generations of later stage calcite cements that exhibit dark brown to bright orange concentrically-zoned CL.

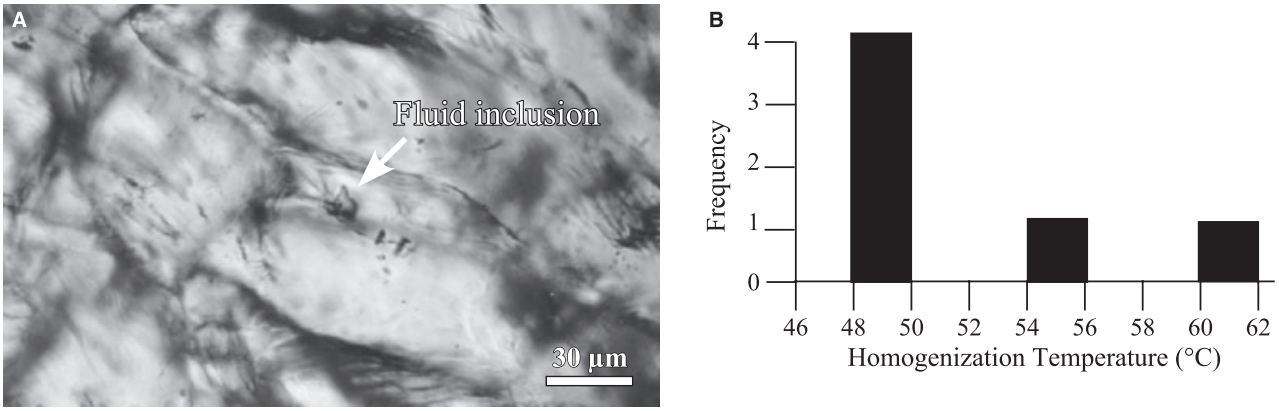


**Fig. 31.** Fluid inclusions within 100 YBP calcite crystals in the pond facies at Highland Terrace in the MHS complex. (A) Plane-light photomicrograph. (B) Frequency histogram of homogenization temperatures.

abiotic geological phenomena (Veysey & Goldenfeld, 2008). Conversely, field experimentation at the mesoscopic and microscopic scales suggests that travertine formation is controlled primarily by biological phenomena (Kandianis *et al.*, 2008). Therefore, a significant next step in Systems Geobiology research at MHS will be to establish a unifying synthesis of how abiotic and biotic factors combine to differentially influence travertine formation across the $10^{16}$ spatial hierarchy to create natural travertine deposits.

Three primary and interrelated phenomena in complex hot-spring environments are acknowledged, which include: (i) *mechanisms:* the most fundamental organizations of microscopic primary entities and activities that will produce changes and transformations (causal attribution, Ahn *et al.*, 1995; Stumm & Morgan, 1996); (ii) *processes:* an observed series of mesoscale interactions, events and changes that result from mechanistic interactions; and (iii) *patterns:* emergent macroscale groupings of organization and behaviour that are produced consistently and reproduced by similar natural systems (either self-organized or externally forced; Paola, 2000). With this conceptual framework in mind, future MHS studies will be able to test controls on travertine precipitation by combining field observation, field experimentation and laboratory experimentation with theoretical modelling.

For example, field and laboratory experiments can now be conducted that directly control microbial content, flow dynamics and precipitation to produce travertine accumulation patterns predicted by cell dynamical system (CDS) simulations. To compliment the field *in situ* kinetic apparatus (ISKA) for these studies (Kandianis *et al.*, 2008), a laboratory *in vitro* kinetic apparatus (IVKA) has also been developed (Fig. 25F). The IVKA can be used to collect coupled travertine–water–microbe samples that document coincident shifts between microbial community composition, spring-water chemistry and flow, and travertine crystalline structure, mineralogy and geomorphology. Iterative comparison and testing can then be completed between strategic travertine samples (natural hot spring, ISKA and IVKA experimental samples) and mathematical models.

Using this type of linked field and experimental approach, future studies of the *Sulfurihydrogenibium*-dominated microbial communities in the apron and channel facies will be able to simultaneously track: (i) highly exergonic reactions involving the oxidation of reduced S species by low-levels of dissolved $O_2$(aq), which include $H_2S/S^o$, $H_2S/SO_4^{-2}$ and $S^o/SO_4^{-2}$; (ii) primitive chemolithotrophic metabolic oxidation of $H_2$ with $S^o$; and (iii) highly exergonic oxidation of $H_2AsO_4^-$ by low-levels of dissolved $O_2$(aq). The vertical and horizontal spatial heterogeneity of these reactions along the primary flow path of the MHS apron and channel facies (Veysey *et al.*, 2008) could then be mechanistically modelled with observed changes in the content of *Sulfurihydrogenibium* lipids, proteins and extracellular matrix materials (Zhang *et al.*, 2004). These co-variations in physical, chemical and biological parameters can then be numerically modelled to determine how microbial activity relates to $CaCO_3$ crystal precipitation dynamics, thus permitting microbial diversity to be correlated with dynamic chemical equilibrium and kinetic models of the spring-water.

## Application to other modern and ancient sedimentary environments

Several promising research opportunities exist to apply the understandings of geological and biological controls on travertine deposition derived from MHS to other important modern and ancient depositional environments. One example is to systematically apply the modern MHS travertine–water–microbe analyses to sequentially older and older fossil travertine deposits back to 8000 YBP at MHS (Fig. 5B) and back to 33 000 YBP in the Gardiner quarries (Figs 27 to 31). Another important opportunity would be to apply the experimental and theoretical approaches developed to study travertine formation at MHS to the siliceous springs that occur throughout the rest of Yosemite National Park (YNP; Fig. 2A). Siliceous hot spring systems such as those in the Hayden Valley of YNP exhibit sinter depositional geomorphologies and facies successions that are strikingly similar to those at MHS (Fig. 32). Previous studies on siliceous hot springs around the world (Campbell *et al.*, 2001; Lowe *et al.*, 2001; Hinman & Walter, 2002; Guidry & Chafetz, 2003a,b; Jones & Renaut, 2003a,b; Vitale *et al.*, 2008) suggest that strong correlations may exist between distinct types of $SiO_2$ mineral deposits (sinter) and microbial community composition. Furthermore, these studies suggest that sinter growth rates may be fast enough to successfully apply the ISKA and IVKA in these siliceous hot-spring systems.

Another example of the potential application of results from MHS is to help better understand the density banding in the aragonitic skeleton of scleractinian corals. It is currently assumed that coral skeletal density banding patterns represent

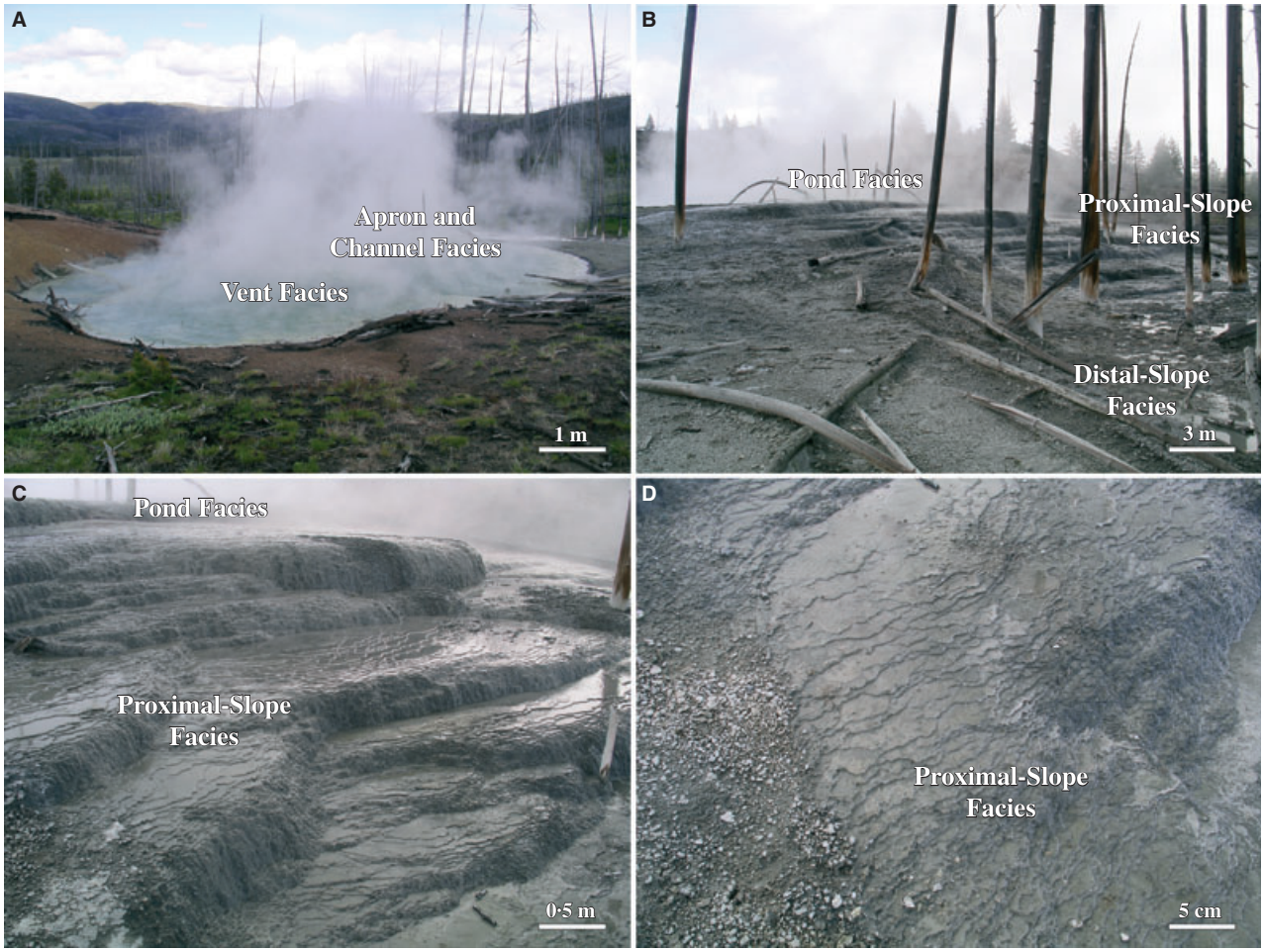


**Fig. 32.** Field photographs of similarities in $SiO_2$ sinter deposits (October 2007) in a spring near Monument at the northern rim of the Yellowstone caldera. Vent spring-water is expelled at a temperature of 100°C and a pH of 3. (A) to (D) Sinter terracette and microterracette distributions along the spring drainage system that, at a gross field-scale geomorphology, resemble those of the travertine vent, apron and channel, pond, proximal-slope and distal-slope facies.

seasonal changes in sea surface temperature and, thus, fossil banding is commonly used for palaeothermometry, palaeoclimatology and palaeoecology reconstructions (Moses *et al.*, 2006; Lough & Barnes, 1997; Barnes & Lough, 1993; Tambutte *et al.*, 2007; Helman *et al.*, 2008; Vago, 2008). However, a detailed understanding of the mechanisms and processes controlling skeletal aragonite nucleation and crystallization events, such as the rate of skeletal growth, remain less certain. Travertine and coral skeleton aragonite are obviously deposited under extremely different environmental and biological conditions, and they exhibit significant structural differences at the scale of *ca* 100 μm and greater. However, there are many chemical and physical similarities between travertine and coral skeletons at the tens of micron-scale and smaller. This observation opens up the possibility that the organic matrix in corals may influence coral skeletal growth rate in a manner that is directly analogous to that of microbial biomass catalysis observed in hot-spring travertine aragonite precipitation (Kandianis *et al.*, 2008). The crystallization rate equations formalization from the results of the ISKA experiment at MHS (Kandianis *et al.*, 2008) will allow this hypothesis to be tested in future Systems Geobiology studies of coral skeletal growth.

## ACKNOWLEDGEMENTS

This work was supported by the National Science Foundation Biocomplexity in the Environment Coupled Biogeochemical Cycles Program (EAR 0221743), the National Science Foundation Geosciences Postdoctoral Research Fellowship Program (EAR-0000501), the Petroleum Research Fund of the American Chemical Society Starter Grant Program (34549-G2), and the University of Illinois Urbana-Champaign Critical Research Initiative. Research was completed under YNP NPS research permit number 3060R. Conclusions in this study are those of the author and do not necessarily reflect those of the funding or permitting agencies. I gratefully acknowledge the many years of colleagueship and close working collaboration with NPS Rangers at YNP that made this work possible. Christie Hendrix, Robert Fuhrman, Ellen Petrick, Brian Suderman and Henry Heasler have been especially pivotal in issuing permits, assisting in the collection of data and co-ordinating multiple research and educational activities for more than a decade. The many invaluable and significant contributions toward this work provided by all members of the Fouke laboratory research group at Illinois are gratefully acknowledged, with special recognition to George Bonheyo, Michael Kandianis, Robert Sanford, Jorge Frias-Lopez, Roy Johnson, Philip Miller, Samantha Dwyer, Holly Vescogni, Shane Butler, Kelly Hutchins, Beth Sanzenbacher, David Fike, Amanda Oehlert, Alan Piggot, James Klaus and Yiran Dong. Results from unpublished MSc theses (Thomas Schickel, Holly Vescogni, Shane Butler and Alexandria Kameda) and BSc theses (Philip Miller and Samantha Dwyer) also made significant contributions to this review. Unpublished fluid inclusion analyses by Robert Goldstein and unpublished molecular microbial ecology analyses conducted by the laboratory group of Alison Murray were also incorporated. Discussions with Abigail Salyers, Carl Woese, Nigel Goldenfeld, Peter Yau, John Veysey, Hector Garcia Martin, Lisa Morgan and Pat Shanks were essential to improving all aspects of the research from data collection through interpretation and synthesis. Robert Goldstein is gratefully acknowledged for providing petrographic and geochemical analyses of travertine fluid inclusions. Extensive reviewer comments provided by James Best, Andrew Knoll, Martyn Pedley and an anonymous reviewer were particularly insightful and served to significantly improve the structure and content of the manuscript.

## REFERENCES

**Agouron** (2001) *Geobiology: Current Technology and Resource Needs*. Agouron Institute, Pasadena, 43 pp.

**Ahn, W.-K., Kalish, C.W., Medin, D.L.** and **Gelman, S.A.** (1995) The role of covariation versus mechanism information in causal attribution. *Cognition*, **54,** 299–352.

**Allen, E.T.** and **Day, A.L.** (1935) *Hot Springs of the Yellowstone National Park*. Carnegie Institution, Washington, DC, 466, 525 pp.

**Allen, C.C., Albert, F.G., Chafetz, H.S., Combie, J., Graham, C.R., Kieft, T.L., Kivett, S.J., McKay, D.S., Steele, A., Taunton, A.E., Taylor, M.R.** and **Thomas-Keptra, K.L.** (2000) Microscopic physical markers in carbonate hot springs: implications in the search for life on Mars. *Icarus*, **147,** 49–67.

**Amend, J.P.** and **Shock, E.L.** (2001) Energetics of overall metabolic reactions of thermophilic and hyperthermophilic Archaea and Bacteria. *FEMS Microbiol. Rev.*, **25,** 175–243.

**Amend, J.P., Rogers, K.L.** and **Meyer-Dombard, D.R.** (2004) Microbially mediated sulfur-redox: energetics in marine hydrothermal vent systems. In: *Sulfur Biogeochemistry – Past and Present* (Eds J.P. Amend, R.A. Edwards and B.Y. Lynne), *Geol. Soc. Am.*, **379,** 17–34.

**Amundson, R.** and **Kelly, E.** (1987) The chemistry and mineralogy of a $CO_2$-rich travertine depositing spring in the

California Coast Range. *Geochim. Cosmochim. Acta*, **51,** 2883–2890.

**Anderson, P.W.** (1972) More is different. *Science*, **177,** 394–396.

**ASM** (2001) *Geobiology: Exploring the Interface Between the Biosphere and the Geosphere*. American Academy of Microbiology, Washington, DC, 57 pp.

**Balmforth, N.J.** and **Mandre, S.** (2004) Dynamics of roll waves. *J. Fluid Mech.*, **514,** 1–33.

**Banfield, J.F.** and **Nealson, K.H.** (1997) Geomicrobiology: interactions between microbes and minerals. *Rev. Mineral.*, **35,** Mineralogical Society of America, Washington, DC, 448.

**Bargar, K.E.** (1978) Geology and thermal history of Mammoth Hot Springs, Yellowstone National Park, Wyoming. *U.S. Geol. Surv. Bull.*, **1444,** 54.

**Barnes, W.M.** (1992) The fidelity of Taq polymerase catalyzing PCR is improved by an N-terminal deletion. *Gene*, **112,** 29–35.

**Barnes, D.J.** and **Lough, J.M.** (1993) On the nature and causes of density banding in massive coral skeletons. *J. Exp. Mar. Biol. Ecol.*, **167,** 91–108.

**Berner, R.A.** (1980) *Early Diagenesis: A Theoretical Approach*. Princeton University Press, Princeton, NJ, 245 pp.

**Blow, N.** (2008) Exploring unseen communities. *Nature*, **453,** 687–690; 687–690.

**Bonheyo, G.T., Frias-Lopez, J.** and **Fouke, B.W.** (2005) A test for airborne dispersal of thermophilic bacteria from hot springs. In: *Geothermal Biology and Geochemistry in Yellowstone National Park. Proceedings of the Thermal Biology Institute Workshop, Yellowstone National Park, WY* (Eds W.P. Inskeep and T.R. McDermott), pp. 327–342. Montana State University Press, Bozeman.

**Bosak, T.** and **Newman, D.K.** (2005) Microbial kinetic controls on calcite morphology in supersaturated solutions. *J. Sediment. Res.*, **75,** 190–199.

**Brock, T.D.** (1978) *Thermophilic Microorganisms and Life at High Temperatures*. Springer-Verlag, New York, 465 pp.

**Buczynski, C.** and **Chafetz, H.S.** (1991) Habit of bacterially induced precipitates of calcium carbonate and the influence of medium viscosity on mineralogy. *J. Sediment. Petrol.*, **61,** 226–233.

**Burton, E.A.** and **Walter, L.M.** (1987) Relative precipitation rates of aragonite and Mg calcite from seawater: temperature or carbonate ion control?. *Geology*, **15,** 111–114.

**Campbell, K.A., Sannazzaro, K., Rodgers, K.A., Herdianta, N.R.** and **Browne, P.R.I.** (2001) Sedimentary facies and mineralogy of the Late Pleistocene Umukuri silica sinter, Taupo Volcanic Zone, New Zealand. *J. Sediment. Res.*, **71,** 727–746.

**Chafetz, H.S.** and **Buczynski, C.** (1992) Bacterially induced lithification of microbial mats. *Palaios*, **7,** 277–293.

**Chafetz, H.S.** and **Folk, R.L.** (1984) Travertines: depositional morphology and the bacterially constructed constituents. *J. Sediment. Petrol.*, **54,** 289–386.

**Chafetz, H.S.** and **Guidry, S.A.** (2003) Deposition and diagenesis of Mammoth hot Springs travertine, Yellowstone National Park, Wyoming, USA. *Canadian J. Earth Sci.*, **40,** 1515–1529.

**Chafetz, H.S., Rush, P.F.** and **Utech, N.M.** (1991) Microenvironmental controls on mineralogy and habit of $CaCO_3$ precipitates: an example from an active travertine system. *Sedimentology*, **38,** 107–126.

**Chan, C.Y.** and **Goldenfeld, N.** (2007) Steady states and linear stability analysis of precipitation pattern formation at geothermal hot springs. *Phys. Rev. E*, **76,** 1–11.

**Chekroun, K.B., Rodriguez-Navarro, C., Gonzalez-Munoz, M.T., Arias, J.M., Cultrone, G.** and **Rodriguez-Gallego, M.** (2004) Precipitation and growth morphology of calcium carbonate induced by Myxococcus Xanthus: Implications for recognition of bacterial carbonates. *J. Sediment. Res.*, **74,** 868–876.

**Christiansen, R.L., Lowenstern, J.B., Morgan, L.A., Nathenson, M., Mastin, L.G., Muffler, L.J.P.** and **Robinson, J.E.** (2007) Preliminary assessment of volcanic and hydrothermal hazards in Yellowstone National Park and vicinity. *U.S. Geol. Surv. Open-File Rep.*, **71,** 94.

**Cross, T.A.** and **Homewood, P.W.** (1997) Amanz Gressly's role in founding modern stratigraphy. *Geol. Soc. Am. Bull.*, **109,** 1617–1630.

**D'Alessio, S.J.D., Pascal, J.P.** and **Jasmine, H.A.** (2009) Instability in gravity-driven flow over uneven surfaces. *Phys. Fluids*, **21,** 1–11.

**Dilek, Y., Furned, H.** and **Muelenbachs, K.** (2008) *Links Between Geological Processes, Microbial Activities and Evolution of Life*. Springer-Verlag and Business Media B.V., Berlin, 348 pp.

**Dinsdale, A.D., Edwards, R.A., Hall, D., Angly, F., Breibart, M., Brulc, J.M., Furlan, M., Desnues, C., Haynes, M., Li, L., McDaniel, L., Moran, M.A., Nelson, K.E., Nilsson, C., Olson, R., Paul, J., Rodriguez Brito, B., Ruan, Y., Swan, B.K., Stevens, R., Valentine, D.L., Vega Thurber, R., Wegley, L., White, B.A.** and **Rohwer, F.** (2008) Functional metagenomic profiling in nine biomes. *Nature*, **452,** 629–633.

**Dodick, J.** and **Orion, N.** (2006) Building an understanding of geological time: a cognitive synthesis of the ''macro'' and ''micro'' scales of time. In: *Earth and Mind: How Geologists Think and Learn About the Earth* (Eds C.A. Manduca and D.W. Mogk), pp. 77–93. Geological Society of America, Boulder, CO.

**Dreybrodt, W., Buhman, D., Michaelis, J.** and **Usdowski, E.** (1992) Geochemically controlled calcite precipitation by $CO_2$ outgassing: Field measurements of precipitation rates in comparison to theoretical predictions. *Chem. Geol.*, **97,** 285–294.

**Dyer, B.D.** (2003) *A Field Guide to Bacteria*. Cornell University Press, Ithaca, NY, 355 pp.

**Ehrlich, H.L.** and **Newman, D.K.** (2009) *Geomicrobiology*. CRC Press, Boca Raton, 606 pp.

**Farmer, J.D.** (2000) Hydrothermal systems: doorways to early biosphere evolution. *GSA Today*, **10,** 1–9.

**Farmer, J.D.** and **Des Marais, D.J.** (1994a) Biological versus inorganic processes in stromatolite morphogenesis: observations from mineralizing sedimentary systems. In: *Microbial Mats: Structure, Development, and Environmental Significance* (Eds L.J. Stal and P. Caumette), *NATO ASI Series Ecol. Sci.*, **G-35,** pp. 61–68. Springer-Verlag, Berlin.

**Farmer, J.D.** and **Des Marais, D.J.** (1994b) Exopaleontology and the search for a fossil record on Mars. *Lunar Planet. Sci.*, **25,** 367–368.

**Ferris, F.G., Phoenix, V., Fujita, Y.** and **Smith, R.W.** (2004) Kinetics of calcite precipitation induced by ureolytic bacteria at 10 to 20°C in artificial groundwater. *Geochim. Cosmochim. Acta*, **68,** 1701–1722.

**Fishbain, S., Dillon, J.G., Heidi, H.L.** and **Stahl, D.A.** (2003) Linkage of high rates of sulfate reduction in Yellowstone Hot Springs to unique sequence types in the dissimilatory sulfate respiration pathway. *Appl. Environ. Microbiol.*, **69,** 3663–3667.

**Flügel, E.** (2004) *Microfacies of Carbonate Rocks: Analysis, Interpretation, and Application*. Springer, Berlin, New York, 976 pp.

**Folk, R.L.** (1993) SEM imaging of bacteria and nannobacteria in carbonate sediments and rocks. *J. Sediment. Petrol.*, **63,** 990–999.

**Folk, R.L.** (1994) Interaction between bacteria, nannobacteria, and mineral precipitation in hot springs of central Italy. *Géograph. Phys. Quatern.*, **48,** 233–246.

**Folk, R.L., Chafetz, H.S.** and **Tiezzi, P.A.** (1985) Bizarre forms of depositional and diagenetic calcite in hot-spring travertines, central Italy. In: *Carbonate Cements* (Eds P. Schneidermann and P.M. Harris), *SEPM Spec. Publ.*, **36,** 349–369.

**Ford, T.D.** and **Pedley, H.M.** (1996) A review of tufa and travertine deposits of the world. *Earth-Sci. Rev.*, **41,** 117–175.

**Fouke, B.W., Farmer, J.D., Des Marais, D.J., Pratt, L., Sturchio, N.C., Burns, P.C.** and **Discipulo, M.K.** (2000) Depositional facies and aqueous-solid geochemistry of travertine-depositing hot springs (Angel Terrace, Mammoth Hot Springs, Yellowstone National Park, USA). *J. Sediment. Res.*, **70,** 265–285.

**Fouke, B.W., Farmer, J.D., Des Marais, D.J., Pratt, L., Sturchio, N.C., Burns, P.C.** and **Discipulo, M.K.** (2001) Reply-Depositional facies and aqueous-solid geochemistry of travertine-depositing hot springs (Angel Terrace, Mammoth Hot Springs, Yellowstone National Park, USA). *J. Sediment. Res.*, **71,** 497–500.

**Fouke, B.W., Bonheyo, G.T., Sanzenbacher, E.** and **Frias-Lopez, J.** (2003) Partitioning of bacterial communities between travertine depositional facies at Mammoth Hot Springs, Yellowstone National Park, USA. *Can. J. Earth. Sci.*, **40,** 1531–1548.

**Fournier, R.O.** (1989) Geochemistry and dynamics of the Yellowstone National Park hydrothermal system. *Annu. Rev. Earth Planet Sci.*, **17,** 13–53.

**Fournier, R.O.** (2005) Geochenistry and dynamics of the Yellowstone National Park hydrothermal system. In: *Geothermal Biology and Geochemistry in Yellowsotne National Park* (Eds W. Inskeep and T. McDermott), pp. 3–30. Montana State University Press, Bozeman.

**Fraser, G.D., Waldorp, H.A.** and **Hyden, H.J.** (1969) *Geology of the Gardiner area, Park County, Montana*, United States Geological Survey Bulletin 1277, 188 pp.

**Frias-Lopez, J., Shi, Y., Tyson, G.W., Coleman, M.L., Schuster, S.C., Chisholm, S.W.** and **Delong, E.F.** (2008) Microbial community gene expression in ocean surface waters. *Proc. Natl Acad. Sci. USA*, **105,** 3805–3810.

**Friedman, I.** (1970) Some investigations of the deposition of travertine from hot springs: I. The isotope chemistry of a travertine-depositing spring. *Geochim. Cosmochim. Acta*, **34,** 1303–1315.

**Garcia, M.H.** (2008) *Sedimentation Engineering: Theorie, Measurements, Modelling and Practice*. American Society for Civil Engineering, Washington, DC, Number 10, 1132 pp.

**Ghosh, W.** and **Dam, B.** (2009) Biochemistryandmolecular biologyof lithotrophic sulfuroxidation by taxonomicallyand ecologicallydiverse bacteria and archaea. *FEMS Microbiol. Rev.* **33,** 999–1043.

**Giovannoni, S.J., Revsbech, N.P., Ward, D.M.** and **Castenholz, R.W.** (1987) Obligately phototrophic Chloroflexus: primary production in anaerobic hot spring microbial mats. *Arch. Microbiol.*, **147,** 80–87.

**Goldenfeld, N.** and **Kadanoff, L.P.** (1999) Simple lessons from complexity. *Science*, **284,** 89–89.

**Goldenfeld, N., Chan, P.Y.** and **Veysey, J.** (2006) Dynamics of precipitation pattern formation at geothermal hot springs. *Phys. Rev. Lett.*, **96,** 1–4.

**Gonfiantini, R.** (1986) Environmental isotopes in lake studies. In: *Handbook of Environmental Isotope Geology: The terrestrial Environment Part B* (Eds P. Fritz and J.C. Fontes), **2**, pp. 113–168. Elsevier, Amsterdam.

**Gressly, A.** (1838) *Observations Géologiques sur le Jura Soleurois*. Nouveaux mémoires de la Société Helvetique des Sciences Naturelles, Neuchâtel, 349 pp.

**Guidry, S.A.** and **Chafetz, H.S.** (2003a) Depositional facies and diagenetic alteration in a relict siliceous hot-spring accumulation: examples from Yellowstone National Park, U.S.A. *J. Sediment. Res.*, **73,** 809–823.

**Guidry, S.A.** and **Chafetz, H.S.** (2003b) Anatomy of siliceous hot springs: examples from Yellowstone National Park, Wyoming, USA. *Sediment. Geol.*, **157,** 71–106.

**Guo, L.** and **Riding, R.** (1992) Aragonite laminae in hot water travertine crusts, Rapolano Terme, Italy. *Sedimentology*, **39,** 1067–1079.

**Guo, L., Andrews, J., Riding, R., Dennis, P.** and **Dresser, Q.** (1996) Possible microbial effects on stable carbon isotopes in hot-spring travertines. *J. Sediment. Res.*, **66,** 468–473.

**Helman, Y., Natale, F., Sherrell, R.M., LaVigne, M., Starovoytov, V., Gorbunov, M.Y.** and **Falkowski, P.G.** (2008) Extracellular matrix production and calcium carbonate precipitation by coral cells in vitro. *Proc. Natl Acad. Sci. USA*, **105,** 54–58.

**Hinman, N.W.** and **Walter, M.R.** (2002) Textural preservation in siliceous hot spring deposits during early diagenesis: examples from Yellowstone National Park and Nevada, U.S.A. *J. Sedment. Res.*, **75,** 200–215.

**Huggenholtz, P., Pitulle, C., Hershberger, K.L.** and **Pace, N.R.** (1998) Novel division level bacterial diversity in a Yellowstone hot spring. *J. Bacteriol.*, **180,** 366–376.

**Hughes, J.B., Hellmann, J.J., Ricketts, T.H.** and **Bohannan, B.J.M.** (2001) Counting the uncountable: statistical approaches to estimating microbial diversity. *Appl. Environ. Microbiol.*, **67,** 4399–4406.

**Hurst, C.J., Crawford, R.L., Knudsen, G.R., McInernery, M.J.** and **Stetzenbach, L.D.** (2002) *Manual of Environmental Microbiology*. American Society for Microbiology Press, Washington, DC, 456 pp.

**Husen, S.** and **Smith, R.B.** (2004) Evidence for gas and magmatic sources beneath the Yellowstone volcanic field from seismic tomographic imaging. *J. Volcanol. Geotherm. Res.*, **131,** 397–410.

**Inskeep, W.P.** and **Bloom, P.R.** (1985) An evaluation of rate equations for calcite precipitation kinetics at $pCO_2$ less than 0.01 atm and pH greater than 8. *Geochim. Cosmochim. Acta*, **49,** 2165–2180.

**Inskeep, W.P.** and **McDermott, T.R.** (2005) Geomicrobiology of acid-sulfate-chloride springs in Yellowsotne National Park. In: *Geothermal Biology and Geochemistry in Yellowstone National Park* (Eds W.P. Inskeep and T.R. McDermott), pp. 143–162. Montana State University Publications, Bozeman.

**Inskeep, W.P., Ackerman, G.G., Taylor, W.P., Kozubal, M., Korf, S.** and **Macur, R.E.** (2005) On the energetics of chemolithotrophy in nonequilibrium systems: case studies of geothermal springs in Yellowstone National Park. *Geobiology*, **3,** 297–317.

**Inskeep, W.P., Rusch, D.B., Jay, Z., Herrgard, M.J., Kozubal, M.A., Richardson, T.B., Macur, R.E., Hamamura, N., Jennings, R., Fouke, B.W., Reysenbach, A.L., Roberto, F., Young, M., Bateson, M., Schwartz, A., Boyd, E., Badger, J., Geesey, G., Mathur, E.** and **Frazier, M.** (2010) Metagenomes from high-temperature chemotrophic systems reveal

importance of geochemical controls on microbial community structure and function. *PLoS ONE*, **5,** 1–15.

**Jones, B.** and **Renaut, R.W.** (2003a) Hot spring and geyser sinters: the integrated product of precipitation, replacement and deposition. *Canadian J. Earth Sci.*, **40,** 1549–1569.

**Jones, B.** and **Renaut, R.W.** (2003b) Petrography and genesis of spicular and columar geyserite from the Whakarewarewa and Orakeikorako geothermal areas, North Island, New Zealand. *Canadian J. Earth Sci.*, **40,** 1585–1610.

**Kandianis, M.T., Fouke, B.W., Veysey, J., Johnson, R.W.** and **Inskeep, W.** (2008) Microbial biomass: a catalyst for $CaCO_3$ precipitation in advection-dominated transport regimes. *Geol. Soc. Am. Bull.*, **120,** 442–450.

**Kharaka, Y.K., Mariner, R.H., Bullen, T.D., Kennedy, B.M.** and **Sturchio, N.C.** (1991) Geochemical investigations of hydraulic connections between Corwin Springs Known Geothermal Area and adjacent parts of Yellowstone National Park. In: *Effects of Potential Geothermal Development in the Corwin Springs KInown Geothermal Resources Area, Montana, on the Thermal Features of Yellowstone National Park* (Ed. M. Sorey), Water-Resources Investigations Report 91-4052, pp. F1–F38. U.S. Geological Survey, Menlo Park, CA.

**Kharaka, Y.K., Sorey, M.L.** and **Thordsen, J.J.** (2000) Large-scale hydrothermal fluid discharges in the Norris–Mammoth corridor, Yellowstone National Park, USA. *J. Geochem. Explor.*, **68–70,** 201–205.

**Knoll, A.H.** (2003) *Life on a Young Planet: The First Three Billion Years of Evolution on Earth*. Princeton University Press, Princeton, NJ, 277 pp.

**Knorre, H.** and **Krumbein, W.E.** (2000) Bacterial calcification. In: *Microbial Sediments* (Eds R.E. Riding and S.M. Awramik), pp. 25–31. Springer-Verlag, Berlin.

**Konhauser, K.** (2007) *Introduction to Geobiology*. Blackwell Publishing, London, 425 pp.

**Lasaga, A.C.** (1998) *Kinetic Theory in the Earth Sciences*. Princeton University Press, Princeton, 810 pp.

**Lipfert, J.** and **Doniach, S.** (2007) Small-angle X-ray scattering from RNA, proteins, and protein complexes. *Annu. Rev. Biophys. Biomol. Struct.*, **36,** 307–327.

**van Lith, Y., Warthman, R.** and **Vasconcelos, C.** (2003) Microbial fossilization in carbonate sediments: a result of the bacterial surface involvement in dolomite precipitation. *Sedimentology*, **50,** 237–245.

**van Lith, Y., Warthmann, R., Vasconcelos, C.** and **McKenzie, J.A.** (2003) Microbial fossilization in carbonate sediments: a result of the bacterial surface involvement in dolomite precipitation. *Sedimentology*, **50,** 237–245.

**Lough, J.M.** and **Barnes, D.J.** (1997) Several centuries of variation in skeletal extension, density and calcification in massive Porites colonies from the Great Barrier Reef: a proxy for seawater temperature and a background of variability against which to identify unnatural change. *J. Exp. Mar. Biol. Ecol.*, **211,** 29–67.

**Lowe, D.R., Anderson, K.S.** and **Braunstein, D.** (2001) The zonation and structuring of siliceous sinter around hot springs, Yellowstone National Park, and the role of thermophilic bacteria in its deposition. In: *Thermophiles: Biodiversity, Ecology and Evolution* (Eds A.L. Reysenbach, M. Voyteek and R. Mancinelli), pp. 143–166. Kluwer Academic Publishers, Dordrect.

**Lowenstam, H.A.** (1981) Minerals formed by organisms. *Science*, **211,** 1126–1131.

**Lowenstam, H.A.** and **Weiner, S.** (1982) Mineralization by organisms and the evolution of biomineralization. In: *Biomineralization and biological metal accumulation* (Eds P. Westbroek and E.W. DeJong), pp. 191–204. D. Reidel, Dordrecht.

**Lowenstern, J.B.** and **Hurwitz, S.** (2008) Monitoring a supervolcano in repose: heat and volatile flux at the Yellowstone caldera. *Elements*, **4,** 35–40.

**Lynne, B.Y.** and **Campbell, K.A.** (2003) Diagenetic transformations (opal-A to quartz) of low- and mid-temperature microbial textures in siliceous deposits, Taupo Volcanic Zone, New Zealand. *Canadian J. Earth Sci.*, **40,** 1679–1696.

**Madigan, M.** (1984) A novel photosynthetic purple bacterium isolated from a Yellowstone hot spring. *Science*, **225,** 313–314.

**Madigan, M.** (1988) Microbiology, physiology, and ecology of phototrophic bacteria. In: *Biology of Anaerobic Microorganisms* (Ed. A.J.B. Zehnder), pp. 39–111. John Wiley & Sons, New York.

**Madigan, M.** (2001) Thermophylic Anoxygenic Phototrophs. In: *Thermophiles: Biodiversity, Ecology and Evolution* (Eds A.L. Reysenbach, M. Voyteek and R. Mancinelli), pp. 103–124. Kluwer Academic Publishers, Dordrect.

**Madigan, M.** (2003) Anoxygenic phototrophs from extreme environments. *Photosynth. Res.*, **76,** 157–171.

**Madigan, M.** (2005) Diversity of anoxygenic phototrophs in contrasting extreme environments. In: *Geothermal Biology and Geochemistry in Yellowstone National Park*. (Eds W. Inskeep and T. McDermot ), pp. 275–304. Montana State University Press, Bozeman.

**Madigan, M.T., Martinko, J.M.** and **Parker, J.** (2006) *Brock: Biology of Microorganisms*. Pearson Prentice Hall, Upper Saddle River, NJ, 992 pp.

**Mann, S.** (2001) *Biomineralization: Principles and Concepts in Bioinorganic Materials Chemistry*. Oxford University Press, Oxford, 201 pp.

**Martin, H.G.** and **Goldenfeld, N.** (2006a) Estimation of microbial cover distributions at Mammoth Hot Springs using a multiple clone library resampling method. *Environ. Microbiol.*, **8,** 1145–1154.

**Martin, H.G.** and **Goldenfeld, N.** (2006b) Origin of the species–area relationship in ecology. *Proc. Natl Acad. Sci. USA*, **103,** 10310–10315.

**Martin, H.G., Veysey, J., Bonheyo, G.T., Frias-Lopez, J., Goldenfeld, N.** and **Fouke, B.W.** (2010) Statistical evaluation of bacterial 16S rRNA gene sequences in relation to travertine mineral precipitation and water chemistry at Mammoth Hot Springs, Yellowstone National Park, USA. In: *Geomicrobiology: Molecular and Environmental Perspective* (Eds L. Barton, M. Mendl and A. Loy), pp. 223–245. Springer, New York.

**van der Meer, M.T.J., Schouten, S., Damste, J.S.S., de Leeuw, J.W.** and **Ward, D.M.** (2003) Compound-Specific Isotopic Fractionation Patterns Suggest Different Carbon Metabolisms among *Chloroflexus*-Like Bacteria in Hot-Spring Microbial Mats. *Appl. Environ. Microbiol.*, **69,** 6000–6006.

**Meyer-Dombard, D.R., Shock, E.L.** and **Amend, J.P.** (2005) Archaeal and bacterial communities in geochemically diverse hot springs of Yellowstone National Park, USA. *Geobiology*, **3,** 211–227.

**Morgan, L.A., Cathey, H.E.** and **Pierce, K.L.** (2009a) The track of the Yellowstone hot spot: multi-disciplinary perspectives on the origin of the Yellowstone-Snake River Plain Volcanic. *J. Volcanol. Geotherm. Res.*, **188,** issues, 304.

**Morgan, L.A., Shanks, W.C.P.** and **Pierce, K.L.** (2009b) Hydrothermal processes above a large magma chamber. Large hydrothermal systems and hydrothermal explosions

in Yellowstone National Park. *Geol. Soc. Am. Spec. Pap.*, **459,** 95.

**Morrison, P., Morrison, P.** and **Eames, O.R.** (1994) *Powers of 10: A Book About the Relative Size of Things in the Universe and the Effect of Adding Another Zero*. W H Freeman and Company, New York, 194 pp.

**Morse, J.W.** (1983) The kinetics of calcium carbonate dissolution and precipitation, *in* Carbonates: Mineralogy and Chemistry. *Rev. Mineral.*, **11,** 227–264.

**Moses, C.S., Swart, P.K.** and **Dodge, R.E.** (2006) Calibration of stable oxygen isotopes in Siderastrea radians (Cnidaria: Scleractinia): Implications for slow-growing corals. *Geochem. Geophys. Geosyst.*, **7,** 14–34.

**Nakagawa, S., Shtaih, Z., Banta, A., Beveridge, T.J.** and **Sako, Y.** (2005) Sulfurihydrogenibium yellowstonense sp. nov., an extremely thermophilic, facultatively heterotrophic, sulfur-oxidizing bacterium from Yellowstone National Park and amended descriptions of the genus Sulfurihydrogenibium, S. subterraneum, and S. azorense. *Int. J. Syst. Evol. Microbiol.*, **55,** 2263–2268.

**Neuweiler, F., Gautret, P., Volker, T., Lange, R., Michaelis, W.** and **Reitner, J.** (1999) Petrology of lower creataceous carbonate mud mounds (Albian, N. Spain): insights into organomineralic deposits of the geological record. *Sedimentology*, **46,** 837–859.

**Nordstrom, D.K., Ball, J.W.** and **McClesky, R.B.** (2005) Groundwater to surface water: chemistry of thermal outflows in Yellowstone National Park. In: *Geothermal Biology and Geochemistry in Yellowsotne National Park* (Eds W. Inskeep and T. McDermott), pp. 73–94. Montana State University Press, Bozeman.

**NRC** (2007) *The New Science of Metagenomics*. National Academies Press, Washington, DC, 158 pp.

**Paola, C.** (2000) Quantitative models of sedimentary basin filling. *Sedimentology*, **47,** 121–178.

**Papke, R.T., Ramsing, N.B., Bateson, M.M.** and **Ward, D.M.** (2003) Geographical isolation in hot spring cyanobacteria. *Environ. Microbiol.*, **5,** 650–659.

**Pedley, H.M., Rogerson, M.** and **Middleton, R.** (2009) Freshwater calcite precipitates from in vitro mesocosm experiments: a case for biomediation of tufas. *Sedimentology*, **56,** 511–527.

**Pentecost, A.** (1990) The formation of travertine shrubs: Mammoth Hot Springs, Wyoming. *Geol. Mag.*, **127,** 159–168.

**Pentecost, A.** (1995) The quaternary travertine deposits of Europe and Asia Minor. *Quatern. Sci. Rev.*, **14,** 1005–1028.

**Pentecost, A.** (2005) *Travertine*. Springer-Verlag, Heidelberg, 445 pp.

**Pentecost, A.** and **Viles, H.** (1994) A review and reassessment of travertine classification. *Géograph. Phys. Quatern.*, **48,** 305–314.

**Pentecost, A., Jones, B.** and **Renaut, R.W.** (2003) What is a hot spring? *Canadian J. Earth Sci.*, **40,** 1443–1446.

**Pierce, K.L., Despain, D.G., Morgan, L.A.** and **Good, J.M.** (2007) The Yellowstone hotspot, greater Yellowstone ecosystem and human geography. In: *Integrated Geoscience Studies in the Greater Yellowstone Area – Volcanic, Tectonic, and Hydrothermal Processes in the Yellowstone Ecosystem* (Ed. L.A. Morgan), pp. 1–40. U.S. Geological Survey, Professional Paper 1717.

**Pierson, B.K.** and **Castenholz, R.W.** (1995) Taxonomy and physiology of filamentous anoxygenic phototrophs. In: *Anoxygenic Photosynthetic Bacteria (Advances in Photosynthesis and Respiration)* (Eds Blankenship R.E., Madigan M.T. and Bauer C.E.) pp. 31–47, Kluwer Academic Publishers, Dordrecht, Germany.

**Ponce, V.M.** and **Maisner, M.P.** (1993) Verification of theory of roll-wave formation. *J. Hydraul. Eng.*, **119,** 768–773.

**Reysenbach, A.-L., Hamamura, N., Podar, M., Griffiths, E., Ferreira, S., Hochstein, R., Heideberg, J., Johnson, J., Mead, D., pohorille, A., Sarmiento, M., Schweighofer, K., Seshari, R.** and **Voytek, M.A.** (2009) Complete and draft genome sequences of six members of the Aquificales. *J. Bacteriol.*, **191,** 1992–1993.

**Ridgwell, A.** and **Zeebe, R.E.** (2005) The role of the global carbonate cycle in the regulation and evolution of the Earth system. *Earth Planet. Sci. Lett.*, **234,** 299–315.

**Riding, R.** (2000) Microbial carbonates: the geological record of calcified bacterial-algal mats and biofilms. *Sedimentology*, **47,** 179–214.

**Rogerson, M., Pedley, H.M., Wadhawan, J.D.** and **Middleton, R.** (2008) New insights into biological influence on the geochemistry of freshwater carbonate deposits. *Geochim. Cosmochim. Acta*, **72,** 4976–4987.

**Rye, R.O.** and **Truesdell, A.H.** (2007) The question of recharge to the deep thermal reservoir underlying the geysers and hot springs of Yellowstone National Park. In: *Integrated Geoscience Studies in the Greater Yellowstone Area - Volcanic, Tectonic, and Hydrothermal Processes in the Yellowsotne Ecosystem* (Ed. L.A. Morgan), pp. 235–270. U.S. Geological Survey, Professional Paper 1717.

**Sanders, J.E.** and **Friedman, G.M.** (1967) Origin and occurence of limestones. In: *Carbonate Rocks* (Eds G.V. Chilinger, H.J. Bissel and R.W. Fairbridge), *Dev. Sedimentol.*, **9A,** pp. 322. Elsevier, Amsterdam.

**Schmidt, M.** and **Lipson, H.** (2009) Distilling free-form natural laws from experimental data. *Science*, **324,** 81–85.

**Schneidermann, N.** and **Harris, P.M.** (1985) *Carbonate Cements*. Society of Economic Paleontologists and Mineralogists, Tulsa, 379 pp.

**Scrima, A., Konícková, R., Czyzewski, B.K., Kawasaki, Y., Jeffrey, P.D., Groisman, R., Nakatani, Y., Iwai, S., Pavletich, N.P.** and **Thomä, N.H.** (2008) Structural basis of UV DNA-damage recognition by the DDB1–DDB2 complex. *Cell*, **135,** 1213–1223.

**Sheehan, K.B., Patterson, D.J., Dicks, B.L.** and **Henson, J.M.** (2005) *Seen and Unseen: Discovering the Microbes of Yellowstone*. Falcon Press, Helena, Montana, 106 pp.

**Shock, E.L., Meyer-Dombard, D., Amend, J.P., Osburn, G.R.** and **Fischer, T.P.** (2010) Quantifying organic sources of geochemical energy in hydrothermal ecosystems, Yellowsotne National Park, USA. *Geochim. Cosmochim. Acta*, **14,** 4005–4043.

**Smith, R.B.** and **Siegel, L.J.** (2000) *Windows into the Earth*. Oxford University Press, New York, 242 pp.

**Sorey, M.L.** 1991. *Effects of potential geothermal development in the Corwin Springs known geothermal resources area, Montana, on the thermal features of Yellowstone National Park*. 91-4052, United States Geological Survey, Menlo Park, CA.

**Sorey, M.L.** and **Colvard, E.M.** (1997) Hydrologic investigations in the Mammoth Corridor, Yellowstone National Park and vicinity, U.S.A. *Geothermics*, **26,** 221–249.

**Spear, J.R., Walker, J.J., McCollum, T.M.** and **Pace, N.R.** (2005) Hydrogen and bioenergetics in the Yellowstone geothermal ecosystem. *Proc. Natl Acad. Sci. USA*, **102,** 2555–2560.

**Stackebrandt, E.** and **Goebel, B.** (1994) Taxonomic Note: a place for DNA-DNA reassociation and 16S rRNA sequence

analysis in the present species definition in bacteriology. *Int. J. Syst. Bacteriol.*, **44,** 846–849.

**Stal, L.J.** (2000) Cyanobacterial mats and stromatolites. In: *The Ecology of Cyanobacteria: Their Diversity in Time and Space* (Ed. B.A. Whitton and M. Potts), pp. 61–120. Kluwer Academic Publishers, Dordrecht.

**Stanley, G.D.** (2001) *The History and Sedimentology of Ancient Reef Systems*. Kluwer Academic/Plenum Publishers, New York, NY, 458 pp.

**Stephens, D.J.** and **Allan, V.J.** (2003) Light microscopy techniques for live cell imaging. *Science*, **300,** 82–86.

**Stock, S.R.** (2008) *MicroComputed Tomography: Methodology and Applications*. CRC Publishers, Boca Raton, Florida, 336 pp.

**Stumm, W.** and **Morgan, J.J.** (1996) *Aquatic Chemistry: Chemical Equilibria and Rates in Natural Waters*. John Wiley and Sons, Inc., New York, 1022 pp.

**Sturchio, N.C.** (1992) Radium isotopes, alkaline earth diagenesis, and age determination of travertine from Mammoth Hot Springs, Wyoming, USA. *Appl. Geochem.*, **5,** 631–640.

**Sturchio, N.C., Pierce, K.L., Murrell, M.T.** and **Sorey, M.L.** (1994) Uranium-series ages of travertines and timing of the last glaciation in the northern Yellowstone area, Wyoming-Montana. *Quatern. Res.*, **41,** 265–277.

**Sweedlow, J.R., Goldberg, I., Brauner, E.** and **Sorger, P.K.** (2003) Informatics and quantitative analysis in biological imaging. *Science*, **300,** 100–102.

**Takacs-Vesbach, C., Mitchell, K., Jackson-Weaver, O.** and **Reysenbach, A.L.** (2008) Volcanic calderas delineate biogeographic provinces among Yellostone thermophiles. *Environ. Microbiol.*, **10,** 1681–1689.

**Tambutte, E., Allemand, D., Zoccola, D., Meibom, A., Lotto, S., Caminiti, N.** and **Tambutte, S.** (2007) Observations of the tissue-skeleton interface in the scleractinian coral Stylophora pistillata. *Coral Reefs*, **26,** 517–529.

**Teng, H.H., Dove, P.M., Orme, C.A.** and **De Yoreo, J.J.** (1998) Thermodynamics of calcite growth: baseline for understanding biomineral formation. *Science*, **282,** 724–727.

**Tindall, K.R.** and **Kunkel, T.A.** (1988) Fidelity of DNA synthesis by the *Thermus aquaticus* DNA polymerase. *Biochemistry*, **27,** 6008–6013.

**Truesdell, A.H.** and **Hulston, J.R.** (1980) Isotopic evidence on environments of geothermal systems. In: *Handbook of Environmental Isotope Geochemistry* (Eds P. Fritz and J.C. Fontes), 1, The Terestrial Environment A, pp. 179–226. Elsevier, Amsterdam.

**U.S. DOE** (2008) *New Frontiers in Characterizing Biological Systems: Report from the May 2009 Workshop*. DOE/SC-0121, U.S. Department of Energy Office of Science, Washington, DC, 56 pp.

**Usdowski, E., Hoefs, J.** and **Menschel, G.** (1979) Relationship between $\delta^{13}C$ and $\delta^{18}O$ fractionation and changes in major element composition in a recent calcite-depositing spring – a model of chemical variations with inorganic $CaCO_3$ precipitation. *Earth Planet. Sci. Lett.*, **42,** 267–276.

**Vago, R.** (2008) Cnidarians biomineral in tissue engineering: a review. *Mar. Biotechnol.*, **10,** 343–349.

**Veysey, J.** and **Goldenfeld, N.** (2008) Watching rocks grow. *Nat. Phys.*, **3,** 1–5.

**Veysey, J., Fouke, B.W., Kandianis, M.T., Schickel, T.J., Johnson, R.W.** and **Goldenfeld, N.** (2008) Reconstruction of water temperature, pH, and flux of ancient hot springs from travertine depositional facies. *J. Sediment. Res.*, **78,** 69–76.

**Vitale, M.V., Gardner, P.** and **Hinman, N.W.** (2008) Surface water-groundwater interaction and chemistry in a mineral-armored hydrothermal outflow channel, Yellowstone National Park, USA. *Hydrogeol. J.*, **16,** 1381–1393.

**Walker, R.G.** and **James, N.P.** (1992) *Facies Models: Response to Sea Level Change*. Geological Association of Canada, St. John's, 454 pp.

**Walter, M.R.** and **Des Marais, D.J.** (1993) Preservation of biological information in thermal spring deposits: Developing a strategy for the the search for fossil life on Mars. *Icarus*, **101,** 129–143.

**Ward, D.M.** and **Castenholz, R.W.** (2000) Cyanobacteria in geothermal habitats. In: *The Ecology of Cyanobacteria: Their Diversity in Time and Space* (Ed. B.A. Whitton and M. Potts), pp. 37–59. Kluwer Academic Publishers, Dordrecht.

**Ward, D.M.** and **Olson, G.J.** (1980) Terminal processes in the anaerobic degradation of an algal-bacterial mat in a high-sulfate hot spring. *Appl. Environ. Microbiol.*, **40,** 67–74.

**Ward, D.M., Weller, R., Shiea, J., Castenholz, R.W.** and **Cohen, Y.** (1989) Anoxygenic and oxygenic mats of possible evolutionary significance. In: *Microbial Mats: Physiological Ecology of Benthic Microbial Communities* (Ed Y. Cohen and E. Rosenberg), pp. 3–15. American Society for Microbiology, Washington, DC.

**Ward, D.M., Bateson, M.M.** and **de Leeuw, J.W.** (2001) Use of 16S rRNA, lipid, and naturally preserved components of hot spring mats and microorganisms to help interpret the record of microbial evolution. In: *Thermophiles: Biodiversity, Ecology and Evolution* (Eds A.L. Reysenbach, M. Voyteek and R. Mancinelli), pp. 167–182. Kluwer Academic Publishers, Dordrecht, Germany.

**Weed, W.H.** (1889) Formation of travertine and siliceous sinter by the vegetation of hot springs, In: Ninth Annual Report of the United States Geological Survey to the Secretary of the Interior, 1887–88 (Ed. J.W. Powell, Director), U.S. Geological Survey, 613–676.

**Weiner, S.** and **Dove, P.M.** (2003) An Overview of Biomineralization Processes and the Problem of the Vital Effect, In: Biomineralization. *Rev. Mineral. Geochem.*, **54,** 1–29.

**White, D.E., Fournier, R.O., Muffler, L.P.J.** and **Truesdell, A.H.** 1975. *Physical Results of Research Drilling in Thermal Areas of Yellowstone National Park, Wyoming*. United States Geological Survey Professional Paper 892, Menlo Park, Ca, 127 pp.

**Wilson, J.L.** (1975) *Carbonate Facies in Geologic History*. Springer-Verlag, New York, 472 pp.

**Zhang, C.L., Fouke, B.W., Bonheyo, G.T., White, D., Huang, Y.** and **Romanek, C.S.** (2004) Lipid biomarkers and carbon isotopes of modern travertine deposits (Yellowstone National Park, USA): Implications for biogeochemical dynamics in hot-spring systems. *Geochim. Cosmochim. Acta*, **68,** 3157–3169.

**Zhong, S.** and **Mucci, A.** (1989) Calcite and aragonite precipitation from seawater solutions of various salinities: Precipitation rates and overgrowth compositions. *Chem. Geol.*, **78,** 283–299.

*Manuscript received 16 July 2010; revision accepted 26 October 2010*